Università degli Studi di Napoli "Federico II"
Polo delle Scienze e delle Tecnologie

Dottorato di Ricerca in Rischio Sismico

XVIII Ciclo

Attenuation and velocity structure in the area of Pozzuoli-Solfatara (Campi Flegrei, Italy) for the estimate of local site response

Candidate: Simona Petrosino

Tutor: Prof. Edoardo Del Pezzo

Co-Tutor: Prof. Leopoldo Milano

Coordinator: Prof. Paolo Gasparini

Abstract

In the present work I infer the 1D shear-wave velocity model in the volcanic area of Pozzuoli-Solfatara using the dispersion properties of both Rayleigh waves generated by artificial explosions and microtremor. The group-velocity dispersion curves are retrieved from application of the Multiple Filter Technique (MFT) to single-station recordings of air-gun sea shots. Seismic signals are filtered in different frequency bands and the dispersion curves are obtained by evaluating the arrival times of the envelope maxima of the filtered signals. Fundamental and higher modes are carefully recognized and separated by using a Phase Matched Filter (PMF). The obtained dispersion curves indicate Rayleigh-wave fundamental-mode group velocities ranging from about 0.8 to 0.6 km/sec over the 1-12 Hz frequency band.

I also propose a new approach based on the autoregressive analysis, to recover group velocity dispersion. I first present a numerical example on a synthetic test signal and then I apply the technique to the data recorded in Solfatara, in order to compare the obtained results with those inferred from the MF analysis

Moreover, I analyse ambient noise data recorded at a dense array, by using Aki's correlation technique (SAC) and an extended version of this method (ESAC) The obtained phase velocities range from 1.5 km/s to 0.3 km/s over the 1-10 Hz frequency band.

The group velocity dispersion curves are then inverted to infer a shallow shear-wave velocity model down to a depth of about 250 m, for the area of Pozzuoli-Solfatara. The shear-wave velocities thus obtained are compatible with those derived both from cross- and down-hole measurements in neighbour wells and from laboratory experiments. These data are eventually interpreted in the light of the geological setting of the area.

I perform an attenuation study on array recordings of the signals generated by the shots. The γ attenuation curve was retrieved by analysing the amplitude spectral decay of Rayleigh waves with the distance, in different frequency bands. The γ attenuation curve was then inverted to infer the shallow Q_β inverse model.

Using the obtained velocity and attenuation model, I calculate the theoretical ground response to a vertically-incident SH wave obtaining two main amplification peaks centered at frequencies of 2.1 and 5.4 Hz. The transfer function was compared

with those obtained experimentally from the application of Nakamura's technique to microtremor data, artificial explosions and local earthquakes. Agreement among the transfer functions is observed only for the amplification peak of frequency 5.4 Hz.

Finally, as a complementary contribution that might be used for the assessment of seismic risk in the investigated area, I evaluate the peak ground acceleration (PGA) for the whole Campi Flegrei caldera and locally for the Pozzuoli-Solfatara area, by performing stochastic simulations of ground motion, partially constrained by the previously described results. Two different methods (random vibration theory (RVT) and ground motion generated from a Gaussian distribution (GMG)) are used, providing the PGA values of 0.04 g and 0.097 g for Campi Flegrei and Pozzuoli-Solfatara, respectively.

Introduction

It is well known that shallow layers with high impedance contrasts affect the ground motion, causing strong amplifications (Bard and Bouchon, 1980; Hough et al., 1990). Therefore the detailed knowledge of the velocity and attenuation structure at shallow depths is of great relevance for the quantitative estimate of the theoretical ground response to a seismic input. Such determinations are crucial especially in densely urbanized areas, where a quantitative assessment of the amplification factors is necessary for a correct evaluation of seismic hazard.

The determination of the subsoil structure often requires expensive drilling. An alternative and more economic approach to investigate the shallow velocity structure is based on the analysis of surface waves. In the last years, the determination of the seismic velocities at shallow depths from the dispersion of surface waves has got an increasing popularity and recent results in seismic engineering (Liu et al., 2000; Louie, 2001; Bettig et al. 2001) have demonstrated that inversions of dispersion data can provide very fine resolution of the velocity structure and constrain shallow shear wave velocities with a minimum level of uncertainty. Single-station methods (MFT; Herrmann, 1973, 1987) have been widely used with the aim of obtaining the group velocity dispersion curves of short period Rayleigh waves and inferring the shallow velocity structure in sedimentary and tectonic areas (Malagnini et al., 1995, 1997; De Lorenzo et al., 2003). These techniques have been also adapted and successfully applied to retrieve the dispersive properties of the seismic signals generated by the volcanic activity, in order to infer the shallow velocity structure in volcanic areas (Petrosino et al., 1999, 2002). The multichannel (MASW, SAC; Louie, 2001; Aki, 1957; Bettig et al., 2001) techniques also represent a very attractive tool for the phase velocity determination because they can be applied to ambient noise and do not require any particular energizing source. These methods have also been used on microtremor data recordeded on active volcanoes such as the Puu Oo crater, Hawaii (Saccorotti et al., 2003), Stromboli (Chouet et al., 1998) and Vesuvius (Saccorotti et al., 2001).

The ground motion amplitude is strongly affected not only by the impedance contrasts, but also by the damping of soils (and hence by the quality factor Q). Studies of seismic attenuation are helpful in delineating the dissipative properties of rocks. In

particular, the attenuation of surface waves can be analyzed to obtain local Q_β models (Malagnini et al., 1995; Malagnini, 1996; Petrosino et al. 2002).

The information coming from velocity and attenuation structures is useful for the estimate of the theoretical transfer function (Malagnini et al., 1996, Margheriti et al., 2000). In this way, the resonance frequencies that could cause amplification of the ground shaking can be determined. In addition, the site transfer function is extremely useful to put constraints for the evaluation of the peak ground acceleration (PGA), that allows to predict the maximum expected ground shaking (Kramer, 1996). Resonance frequencies, amplification levels and PGA are important parameters that should be taken into account in the assessment of seismic hazard.

In the recent years, experimentally measurements of the site transfer function have been obtained by Nakamura's spectral ratio technique (Nakamura, 1989). In particular, the maxima of the horizontal to vertical (H/V) function, under certain assumptions, correctly indicate the resonance frequencies of soft shallow sediments overlying the bedrock. Many authors have proved the validity of the technique by empirical, theoretical, and numerical results (Field and Jacob, 1993; Lermo and Chavez-Garcia, 1993; Lachet and Bard, 1994; Lermo and Chavez-Garcia, 1994; Field and Jacob, 1995; Castro et al., 1997). However other authors (Luzon et al., 2001; Malischewsky and Scherbaum, 2004) have found that in the case of low impedance contrast, the method does not predict accurately the resonance frequencies and the amplification levels. Moreover it is still not clear if the technique can be applied only to the ambient noise or also to earthquakes and artificial explosions. Actually some authors have found a discrepancy in the H/V functions for noise and earthquakes (Malagnini et al, 1996), while others have observed a good agreement (at least in certain frequency ranges) between the H/V ratio of microtremor and S waves (Seekins at al., 1996; Satoh, 2001). In this framework, further investigations and more tests on data are still needed to establish the range of applicability of Nakamura's technique.

In the present work I will focus on the volcanic area of Pozzuoli-Solfatara and carry on a complete study according to the following tasks:

1) Analysis of Rayleigh wave dispersion and inversion for the velocity structure
2) Analysis of Rayleigh wave attenuation and inversion for the Q_β model
3) Estimate of the theoretical transfer function
4) Determination of the experimental transfer function
5) Estimate of the peak ground acceleration (PGA)

For task 1) I use the Multiple Filter (MFT), the Spatial AutoCorrelation (SAC) and the Extended Spatial AutoCorrelation (ESAC) techniques. Moreover, I propose a new alternative approach based on the autoregressive signal analysis to recover group velocity dispersion. I first present a numerical example on synthetics and then I apply the technique to the data recorded in Solfatara, to compare the obtained results with those inferred from the MFT analysis.

With task 1) and 2) I want to contribute to the knowledge of the very shallow structure of the area of Pozzuoli-Solfatara and provide some complementary information to that given by the available velocity and attenuation tomography, that has greater depths of investigation but cannot resolve the finer structure (first 250 m) of the subsoil.

Task 3) is carried on by using the results obtained from task 1) and 2). Velocity and attenuation structures are used to calculate the ground response to a vertically propagating SH wave in a multiple layered medium. The obtained transfer function might be considered for assessing seismic hazard in the densely-populated volcanic area of Pozzuoli-Solfatara.

For task 4) I will use Nakamura's spectral ratio technique applied to both microtremor data, explosions and local earthquakes and compare it with the theoretical transfer function obtained in task 3). At the present there is a great scientific debate about the validity, the range of applicability of Nakamura's method and if it suitable

only for ambient noise or can be applied to earthquakes too. I want to give my contribution by proposing some examples of application to different kind of data recorded in an area with low-impedance contrast.

Finally, as complementary result in task 5) I provide an estimate of the expected peak ground acceleration for the Campi Flegrei area, by simulating the ground motion produced by local earthquakes. Moreover for the area of Pozzuoli-Solfatara, I estimate the PGA taking into account the local site effects evidenced by the resonance frequencies in the transfer function derived in 3). These evaluations refine the present PGA values for the Phlegraen area reported in the hazard maps (www.mi.ingv.it; Slejko et al., 1998), which have been calculated considering the ground motion produced by strong tectonic earthquakes occurring in the Apennines.

In the next chapters I first illustrate the geological setting of the Campi Fegrei area (Chapter I), I describe the techniques used for this study (Chapter II) and finally I present the obtained results (Chapter III) with the relative discussion.

Chapter I
The Campi Flegrei volcanic complex

1.1 Geological setting

The Campi Flegrei is a nested caldera originated by two large collapses occurred during the Campanian Ignimbrite (39 ka) and the Neapolitan Yellow Tuff (NYT, 15 ka) eruptions (Orsi et al., 1996; Di Vito et al., 1999; Orsi et. al., 2003).

The Campanian Ignimbrite is one of the major explosive eruption occurred in the Mediterranean area in the last 200,000 years and its deposits buried a large part of the Campania region. The Campanian Ignimbrite caldera, which formed after the collapse includes the present area of the Campi Flegrei, the city of Naples, the western part of the bay of Naples and the bay of Pozzuoli.

During the Neapolitan Yellow Tuff eruption several tens of km^3 of magma were emitted and an area of approximately 1,000 km^2 was covered by pyroclastic deposits. These deposits have been found in Neapolitan-Phlegraean area and the Campanian Plain as far as in the Appennines. The NYT caldera is nested inside the Campanian Ignimbrite caldera, it includes part of the present Campi Flegrei area and the bay of Pozzuoli. The caldera floor is affected by brittle deformation, being its continental north-eastern sector crossed by faults oriented NW-SE and NE-SW, which are the same directions as those of the faults affecting the Campanian Plain and the inner sectors of the Apennine belt.

Since 15 ka the volcanic activity concentrated inside the NYT caldera and many eruptions took place during three distinct epochs of activity, alternated to two periods of quiescence. In particular, volcanism of the I epoch (15-9.5 ka) includes 34 variable magnitude explosive eruptions. During this epoch several tuff-cones were formed near the present coast of Pozzuoli (Rione Terra, La Pietra).

During the II epoch (8.6-8.2 ka), the volcanic activity occurred along the north-eastern structural boundary of the NYT caldera, whereas vents (Solfatara, Accademia, Monte Olibano) of the III epoch (4.8–3.8 ka) were mainly located in the north-eastern sector of the caldera floor, near the present town Pozzuoli.

The last eruption (Monte Nuovo) occurred in 1538, after a period of quiescence which lasted approximately 3,000 years.

Since the NYT collapse, the whole Campi Flegrei caldera is affected by subsidence, while the younger central part of the caldera floor is characterized by resurgence. In particular, during the three epochs of volcanic activity, the La Starza marine terrace (the most uplifted part of the resurgent block) alternated periods of emersion and submersion and after the onset of the III epoch it definitely emerged.

The stratigraphic, structural and geochronological observations have widely contributed to define this complex volcanological evolution. For example, evidences of the eruptive activity of the I and III epoch and the sequence of La Starza comes from the stratigraphic data and borehole drillings in the area of Pozzuoli which show the presence of tuff rocks overlaid by pyroclastic and marine deposit layers of variable thickness. These data were also used to trace a possible geological section across the town of Pozzuoli, moving from the shore (Rione Terra) towards the Solfatara, along a NNE-SSW profile (Lirer et al., 1987).

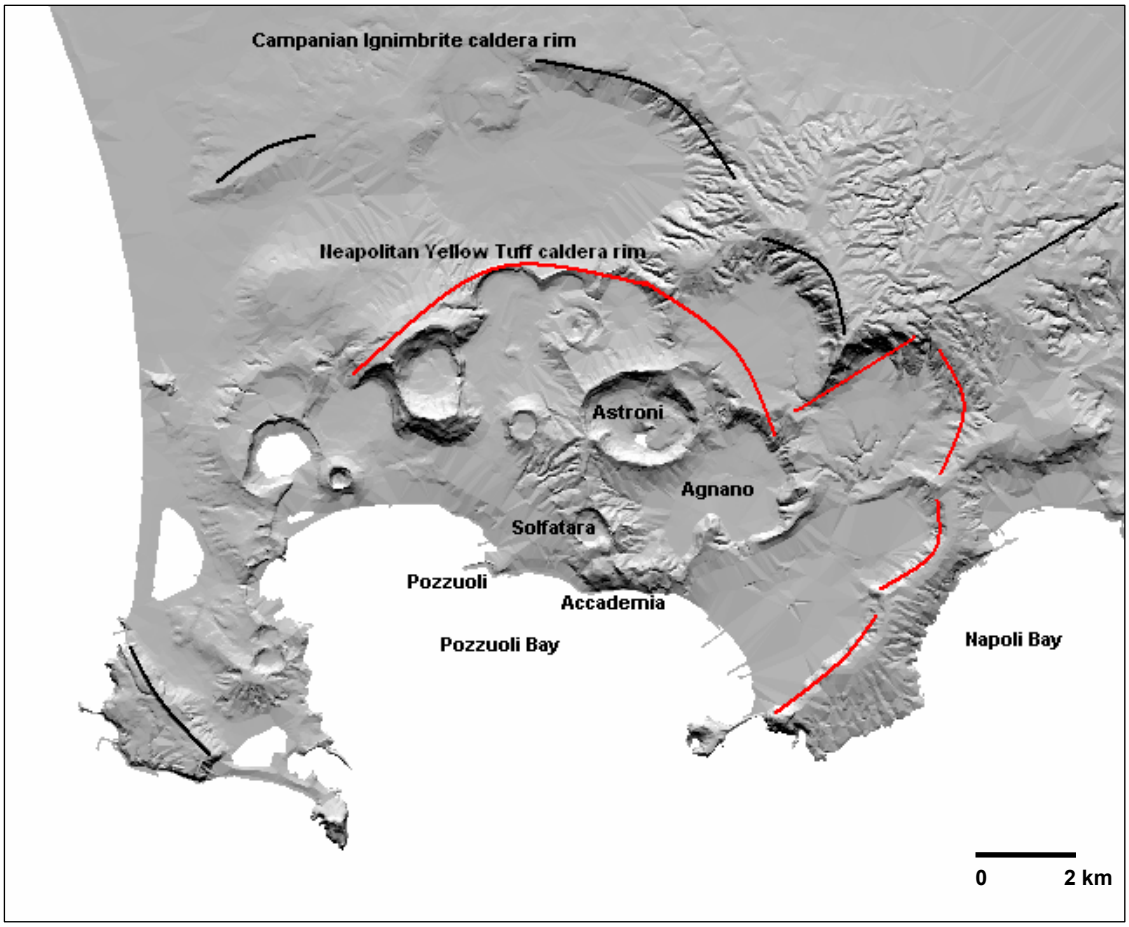

Fig. 1.1- Sketch map of the Campi Flegrei caldera.

1.2 Seismicity and ground deformation

Seismicity in the Campi Flegrei area generally occurs during the phases of ground uplift, while it is absent during the periods of subsidence.

The major uplift episodes occurred in 1969-1972 and in 1982-1984 (Orsi et al., 1999). During the bradyseismic crisis of 1969-1972, the ground lifted by approximately 1.5 m. The seismic activity began with some low-energy events which preceded a 1.8 magnitude earthquake occurred on 1970, March 26th. Other seismic swarms followed on 1970, April 2nd, July 21st and November 26th. The strongest earthquake was recorded on 1972, March 2nd. In the summer of 1972 the ground stopped to rise and, at the same time, the seismic activity ended. Between 1973 and 1981 the Campi Flegrei area was subjected to a slow process of subsidence, interrupted by a small uplift episode (less than 10 cm) in the month of September 1976 which was accompanied by about 12 earthquakes located in the Solfatara area.

During the 1982-1984 crisis a ground uplift of 1.79 m took place. This was accompanied by intense seismic activity: swarms of earthquakes were recorded with a magnitude between 0.6 and 4.2, generally at a depth of 1.5 to 5 Km. The most significant swarm (513 earthquakes in about 6 hours) was detected on 1984, April 1st. The strongest earthquake (magnitude 4.2) occurred on 1983, December 8th. During this seismic crisis, over 10,000 earthquakes were recorded. Most of the seismicity concentrated in the area of Pozzuoli-Solfatara. In Pozzuoli, the seismic activity was characterized by low-energy swarms, while the Solfatara area was the epicentral zone for the most energetic earthquakes (Vilardo et al., 1991).

After the 1982-1984 episode, no further seismic activity was recorded in the Phlegrean area until 1987, when on April 10th and November 4th two seismic swarms consisting of 50 and 26 earthquakes respectively, were recorded and located in the Solfatara area. Between April and June 1989, at the time of an episode of renewed ground uplift (about 7.5 cm), there were 316 earthquakes, located SE of the Solfatara crater. In particular on April 3rd a seismic swarm was recorded, consisting of 82 events, while the severest earthquake of this period happened June on 6th. After the 1989 episode, no further significant events were recorded until July 2000.

In the period July-August 2000 a net uplift of 4 cm centered on Pozzuoli occurred. This phase was accompanied by two low-energy seismic swarms on July 2nd and August

22nd (Bianco et al., 2004). Seismic activity started between July 2nd and 10th, when about ten low-energy low-frequency events were recorded. On August 22nd there was a seismic swarm of about sixty volcano-tectonic earthquakes, some of them felt by the population living in the area of the Solfatara. The high frequency pattern of this swarm is similar to that shown by the volcano-tectonic events recorded during the 1983-84 uplifting episode. The strongest earthquake had magnitude 2.2. The seismic swarm was located in the Solfatara area, at a depth of about 2 Km.

Since October 2004 a weak uplifting episode started and reached its maximum value (11 mm) in May 2005. The last seismic swarm was recorded on 2005, October 5th and consisted of about 70 low-energy earthquakes occurred in about 8 hours, with the maximum magnitude of 1.1. Some of these earthquakes were felt by the population of the area of Pozzuoli-Solfatara. The most energetic events were located in the area of Solfatara - Monte Spina (Agnano), with hypocentral depths in the first 2 km.

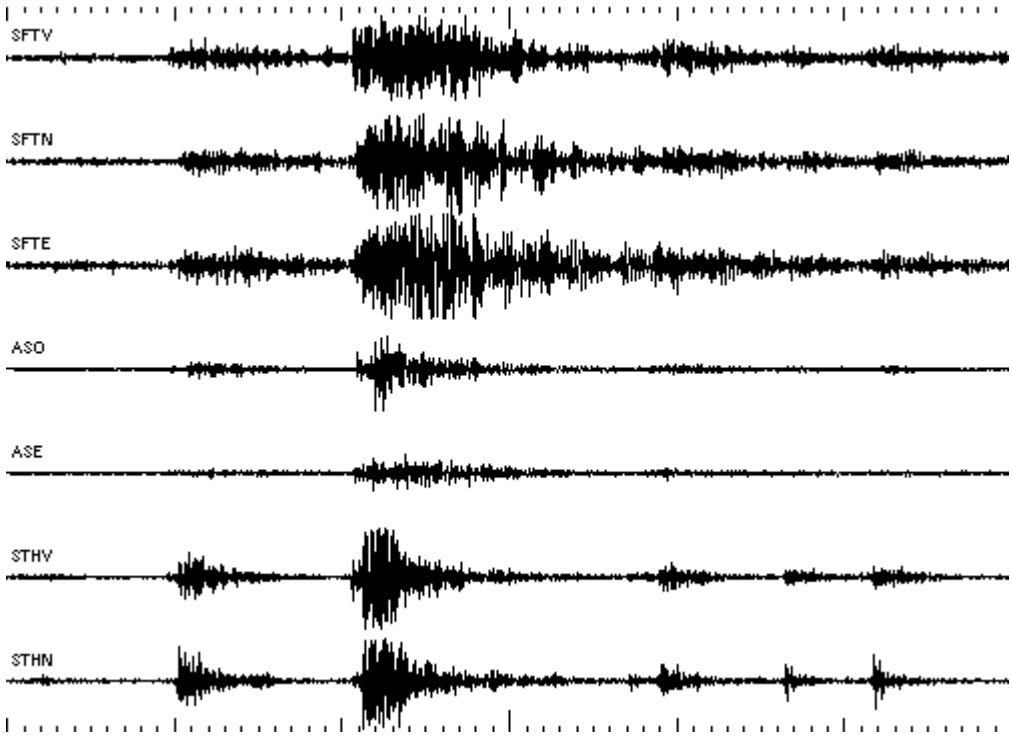

Fig. 1.2 - Example of earthquakes recorded on 2005/10/05 by the seismic stations of the Osservatorio Vesuviano.

Fig. 1.3 – Aerial view of the area of Pozzuoli-Solfatara. Photo courtesy of Laboratorio di Geomatica e Cartografia - Osservatorio Vesuviano.

Chapter II
Techniques of analysis

2.1 Techniques for surface wave dispersion analysis

A brief review of the techniques that I used for the analysis of surface wave dispersion is reported in the following sections.

2.1.1 The Multiple Filter Technique

The Multiple Filter Technique (MFT; Dziewonski et al.,1969; Herrmann, 1987) is a single station method based on the evidence that for dispersive signals, different wave packets arrive at different times, depending on the frequency. The method consists in the application of gaussian band-pass filters to multi-modal dispersive signals associated to the propagation of surface waves. Then, the arrival times of the maxima of the envelope of the filtered signal are estimated and used to calculate group velocity. By Repeating the procedure for different frequencies, the group velocity dispersion curve can be inferred.

The technique is based on the following theory. The displacement caused by a dispersive wave packet at time t and distance r from the source is represented as superposition of the M+1 modes present in the signal (Aki and Richards, 1980):

$$f(t,r)=\frac{1}{2\pi}\int_{-\infty}^{\infty}F(\omega,r)\exp(i\omega t)d\omega=\frac{1}{2\pi}\int_{-\infty}^{\infty}\sum_{j=0}^{M}A_j(\omega,r)\exp[i(\omega t-k_j r)]d\omega$$

where ω is the angular frequency, k_j and A_j are the wave number and the complex amplitude of the *j*-th mode, respectively. First consider the application of a gaussian band-pass filter to a single-mode signal. If $H(\omega-\omega_0)$ is a gaussian filter centered at $\omega=\omega_0$ with cutoff frequency at $\omega=\omega_0\pm\omega_c$:

$$H(\omega)=\begin{cases}\exp(-\alpha\,\omega^2/\omega_0) & |\omega|\le\omega_c\\ 0 & |\omega|>\omega_c\end{cases}$$

the expression of the filtered signal will be:

$$g(r,t)=\frac{1}{2\pi}\int_{\omega_0-\omega_c}^{\omega_0+\omega_c}H(\omega-\omega_0)A(\omega,r)\exp[i(\omega t-kr)]d\omega$$

After changing variable, the integral becomes:

$$g(r,t) = \frac{1}{2\pi} \int_{-\omega_c}^{\omega_c} H(\omega) A(\omega + \omega_0, r) \exp\{i[(\omega + \omega_0)t - k(\omega + \omega_0)r]\} d\omega \tag{2.1}$$

After an expansion in Taylor series of $A(\omega, r)$ and of $k(\omega)$ around ω_0, Herrmann (1973) demonstrated that equation (2.1) can be written as (see appendix A):

$$g(t,r) = \frac{A\omega_0}{2\pi} \sqrt{\frac{\pi}{\alpha}} \exp[i(\omega_0 t - k_0 r)] \exp\left[-\frac{\omega_0^2}{4\alpha} \left(t - \frac{r}{U_0} \right)^2 \right] \tag{2.2}$$

where U_0 is the group velocity. From (2.2) one can easily see that the envelope (or magnitude) of the function $g(t,r)$ has the maximum at the time $t = r/U_0$.

In case of multi-modal signals, the equation (2.2) assumes the form:

$$g(t,r) = \frac{\omega_0}{2\pi} \sqrt{\frac{\pi}{\alpha}} \sum_{j=0}^{M} A_j(\omega_0, r) \exp[i(\omega_0 t - k_{0j} r)] \exp\left[-\frac{\omega_0^2}{4\alpha} \left(t - \frac{r}{U_{0j}} \right)^2 \right] \tag{2.3}$$

where the index *j* represents the value of *U* and *A* for the *j*-th mode. Taking the envelope of (2.3), the individual maxima correspond to the arrivals $t = r/U_{0j}$ relative to the different modes, each of them propagating with group velocity U_{0j}. If the individual maxima are well separated and the source-to-receiver distance *r* is known, the group velocities U_{0j} can be calculated.

2.1.2 Phase-matched filters

The phase-matched filters (PMF; Herrin and Goforth, 1977) are defined as the class of linear filters for which the Fourier phase is equal to that of a given signal. Considering the convolution and the cross-correlation of a signal $s(t)$ with the filter $f(t)$ and taking the Fourier transform, one obtains:

$$s(t) * f(t) \Rightarrow |S(\omega)||F(\omega)| \exp i[\sigma(\omega) + \phi(\omega)] \tag{2.4}$$

$$s(t) \otimes f(t) \Rightarrow |S(\omega)||F(\omega)| \exp i[\sigma(\omega) - \phi(\omega)] \tag{2.5}$$

where the symbol $\Rightarrow$ denotes the Fourier transform operation. If $f(t)$ is a phase-matched filter, then $\sigma(\omega) = \phi(\omega)$. With this choice, the Fourier transform of equation (2.5) will be $|S(\omega)||F(\omega)|$. The same result can be obtained from (2.4) if one considers

the Fourier transform of the convolution of $s(t)$ with $f(-t)$. The quantity $|S(\omega)||F(\omega)|$ is defined pseudo-correlation function (PAF). Generally, $|F(\omega)|$ is chosen to be equal to 1, in order to have a good compromise between maximum signal-to-noise improvement and maximum time resolution.

The application of the phase-matched filters allows to remove multiple arrivals, non-dispersive arrivals of body waves and higher oscillation modes from the signal and therefore to isolate a selected wave packet. The PM filters are generally combined with the Multiple Filter analysis in order to avoid the contamination of the different modes in the analysed signal and to obtain well separated dispersion curves.

Assuming that the seismogram is formed by a certain number *m* of modes, the action of the phase-matched filter can be expressed as:

$$\psi_j(t) = \frac{1}{2\pi}\int_{-\infty}^{\infty}\left\{e^{ik_j^* t}\right\}\sum_m A_m e^{i(\omega t - k_m x)}d\omega \tag{2.6}$$

where $\psi_j(t)$ is the PAF, $e^{ik_j^* t}$ is the phase of the phase-matched filter and k_j^* is the estimate of the wavenumber of the *j*-th mode. Equation (2.6) can be rewritten as:

$$\psi_j(t) = \frac{1}{2\pi}\int_{-\infty}^{\infty} A_j e^{i\left(k_j^* - k_j\right)x} e^{i\omega t}d\omega + \frac{1}{2\pi}\int_{-\infty}^{\infty}\sum_{m\neq j} A_m e^{i(\omega t - k_m x)}d\omega$$

If $k_j^* \approx k_j$, the first integral will have the phase approximately equal to zero, obtaining a zero-lag signal. If one multiplies the PAF with a symmetric zero-phase time window $w(t)$, the effects of the other modes ($\neq j$) will be removed:

$$\psi_j(t)w(t) = w(t)\frac{1}{2\pi}\int_{-\infty}^{+\infty} A_j e^{i\delta k x} e^{i\omega t}d\omega \tag{2.7}$$

where $\delta k = k_j^* - k_j$. Taking the Fourier transform of equation (2.7), the amplitude spectrum of the desired mode is obtained:

$$A_j e^{i\delta k x} = \int_{-\infty}^{\infty}\psi(t)w(t)e^{-i\omega t}d\omega$$

The residual error $\delta k x$ affecting the phase can be used to obtain a new estimate of the real wavenumber:

$$k_j^{*new} = k_j^* - \delta k$$

The procedure can be iterated to obtain a precise estimate of the wavenumber (and hence of the group velocity) for the mode of interest.

2.1.3 Spatial Autocorrelation technique (SAC and ESAC)

The Spatial Autocorrelation method (SAC) of Aki (1957) is a multichannel technique and it allows the estimate of the phase velocity dispersion curve of surface waves in the hypothesis that the noise wavefield is stationary in time and space.

Given two receivers, the normalized spatial autocorrelation coefficient is defined as:

$$\rho(r,\varphi) = \frac{\langle u(x,y,t) \cdot u(xr\cos\varphi, y + r\sin\varphi)\rangle}{\langle u(x,y,t) \cdot u(x,y,t)\rangle}$$

The symbols $\langle\rangle$ indicate the average over time, u is the ground motion, x and y are the Cartesian coordinates of the receivers, r is the distance between the receivers and φ is the azimuth of the two receivers measured counter clockwise from the direction of the x-axis. The correlation coefficients range between -1 and 1, assuming the maximum value when the waveforms are equal. If the signal is filtered in a narrow frequency band around ω_0, Aki demonstrated that the correlation coefficient takes the form:

$$\rho(r,\varphi,\omega_0) = \cos\left[\frac{\omega_0}{c(\omega_0)} r\cos(\theta - \varphi)\right] \tag{2.8}$$

where θ is the propagation azimuth and $c(\omega_0)$ is the wave phase velocity at the angular frequency ω_0. Taking into account equation (2.8), for an array of receivers in a semi-circular configuration around a reference receiver, the azimuthal average of the correlation coefficients for the vertical component is expressed:

$$\overline{\rho}(r,\omega_0) = J_0\left[\frac{\omega_0}{c(\omega_0)} r\right] \tag{2.9}$$

where J_0 is the 0-th order Bessel function. From equation (2.9), the phase velocity $c(\omega_0)$ can be obtained by fitting the Bessel function to the azimuthal average of the autocorrelation coefficients, estimated 1) at a fixed angular frequency ω_0 or 2) at a fixed distance r. In case 1), $\overline{\rho}$ will be a function of the distance r. Otherwise, in case 2), $\overline{\rho}$ will be a function of the frequency and in the fitting procedure it will be necessary to

assume an a-priori dispersion law $c(\omega_0)$. In this case, the phase velocity is usually assumed to have a frequency dependence described by a power-law function:

$c(f) = Af^{-b}$

The choice 1), which is the best because no a priori dispersion should be assumed, is generally possible when the array is formed by a large number of sensors and the correlation coefficients can be evaluated for a relatively high number of inter-station distances. This requires a particular geometry of the seismic array, with the sensors deployed along many semicircles with different radius.

Extension of Aki's SAC method to non-semicircular arrays (ESAC) was proposed by Bettig (2001) and consists in averaging, for each individual target frequency, the correlation coefficients evaluated at subsets of M station pairs whose distances range between *r-dr* and *r+dr*. This procedure allows a robust assessment of the azimuthally-averaged correlation coefficients, once the relative position vectors of the selected station pairs depict an uniform and tight sampling of the 0-180° azimuthal range. In this case the condition of having a large number of available inter-station distances can be achieved without the constraint of adopting a particular geometry for the array deployment. For this reason, the advantage of ESAC compared to the conventional SAC is that the evaluation of (2.9) at a fixed frequency can be easily carried on, and the estimates of phase velocities may be retrieved at any individual frequency without the need of assuming any a-priori dispersion relationship.

2.1.4 Autoregressive analysis for complex travel time determination

In this section I discuss a new approach to recover the group velocity dispersion curve of surface waves.

Consider a pulse occurring at a certain point at time t = 0. As an effect of the propagation, the signal observed at the given point can be represented by the superposition of a certain number *j* of pulses that may have been propagating along different paths, with different phase velocities, *c*, (Aki and Richards, 1980) :

$$f(t) = \sum_j A_j \exp(i\omega(t - \frac{k_j}{\omega} x_j) = \sum_j A_j \exp\left[i\omega(t - q_j)\right] \qquad (2.10)$$

where A_j is the amplitude of the j-th pulse and ω is the angular frequency. In case of dissipative medium, k is the complex wavenumber and the quantity q is defined as the complex travel-time:

$$k_j = \frac{\omega}{c_j}\left(1 - \frac{i}{2Q}\right)$$

$$q_j = \tau_j + iv_j$$

The real part of q represents the arrival time $\tau = x/c = kx/\omega$ and the imaginary part is expressed as:

$$v = -\frac{x}{2cQ}$$

with c phase velocity and Q quality factor.

In the frequency domain, the sequence of pulses is represented by the Fourier transform of (2.10):

$$F(\omega) = \sum_j A_j \exp(-iq_j\omega) = \sum_j A_j \exp(-ik_j x_j) \tag{2.11}$$

The real and imaginary part of (2.11) correspond to oscillating signals in the frequency domain. Hasada et al. (2001) proposed an impulse model corresponding to equation (2.11). Actually it can be demonstrated that the inverse Fourier transform of the function $F(\omega)$ corresponds to the real part of the complex Lorentzian function $L(t)$:

$$h(t) = \frac{1}{\pi}\sum_j \mathrm{Re}\left(\frac{iA_j}{t - q_j}\right) = \frac{1}{\pi}\sum_j \mathrm{Re}(L_j(t))$$

As the amplitude A can be expressed as $A = A_0 \exp(i\omega\phi)$, for ϕ=0 the real part of the function $L(t)$ is a Lorentzian function centered at τ, with a width of w_j=-$2v_j$ and the imaginary part is asymmetric respect $t = \tau$. In general, for different values of ϕ, $Re(L(t))$ is a linear combination of a symmetric and asymmetric components.

For dispersive wave packets, the complex wavenumber k is a function of frequency and can be expanded in a Taylor series around the point ω_0:

$$k_j(\omega) = k_0(\omega) + \left.\frac{\partial k_j}{\partial \omega}\right|_{\omega=\omega_0}(\omega - \omega_0) = k_0(\omega) + \frac{1}{u_j(\omega_0)}(\omega - \omega_0)$$

where u is the group velocity. Substituting this expression in the equation (2.11) one obtains:

$$F(\omega) = \sum_j A_j \left[\exp(-ik_j(\omega_0)x_j)\right]\left[\exp(-iq_j^g(\omega_0)(\omega-\omega_0)\right] =$$

$$= \sum_j A_j \left[\exp(-iq_j(\omega_0)\omega\right]\left[\exp(-iq_j^g(\omega_0)(\omega-\omega_0)\right]$$

q_j^g is the complex group delay that is related to the complex group velocity:

$$q_l^g(\omega_0) = \frac{x_j}{u_j(\omega_0)}$$

Consider now the function $F(\omega)$ in a narrow frequency band centered around ω_0; it will assume the following form:

$$H(\omega_0,\omega) = \sum_j A_j \left[\exp(-i(q_j(\omega_0) - q_j^g(\omega_0))\omega_0)\right]\left[\exp(-iq_j^g(\omega_0)\omega)\right] =$$

$$= \sum_j B_j(\omega_0)\exp(-iq_j^g(\omega_0)\omega) \qquad (2.12)$$

Comparing this expression with (2.11), one notes that the two transfer functions have the same form with the difference that in the case of dispersive media the amplitude A_j and the phase delay q_j in equation (2.11) have been replaced by B_j and the group delay q_j^g at the frequency ω_0. Therefore, the impulse sequence model corresponding to the complex Lorentzian function can also be applied to the case of dispersive media if one considers a narrow frequency band. In this case the real part of the complex travel time corresponds to the travel time of the group velocity at the frequency f_0. Taking this into account, a dispersion curve can be obtained by estimating the real part of complex travel time for a set of center frequencies.

The problem of providing a reliable estimate of the complex travel times (and therefore of the group arrivals) can be carried on by using an autoregressive (AR) approach. In the following I will describe some general concepts of the autoregressive method applied to complex frequency series, then in appendix B I will show an application to a synthetic signal to demonstrate the ability of the technique in discriminating closely spaced pulses and hence in reliably determining the travel times.

The complex frequency series corresponding to expression (2.11) can be considered as the superposition of two independent components, the signal H and the Gaussian white noise E:

$Y_i = H_i + E_i \quad \text{i} = 0\ldots\text{N-1}$

where N is the number of points of the complex frequency series. The signal H consists of decaying oscillations and satisfies an m order AR equation:

$$A(z)H_j = 0 = \sum_{k=0}^{m} a_k z^{-k} H_j \tag{2.13}$$

$A(z)$ is a complex AR operator of order m, a_k are the AR coefficients and z is the unit-frequency-shift operator:

$$zH_j = H_{j+1}$$

$$z = \exp(-i2\pi q \Delta f)$$

with Δf the unit of frequency discretization. To estimate the unknown parameters (the complex travel times q which are related to the z operator) in the given complex frequency series, several approaches exist. I will follow that proposed by Hori et al. (1989) based on the minimization of the prediction error, that leads to the determination of the AR a_k coefficients by solving an eigenvalue problem. Taking into account (2.13), the prediction error is:

$$F = \frac{1}{N-m} \sum_{j=m}^{N-1} \left(\sum_{k=0}^{m} a_k Y_{j-k} \right) \overline{\left(\sum_{k=0}^{m} a_k Y_{j-k} \right)}$$

The prediction error can be minimized by using the method of the Lagrange multiplier with the constraint $|\vec{a}|^2 = 1$, in order to exclude trivial solutions:

$$\frac{\partial}{\partial a_l} \left[F - \lambda \left(\sum_{k=0}^{m} a_k \overline{a}_k - 1 \right) \right] = 0$$

If one introduces the non-Toeplitz Hermitian autocovariance matrix of Y_i whose elements are given by:

$$P_{k,l} = \overline{P}_{l,k} = \frac{1}{N-m} \sum_{j=m}^{N-1} Y_{j-k} \overline{Y}_{j-l} \qquad 0 \le k, l \le m$$

the problem of the prediction error minimization reduces to the eigenvalue problem:

$$\vec{P}\vec{a}^{\,\mu} = \lambda^{\mu} \vec{a}^{\,\mu} \qquad \mu = 0,1....m \qquad \vec{a}^{\,\mu} = \begin{bmatrix} a_0^{\mu} \\ a_1^{\mu} \\ \dots \\ a_m^{\mu} \end{bmatrix}$$

where λ^{μ} and a^{μ} are the eigenvalues and eigenvectors of $\vec{P}$. The eigenvalue problem is solved through the diagonalization of the matrix $\vec{P}$, obtaining a set of m+1 eigenvalues.

From this set one chooses the minimum eigenvalue λ^0 which corresponds to minimum noise power, and determines the m+1 eigenvectors a_k^0. In terms of the eigenvalue λ^0, one can quantify the Akaike Information Criterion (Matsuura et al. 1990) as:

$$AIC = N \log \lambda^0 + 2(m+1)$$

This quantity can be used to determine the minimum AR filter order required to resolve the wave elements in the complex frequency series.

Once the eigenvectors a_k have been determined, the next step is to calculate z and hence the complex travel times q. The AR equation (2.13) can be satisfied (excluding the trivial condition $H_j = 0$) if one requires:

$$\sum_{k=0}^{m} a_k^0 z^{-k} = 0 \qquad (2.14)$$

where a_k^0 are the eigenvectors corresponding to the minimum eigenvalue λ_0. This characteristic equation is an m-th algebraic equation for z^{-1} whose solutions are:

$$z_k = \exp(-i 2\pi q_k \Delta f)$$

Therefore, from the characteristic roots of (2.14) the complex travel times are calculated according to:

$$q_k = \tau_k + i v_k = \frac{i \ln z_k}{2\pi \Delta f}$$

If the complex frequency series corresponds to a dispersive signal represented by (2.12), the quantity τ_k represents the group-velocity travel time.

In the analysis of complex frequency series a Nyquist travel time t_N exists: 0 and $2t_N$ represent the lower and upper limits of the time band in which the travel times can be resolved. The Nyquist travel time is defined in terms of the unit of frequency discretization Δf:

$$\tau_N = \frac{1}{2\Delta f}$$

The travel times τ_k corresponding to the solutions of the characteristic equation will be distributed in the 0-2 t_N Nyquist time band. As suggested by Kumazawa et al. (1990), an empirical way to select the solutions corresponding to the signal and discard those representing noise, is to construct the so-called cumulative "τ-v plot". If one reports in a 2D plane the τ values versus the v values for all the AR filter orders, a

clustering of the data points will be observed for the true arrival times τ, while scattered points correspond to the noise.

Once the travel times have been obtained, the group velocity can be calculated by simply dividing the source-to-receiver distance *D* to the t_k:

$$u_k = D \big/ \tau_k$$

To obtain the group velocity dispersion curves, the whole procedure have to be applied to a windowed complex frequency series. In this way, a particular frequency band centered on a certain value f_0 is chosen and the application of the AR filter will provide the group velocity values relative to that selected frequency. The dispersion curve will be obtained by repeating the analysis for different segments of the complex frequency series corresponding to the selected center frequencies.

Although AR techniques are well known in spectral analysis, until now this approach has never been applied to real data for the estimate of dispersion curves. The unique application of the AR method for complex travel time determination in surface waves dispersion studies is that proposed by Hasada et al. (2001). However in their work, the authors test the method only on synthetic complex frequency series and do not use real data.

In this thesis I first apply the technique to synthetic data simulating a dispersive wave packet, confirming the ability of the method in resolving closely time-spaced pulses (as shown in appendix B), and then in section 3.2.2 I present a completely new application to a real data set.

2.2 Attenuation analysis: the spectral amplitude decay with distance

The study of the attenuation of seismic waves can be carried out analysing the decay of the spectral amplitude with the distance. The amplitude spectrum of the *j*-th signal recorded at the *i*-th station is expressed as (Aki and Richards, 1980):

$$A_{ij}(R_i, \omega) = \frac{A_{0j}(\omega)}{(R_i)^n} \exp(-\gamma R_i) \qquad (2.15)$$

where γ is the attenuation coefficient defined as:

$$\gamma = \frac{\omega}{2\pi v Q}$$

and A_0 is the source spectral amplitude at the angular frequency ω, R_i is the source-to-station distance, n is the geometrical spreading coefficient (1 for body waves and 0.5 for surface waves), v is the wave velocity, and Q is the quality factor assumed as frequency-independent.Taking the logarithm the equation (2.15) becomes:

$$\ln A_{ij} + n \ln R_i = \ln A_{0j} - \gamma R_i \qquad i = 1\ldots\mathrm{N},\ j = 1\ldots\mathrm{M} \tag{2.16}$$

where N is the number of stations and M is the number of signals to be analysed. Extending relation (2.16) to N stations and M signals, one obtains an overdetermined system of NxM equations with unknowns A_{0j} and γ which can be rewritten in the matrix form:

$$\mathbf{d} = \mathbf{G}\mathbf{m} \tag{2.17}$$

where **d** is a vector of NxM rows that contains the observational data, **G** is the (M+1)x(NxM) coefficient matrix and **m** is the vector of length (M+1) that contains the unknown model parameters. The explicit form of equation (2.17) is:

$$\begin{bmatrix} \ln A_{11} + n \ln R_1 \\ \ln A_{21} + n \ln R_2 \\ \ldots \\ \ln A_{N1} + n \ln R_N \\ \ln A_{12} + n \ln R_1 \\ \ldots \\ \ln A_{NM} + n \ln R_N \end{bmatrix} = \begin{bmatrix} 1 & 0 & \ldots & \ldots & \ldots & R_1 \\ 1 & 0 & \ldots & \ldots & \ldots & R_2 \\ \ldots & \ldots & \ldots & \ldots & \ldots & \ldots \\ 1 & 0 & \ldots & \ldots & \ldots & R_N \\ 0 & 1 & \ldots & \ldots & \ldots & R_1 \\ \ldots & \ldots & \ldots & \ldots & \ldots & \ldots \\ 0 & 0 & 0 & \ldots & 1 & R_N \end{bmatrix} \cdot \begin{bmatrix} A_{01} \\ A_{02} \\ \ldots \\ \ldots \\ \ldots \\ A_{0M} \\ -\gamma \end{bmatrix}$$

This problem can be solved by using a least square inversion technique to find the best solution for **m** (and hence for γ), according to the generalized inverse formulation:

$$(\mathbf{G}^{\mathrm{T}}\mathbf{G})^{-1}\,\mathbf{G}^{\mathrm{T}}\,\mathbf{d} = \mathbf{m}$$

When this analysis is applied to surface waves in different frequency bands, the γ attenuation curve (that is the trend of the attenuation coefficient as a function of frequency) can be recovered.

2.3 The horizontal to vertical spectral ratio technique

The idea that the horizontal to vertical (H/V) spectral ratio of microtremor was representative of the site transfer function was initially proposed Nogoshi and Igarashi (1971). These authors justified their assumption suggesting that the observed peak of the H/V ratio was related to the ellipticity curve of fundamental mode Rayleigh waves and it was indicative of the shallow soil structure.

In 1989 Nakamura revisited the method proposing a new semi-qualitative theoretical explanation in terms of multiple refractions of SH waves. He claimed that the peak in the H/V spectral ratio cannot be explained in terms of Rayleigh waves, but it is due to vertical incident SH wave, therefore it represents a reliable estimate for the site transfer function of the S waves.

Both the interpretations are based on some strong assumptions and for this reason at the present there is still a great scientific debate about the correct definition of the theoretical background of the technique and about the validity of the results (see for example Bard, 1999). The present efforts of the scientific community, mainly addressed to provide more robust theoretical basis, essentially follow two aprroaches: 1) the use of numerical simulations aimed at understanding both if the H/V ratio is related to Rayleigh or S waves (Fäh et al., 2001; Malischewsky and Scherbaum, 2004) and if it can be representative of a site true transfer function (Luzon, et al., 2001) and 2) the application to real data in order to compare the experimental results with the theory (Lermo and Chavez-Garcia, 1994; Konno and Omachi, 1998).

In the next sections, I report a brief review about the two interpretations (Bard, 1999).

2.3.1 Interpretation of Nakamura

Nakamura (1989, 1996) provides only a semi-qualitative theoretical explanation that is based on some strong assumptions. The noise can be separated into body and surface waves:

$$S^H(f) = S_b^H(f) + S_s^H(f) = H_T(f)R_b^H(f) + S_s^H$$

$$S^V(f) = S_b^V(f) + S_s^V(f) = V_T(f)R_b^V(f) + S_s^V$$

where the subscripts and superscripts ^{H} and ^{V} stand for horizontal and vertical component respectively, *b* and *s* stand for body and surface waves, *S* is the Fourier spectrum of the noise, *R* is the spectrum of the body-wave part of the noise at the reference site and H_T and V_T represent the true site amplification function for the horizontal and vertical component respectively. The H/V spectral ratio between the amplitude spectra of the noise can be expressed as:

$$A^{HV} = \frac{H_T A_r^{HV} + \beta A_s}{V_T + \beta}$$

where A_r^{HV} is the H/V noise spectral ratio at a rock site, $\beta = S_s^V / S_b^V$ is the relative part of surface waves in the noise wavefield and $A_s = S_s^H / S_s^V$ is the horizontal to vertical spectral ratio due only to surface waves. Nakamura claims that the ratio between the horizontal and vertical noise spectra is equal to the true site amplification function for the horizontal component:

$$A^{HV} = H_T$$

Consider first the previous relation evaluated at the fundamental resonance frequency f_0:

$$A^{HV}(f_0) = H_T(f_0) \tag{2.18}$$

This equality requires the following assumptions:

1) the vertical component is not amplified at f_0
2) The H/V spectral ratio on the rock site is equal to 1 at f_0
3) β is much smaller than 1 at f_0
4) $\beta A_s(f_0)$ is much smaller than $H_T(f_0)$

The point 1) and 2) can be justified on the basis of the experimental evidences. However 1) and 2) are not obviously extended to the case that equation (2.18) should hold for all the frequencies. The other two points are very controversial and seem to be in contradiction, as the assumption in 3) can be valid in the presence of a high-impedance contrast, since S_s^V vanishes around f_0. On the contrary point 4) cannot be accepted since the second term of the product $A_s(f_0)$ is very large. The whole quantity $\beta A_s(f_0)$ is equal to $S_s^H(f_0)/R_b^V(f_0)$ that is the ratio of the horizontal amplitude of surface waves compared to the vertical amplitude of body waves at the rock; there is no obvious reason that this ratio is small compared to the S-wave amplification.

2.3.2 Interpretation based on Rayleigh waves

The basic assumption of this interpretation is that the noise wavefield mainly consists of surface waves. In particular one assumes that the H/V ratio is related to the Rayleigh wave ellipticity, due to the predominance of Rayleigh waves in the vertical component. In this hypothesis, introducing the Rayleigh wave eigenfunctions evaluated at the free surface $U_i(0)$ (i=1,2,3 where 1 is the direction of motion and 3 is the vertical direction), it follows:

$$\frac{H}{V} = \frac{U_1(0)}{U_3(0)}$$

The ellipticity depends on the frequency and shows a sharp peak around the fundamental frequency for site characterized by a high impedance contrasts. This peak is related with the vanishing of the vertical component, due to the inversion of the elliptical motion of Rayleigh wave fundamental mode from counter clockwise to clockwise.

Recently, the H/V method has been extended to other kinds of signals such as earthquakes and artificial explosions (see for example the analyses reported in Malagnini et al.1996; Satoh et al., 2001; Seekins et al. 1996). Also in these applications, the results are controversial and at present it is still not clear if the method yields unambiguous results when it is applied to different types of signals.

2.4 Ground motion simulation for the estimate of the peak ground acceleration (PGA)

The determination of ground motion parameters like peak ground acceleration (PGA) can be carried on by numerically simulating the time history related to the maximum expected earthquake in a given area. Among the techniques used for such estimate, the stochastic method (Boore, 2003) is widely applied to predict the ground motion due to a seismic input, which can be modelled taking into account source, path and site effects. The method is particularly useful to simulate the ground motion for the frequency range usually investigated by earthquake engineering. The basis of the stochastic method is the knowledge of the spectrum of the ground motion A, that can be considered as the contribution of source S, path P ad site G:

$$A(M_0, R, f) = S(M_0, f)P(R, f)G(f) \tag{2.19}$$

where M_0 is the seismic moment, R is the distance from the source and f is the frequency. Once the spectrum of ground motion has been defined in terms of the source, site and path contributions, the PGA estimate can be obtained by using the random vibration theory (RVT) and Parseval's theorem. The RVT provides the estimate of the ratio of the peak motion (a_{max}) to rms motion (a_{rms}), while Parseval's theorem is applied to calculate a_{rms}, therefore the combined use of the two results allows for the PGA estimate. The ratio of peak to rms motion can be calculated by using the Cartwrigth and Longuet-Higgins equation (1956):

$$\frac{a_{\max}}{a_{rms}} = 2\int_0^{\infty}\left[1-\left(1-\xi\exp(-z^2)\right)^{Ne}\right]dz \tag{2.20}$$

with $\xi = Nz/Ne$

Nz and Ne are the number of zero crossings and extrema of the time series. If N is large:

$$\frac{a_{\max}}{a_{rms}} = \sqrt{[2\ln(Nz]} + \frac{0.5772}{\sqrt{[2\ln(Nz)]}}$$

In the above equations the number of zero crossing Nz and extrema Ne are related to the frequencies of zero crossings f_z and extrema f_e, respectively, and to the duration T according to:

$$Nz = 2T\tilde{f}_z \qquad \tilde{f}_z = \frac{\sqrt{(m_2/m_0)}}{2\pi}$$

$$Ne = 2T\tilde{f}_e \qquad \tilde{f}_e = \frac{\sqrt{(m_4/m_2)}}{2\pi}$$

The quantities m_k are the moments of the squared spectral amplitude, defined as:

$$m_k = 2\int_0^{\infty}(2\pi f)^k \left|A(f)\right|^2 df$$

where $A(f)$ is the spectrum of the motion, defined in (2.19).

From Parseval's theorem, a_{rms} can be estimated:

$$a_{rms} = \sqrt{f \cdot 2\int_0^{\infty}\left|A(f)\right|^2 df} = \sqrt{m_0/T} \tag{2.21}$$

Combining equation (2.20) and (2.21), the value of the PGA can be calculated:

$$a_{\max} = \left[2\int_0^{\infty} \left[1 - \left(1 - \xi \exp(-z^2) \right)^{Ne} \right] dz \right] \cdot \left[\sqrt{m_0 / T} \right]$$

Besides this methodology, in the present thesis I also apply another method (GMG) which can be considered a slight modification to the RVT. The details of the modified technique will be given in the section 3.8 dedicated to the PGA estimate for the Campi Flegrei area, together with the definition of the spectrum of ground motion $A(M_0,R,f)$ in terms of source, site and path for the investigated site.

Chapter III

Data analysis and results

3.1 Data set

The data set used for the dispersion analysis of Rayleigh waves in the Pozzuoli-Solfatara area consisted of both air-gun explosions and seismic noise.

The explosions were shot in the Gulf of Pozzuoli in the framework of the "Serapis" active seismic experiment performed in September 2001 (Zollo et al., 2003). The seismic signals generated by the shots were recorded by the stations SLF and SFT of the Osservatorio Vesuviano seismic network, located in the Solfatara crater at an inter-station distance of about 160 m (fig 3.1). An example of recording is shown in fig. 3.2. The SLF Mars Lite digital seismic station was equipped with a three-component 1-Hz LE3DLITE geophone. The SFT analogic station was equipped with a L4-3D Mark Products seismometer with natural frequency of 1 Hz. The sampling rate was 125 and 100 sps for SLF and SFT stations, respectively.

The seismic noise was recorded by an array deployed in the Solfatara crater with a maximum aperture of about 250 m and composed by 24 vertical-component and 4 three-component Mark Products L4C seismometers, with a natural frequency of 1 Hz. The seismic signals were sampled at 200 sps (fig 3.8).

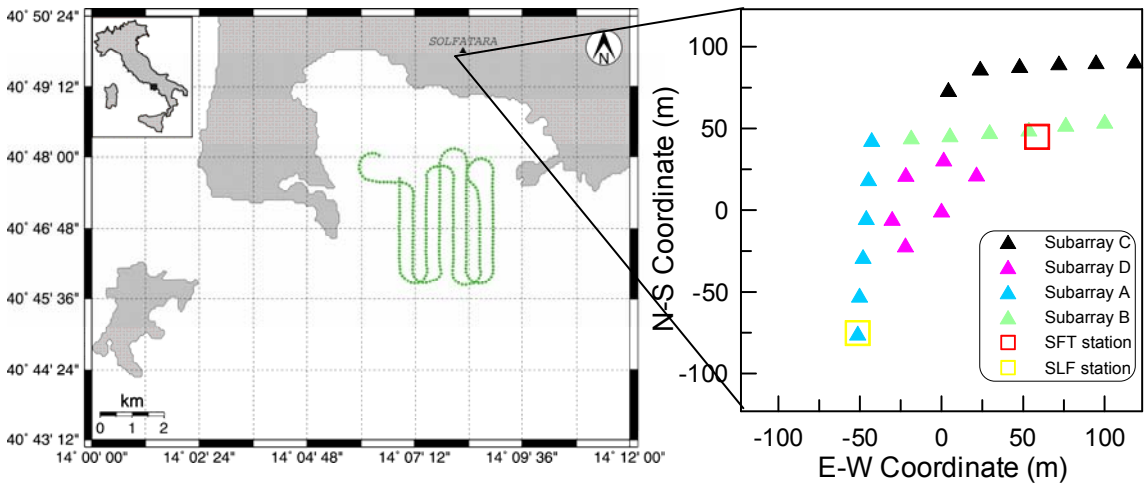

Fig. 3.1 – On the left, map of the Campi Flegrei area. Dots represents the location of the air-gun shots fired on 2001/09/21. On the right, deployment of the array and seismic stations

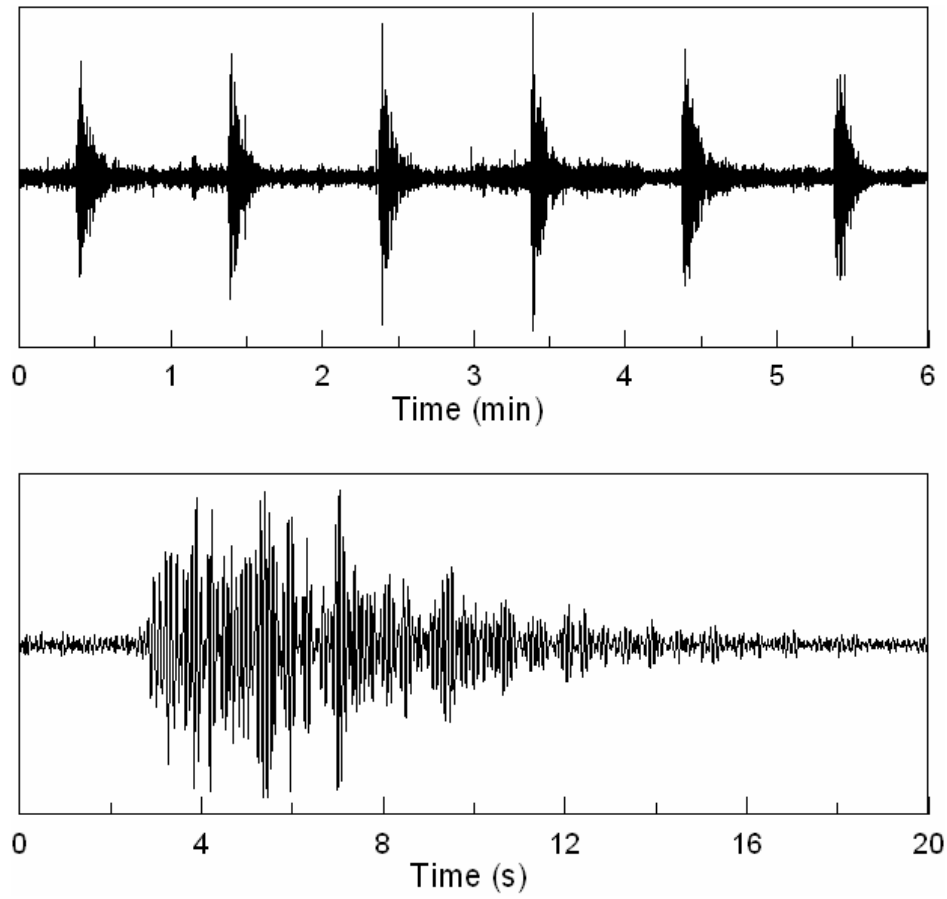

Fig. 3.2 – Seismograms of the shots recorded at SFT station.

3.2 Surface wave dispersion analysis

In the following sections I present the results obtained from the application of different techniques (MFT, AR analysis, SAC and ESAC) for the estimate of surface wave dispersion curve.

3.2.1 Multiple Filter analysis

From the whole data-set consisting of about 5000 shots, I selected 36 recordings associated with source-receiver distances ranging from 2.5 to 4.0 km and high signal-to-noise ratios. I obtained preliminary group velocity dispersion curves applying the MFT to the vertical-component seismograms recorded by station SLF. I windowed the signals by taking 2048 samples starting from the P-wave onset, then each seismogram was bandpass filtered for a set of center frequencies spanning the 1–12 Hz frequency range with a step of 0.2 Hz; the bandwidth of the gaussian filter was set equal to a half of the center frequency. The occurrence time of the envelope maximum of the filtered signal was used to calculate the group velocity at each frequency. For each shot, the

MFT produces a plot (hereinafter referred to as MF plot; see examples in fig. 3.3 and 3.4) of the contoured normalized envelope amplitude as a function of frequency and group velocity, where the four largest envelope maxima are marked by a symbol. The group velocity dispersion curves can be extracted by picking the adjacent symbols that depict a continuous pattern.

A great problem in surface wave analysis of multi-modal signals is the contamination of the higher modes that could mask the real dispersive patterns and bias the picking of the dispersion curves. To avoid this, the signals need to be filtered by using a phase-matched filter. This filter, that allows the separation of different modes, requires the estimate of a trial approximate dispersion curve that will be refined at the end of the filtering iterative procedure.

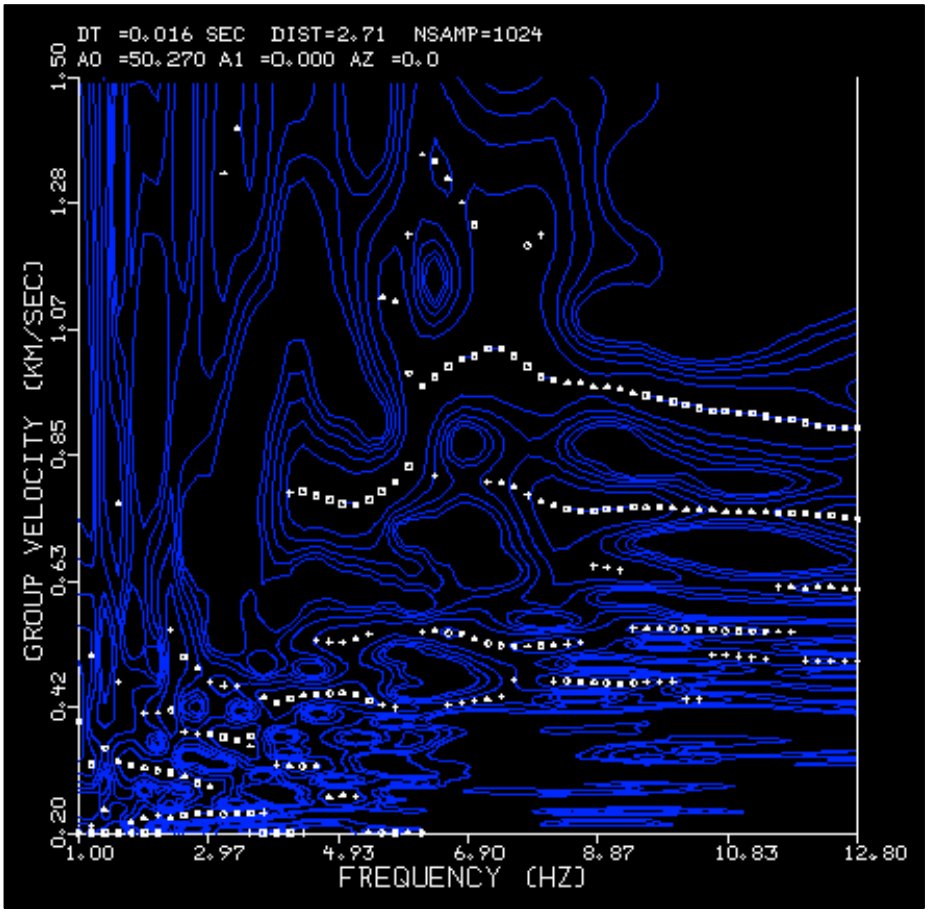

Fig 3.3 – Result of MF analysis applied to a shot recorded at SLF station. Blue lines contour equal values of the envelope amplitude. Symbols represent the four largest maxima of the envelope at each frequency: from the largest maxima to the smallest ones, the symbols used are squares, circles, triangles, and crosses.

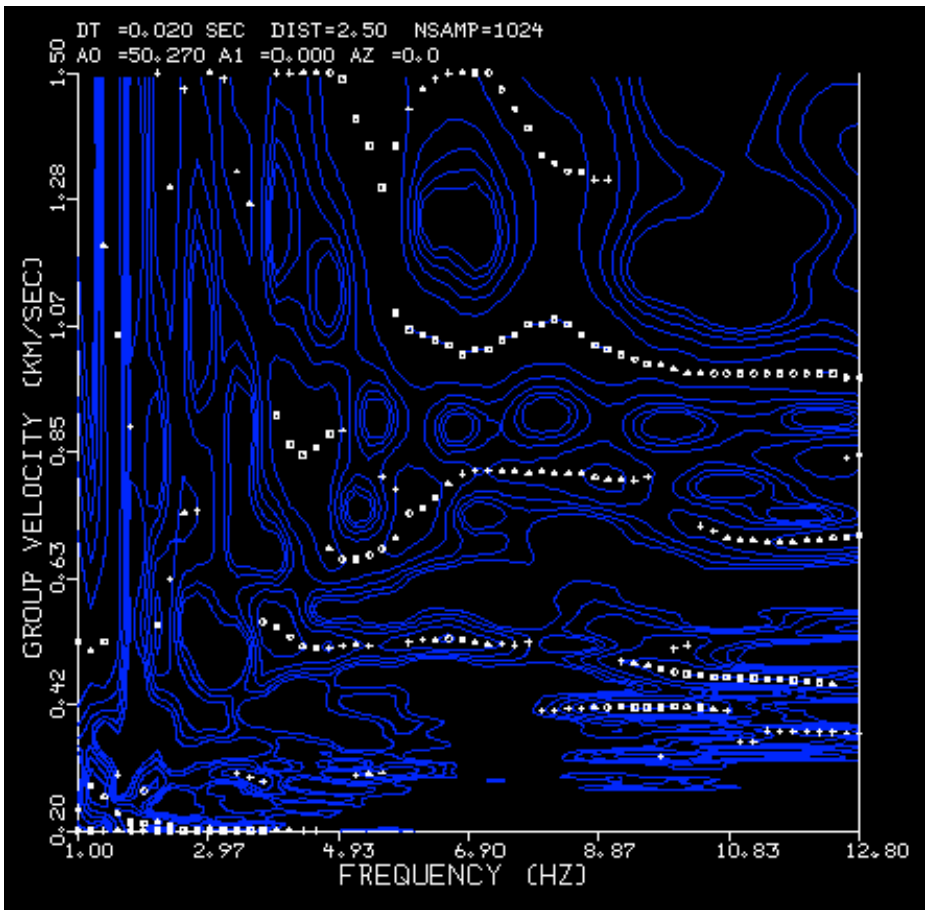

Fig 3.4 - Result of MF analysis applied to a shot recorded at SFT station. Blue lines contour equal values of the envelope amplitude. Symbols represent the four largest maxima of the envelope at each frequency: from the largest maxima to the smallest ones, the symbols used are squares, circles, triangles, and crosses.

To apply the PMF to the data set, I selected the trial dispersions by carefully visually inspecting the MF plots associated to the recordings of SLF station and searching for clear and well separated dispersion curves. The dispersion curve of the first higher mode was always very clear for every analysed shot, with group velocities ranging from ~820 m/s to ~740 m/s in the 6-12 Hz frequency band. For a great number of MF plots I could also identify the second higher mode, while the fundamental mode sometimes appeared contaminated by the higher modes and did not show a clear dispersive pattern (see for example fig. 3.3 where the fundamental mode seems to have a double branch). For this reason I decided to not pick the fundamental mode curve at SLF station. Conversely, I was able to successfully pick a clear fundamental mode dispersion from the MF plots associated with recordings from station SFT.

The fundamental mode and two higher-mode dispersions previously derived, were used as trial curves for the PMF, which I first applied to the signals from station SLF. This procedure is summarized in the following steps:

1) The 36 waveforms were filtered by using the trial curve of the first higher mode to allow the separation of the first mode wave packet from the residual seismograms.
2) The residual seismograms were filtered by using the trial curve of the second higher mode, to separate the second mode wave packet from the new residual seismograms.
3) The new residual waveforms were filtered by using the trial curve of the fundamental mode, to extract the fundamental mode wave packet.

To validate the results obtained for the fundamental mode at station SLF, a further phase-matched filtering was performed by using the trial fundamental dispersion on the seismograms recorded by the station SFT, in order to extract the fundamental mode wave packet.

The MFT was applied once again to all the filtered signals (both for stations SLF and SFT). As the filtered signal contains single mode wave packet, the MFT produces a plot in which the dispersion curve relative to that mode is greatly enhanced respect to

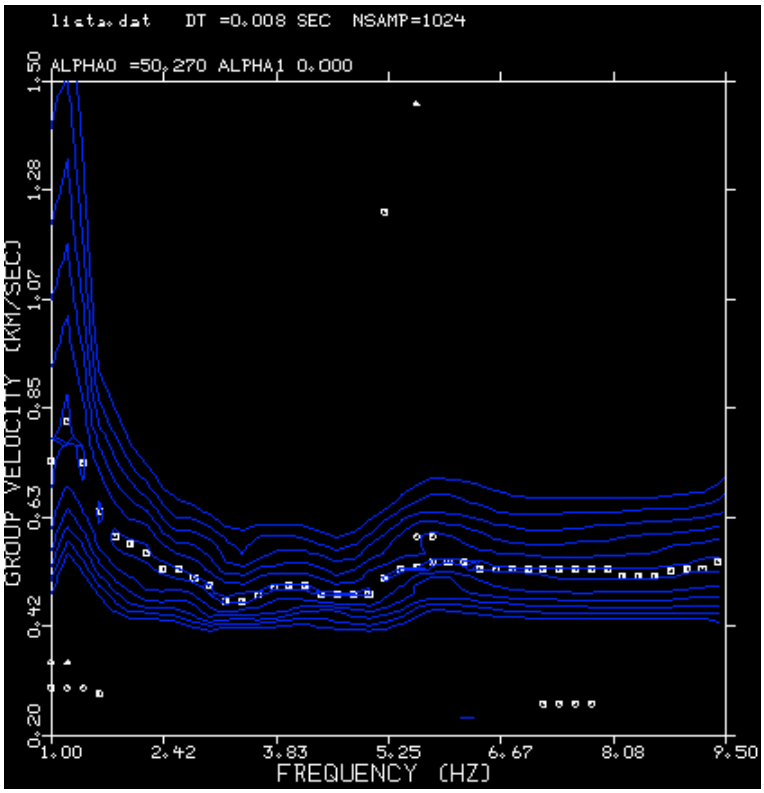

Fig. 3.5 – Stacked dispersion curve of the fundamental mode obtained after the application of PMF and MFT to data recorded at station SLF.

the non-filtered signal. Finally, a more robust and reliable estimate of the final dispersion relations is achieved by performing the stacking of a certain number of selected curves. As one can appreciate from the example in fig. 3.5, the combined use of MFT-PMF and the stacking procedure yield a very clear dispersive pattern which is no more affected by higher mode contamination.

The final stacked dispersion relations for the fundamental, first and second mode are shown in fig. 3.6. They were obtained by the following stacks:

- 26 curves of the fundamental mode at station SLF
- 11 curves of the fundamental mode at station SFT
- 36 curves of the first higher mode at station SLF
- 28 curves of the second higher mode at station SLF

The comparison between the group velocity dispersion curves of the fundamental mode for stations SLF and SFT shows an excellent agreement of the two results.

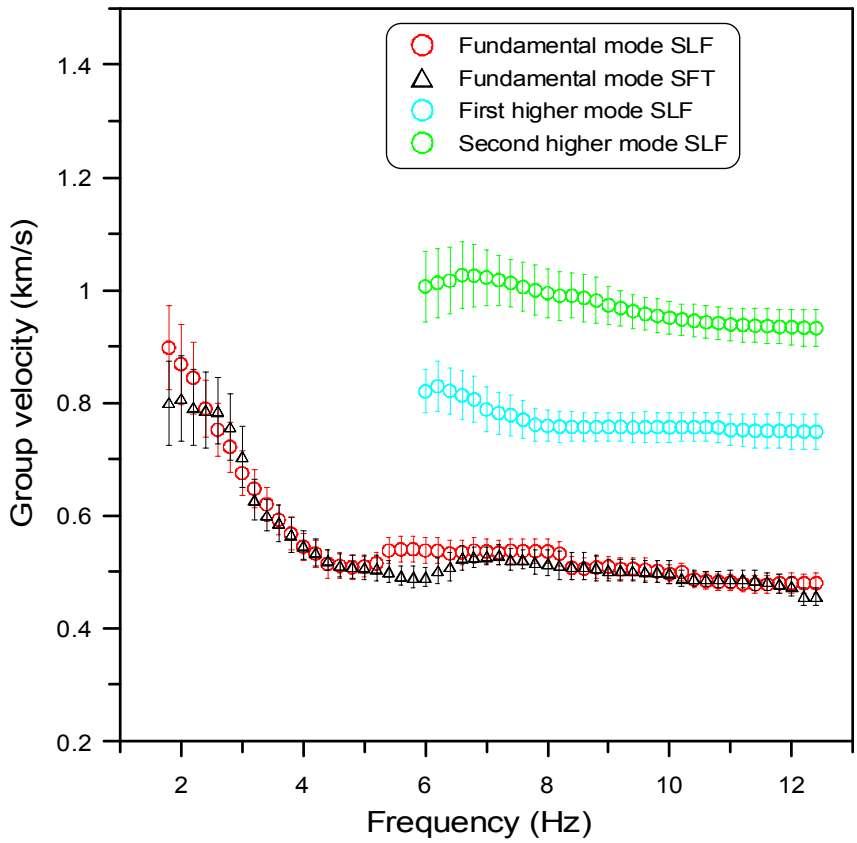

Fig. 3.6 - Stacked dispersion curves with the 1σ-width error bars, obtained from the application of MFT and PMF to data recorded at station SLF. In the plot the fundamental (red circles), first (cyan circles) and second (green circles) mode dispersions are represented. Fundamental mode dispersion curve (black triangles) for data recorded at station SFT is also shown.

Finally, I also performed an MF analysis on the shots recorded at POZ station, which is located near the coast line of Pozzuoli. No significant dispersive features were observed in the MF plots obtained for this data set. This means that the wave propagation in the sea-water does not affect the dispersive pattern observed at the inner stations SFT and SLF, which is only due to the propagation of Rayleigh waves in a layered medium encompassed between the coast of Pozzuoli and the Solfatara crater. This fact ensures that the obtained group velocity dispersions of fig. 3.6 are to be considered representative of the average properties of the medium along this path.

3.2.2 The test of the new method based on autoregressive analysis

I applied the method described in section 2.1.4, to 4 seismic signals associated to the shots fired during the Serapis experiment and recorded at the stations SLF, SFT and 8A (that is the station of the sub-array A closest to SLF). As the application of the AR technique for the determination of group arrivals of dispersive wave packets of real seismic signals is completely new, I will describe in details the whole procedure. First, by integration, I transformed 14 seconds (starting from the P-wave onset) of the vertical component velocity-seismogram in the equivalent displacement time history, then I obtained the pulse time series by using the Hilbert transform $h(t)$ of the displacement $u(t)$:

$$x(t) = \sqrt{(u(t))^2 + (h(t))^2}$$

I calculated the FFT of the pulse sequence $x(t)$ to obtain the complex frequency series $x(f)$. The Nyquist travel time is determined from length T of the time series according to:

$$\tau_N = \frac{1}{2\Delta f} \qquad \Delta f = \frac{1}{T}$$

therefore group arrivals comprised in the Nyquist time band 0-14 s can be resolved.

Once obtained the complex frequency series $x(f)$, I windowed it by using a boxcar in order to select the frequency band in which perform the autoregressive analysis. I performed the segmentation of the complex series using frequency windows of 1 Hz width, with an overlapping of 25%. The center frequencies were selected in the 2-12 Hz frequency range. The segmentation of the complex series in the frequency domain can be seen as equivalent to the band-pass filtering performed in applying the Multiple Filter Technique. However, the advantage in handling complex frequency series is that

the filtering procedure in this case reduces to a simple segmentation of the signal. At this point, each segment of the complex frequency series can be analysed by using the autoregressive technique. On the basis of the Akaike criterion, I chose the filter order m from 2 to 14 and solved the eigenvalue problem (section 2.1.4) for each value of m. The roots z of the characteristic equation, that corresponds to the group arrival τ and v factor (or equivalently $w = -2v$) are therefore obtained for each filter order and represented in a cumulative τ-w plot. In this plot, the group arrival times relative to the different wave packets are represented by clustered points, while the noise corresponds to the scattered points. As the distance between the source of the shot and the receiver is known, the clustered points corresponding to the group travel times are transformed in group velocity. Finally, plotting the group velocity clusters calculated for each segment of the complex series as a function of frequency, I obtained the final group velocity dispersion curve. I implemented the whole procedure in a Mathcad worksheet, similar to that I set up for the analysis of the synthetic signal. In fact, for the dispersion analysis I slightly modified the worksheet reported in appendix B by simply adding a routine that performs the complex series segmentation and allows to reiterate the analysis in different frequency bands.

In fig. 3.7 I report the fundamental mode dispersion curves obtained from the autoregressive analysis applied to 4 selected shots. The curves are in agreement with that derived from MF and PMF analysis (also reported in the same figure). It is important to remark that although the curves obtained from the AR technique seem to have a quite large scatter around the group velocity values, they are relative to the analysis of single events. On the other hand, the curve obtained from the combined use of MFT and PMF is the result of a stacking procedure over a certain number of events and therefore it is affected by lower uncertainties. Surely, in the future, it will be very useful to introduce a stacking procedure in the AR analysis too, in order to reduce the spreading in the group velocity values.

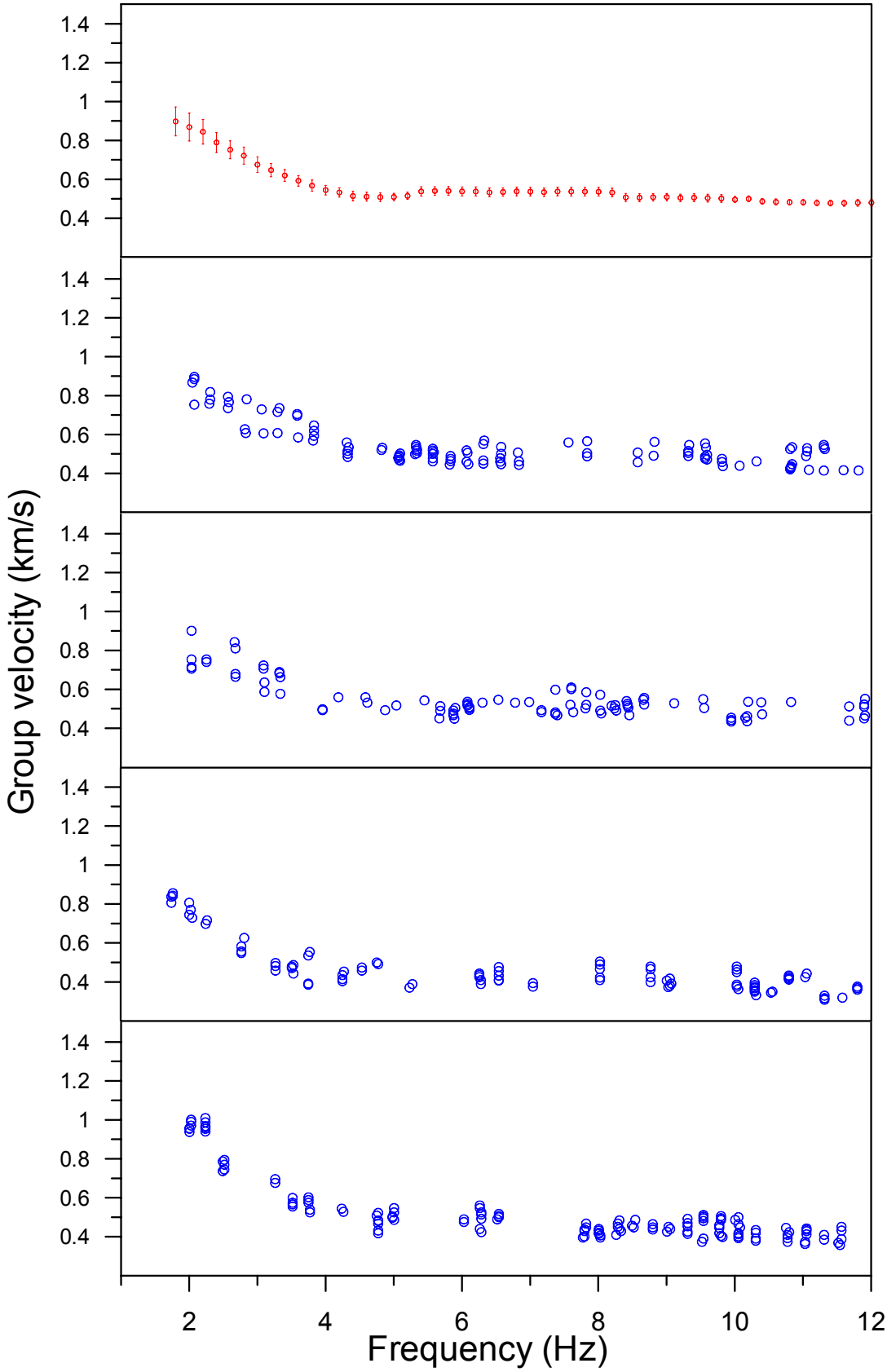

Fig. 3.7 - In the upper panel, stacked dispersion curve (red circles) obtained from MF and PMF analysis. The other 4 panels represent the fundamental mode dispersion curves (blue circles) for 4 shots, obtained from the AR technique.

3.2.3 Spatial Autocorrelation and Extended Spatial Autocorrelation analysis

In this section I describe the application of ESAC and SAC techniques to ambient noise recorded at Solfatara array.

In order to apply ESAC method, I selected twenty 90-s-long windows of noise samples, excluding recordings from the sub-array C array because of the low quality of these data.

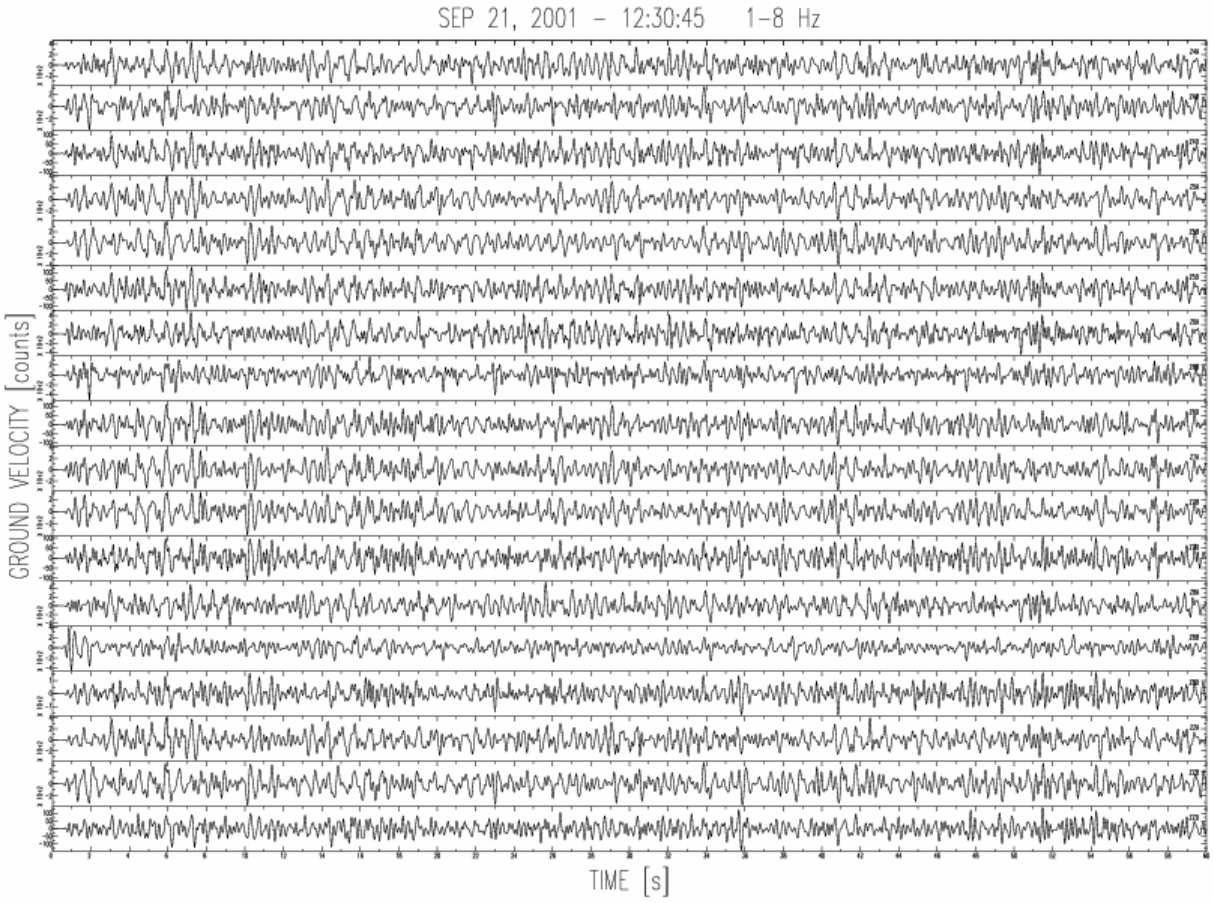

Fig. 3.8 - Recording of seismic noise at the array.

For the data analysis, I adopted the procedure described through the following steps:

1) for all the N(N-1)/2 independent station pairs I evaluated the zero-lag correlation coefficients by filtering the signals at frequency f_0 with a bandwidth of 0.5-Hz.
2) the correlation coefficients were averaged over those station pairs whose distances are included into consecutive distance bins, *dr*, of 5 m spanning the 15-200 m distance range.

3) the above steps were repeated for individual central frequencies f_0 spanning the 1–8 Hz frequency range. This upper frequency bound was adopted due to the poor correlation of seismic noise recordings at frequencies higher than 8-10 Hz. The overlapping of two consecutive frequency bands was set equal to 50%. Step 3) allows to retrieve the correlation coefficients as a function of frequency and distance: C=C(f,r)
4) steps 1-3 were iterated through the i=1…20 noise windows selected for the analysis, and the different $C_i(f,r)$ thus obtained were eventually averaged over these different time measurement windows.

After this procedure, I obtained at any given frequency f_0, the correlation coefficients as a function of the distance r. By performing a fit with a 0-th order Bessel function the value of the phase velocity, *c*, at that particular frequency was obtained. The phase velocity dispersion was then inferred by fitting the correlation coefficients calculated for the different frequencies in the 1-8 Hz band. Fig. 3.9 shows the correlation coefficients as a function of distance and the Bessel fit at 8 sample frequencies. The retrieved phase velocity dispersion is shown in fig. 3.13.

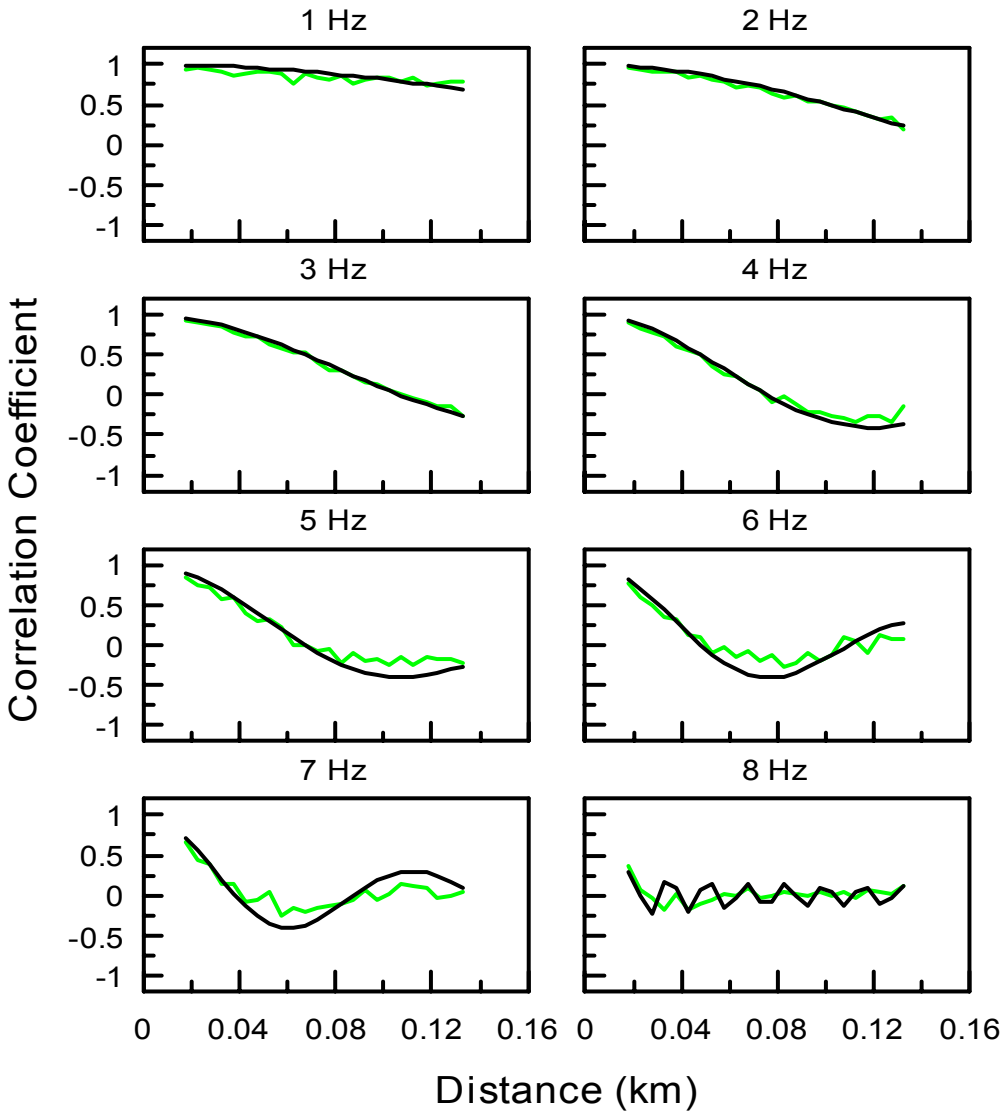

Fig. 3.9 - Correlation coefficients (green line) from ESAC technique, as a function of the distance, for 8 sample frequencies. The Bessel function fitting the data is represented by the black line.

In addition, I applied traditional SAC technique to the same data set recorded at the semicircular array D (fig. 3.1). I evaluated the zero-lag correlation coefficients between the station located at the hub of the array and the stations located along the semicircle of radius 30 m, using 0.5-Hz-wide frequency bands overlapping by 50% of their width, and spanning the 1-8 Hz frequency range. For each window of analysis, azimuthally-averaged correlation curves are obtained from the average of the frequency-dependent correlation coefficients calculated for the different station pairs. From SAC analysis, I obtained a single correlation curve (fig. 3.10) which is function of frequency, for the fixed distance of 30 m (the radius of the D semicircular array). As explained in

section 2.1.3, in this case the Bessel fit over the azimuthal-averaged correlation coefficients can be performed assuming a priori a dispersion law of the form:

$$c(f) = Af^{-b}$$

The best-fit coefficients A and b took the values 0.8 and 0.12, respectively.

The resulting phase velocity dispersion curve is shown in fig. 3.13. For both SAC and ESAC method the relative uncertainties on the phase velocity estimates are of the order of 20%.

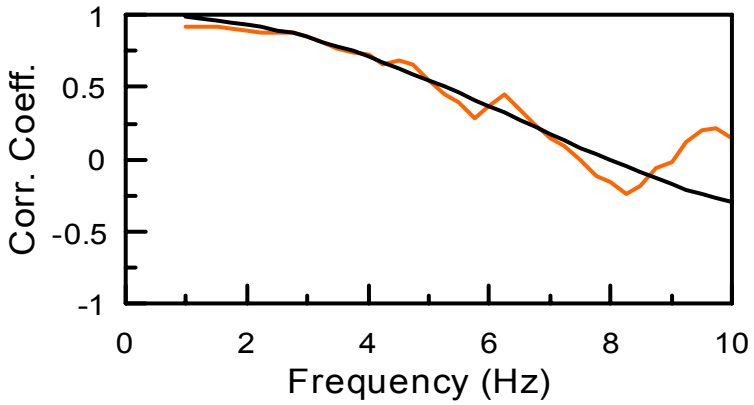

Fig. 3.10 - Correlation curve (orange line) obtained from application of SAC method to microtremors data from semicircular array D. The black line is the Bessel function fitting the correlation data.

3.3 Inversion of the group velocity dispersion

The group velocity dispersion curves obtained from the Multiple Filter analysis were inverted for a plane-layered earth structure to infer the shallow shear-wave velocity model for the area of Pozzuoli-Solfatara. Basing on the available geological and geophysical observations, I build up a set of possible starting models with a variable number of layers (from the simple single-layer-models to 5-layer-models) and different shear-wave velocities (chosen in the range 200-1500 m/s, which is compatible with the S-velocities typically observed for shallow soils and rocks in volcanic areas). Constraints for the minimum and maximum resolvable layer thickness and depth were imposed on the basis of the empirical relationships (Midzi, 2001). For the frequency range I investigated, the minimum resolvable layer thickness is on the order of 20 m, and the maximum resolvable depth is on the order of 250 m. I performed a first selection of the velocity structures by using a trial and error procedure to look for models which produced theoretical dispersion curves compatible with those experimentally observed. On this basis, some of the initial starting models with large

misfit between observed and predicted data where rejected, while others were modified, adjusting layer thicknesses and velocities to better reproduce the dispersive pattern. The new subset of starting models was then inverted both for velocities and layer thicknesses by using an iterative procedure (Herrmann, 1987). After the iterative inversion of the whole new subset I selected the 3-layer-model because it yields the lowest rms value between observed and theoretical data and it fitted the greatest number of observations.

The three dispersion curves for the fundamental, first and second higher mode were inverted both separately and simultaneously to better constrain the results. The resolution kernels relative to the different inversions are reported in appendix C. All the inversions yield similar velocity models and stable results, whose robustness is evidenced by the excellent fits between experimental and theoretical dispersions (fig. 3.11).

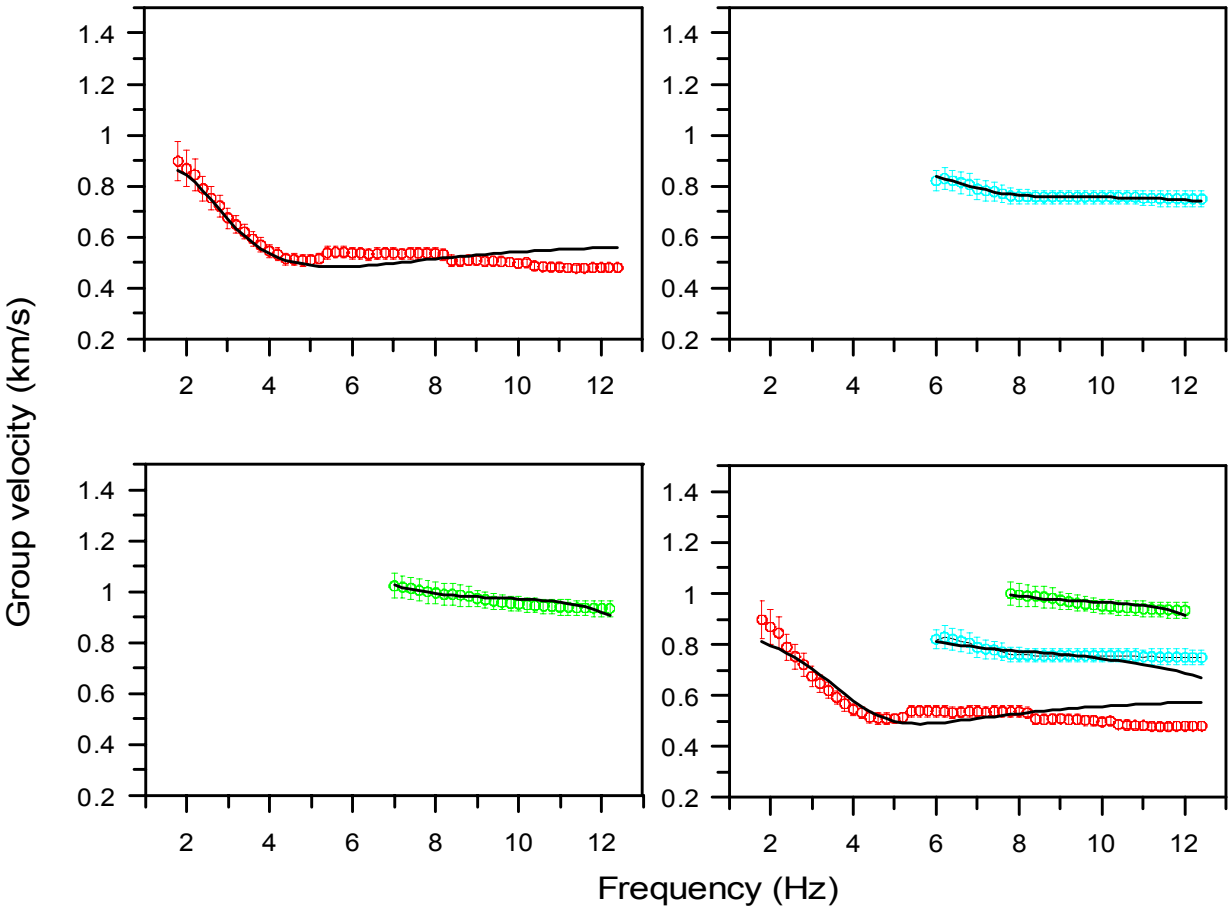

Fig. 3.11 - Results of the single-mode and simultaneous inversion of the fundamental, first and second higher mode dispersion curves. The solid lines superimposed to the experimental data represent the theoretical dispersions obtained from the inferred shear-wave velocity model.

The inferred velocity models (fig. 3.12) show a marked discontinuity at a depth of about 50 m where the shear-wave velocity abruptly changes from about 650 m/s to 900 m/s. Another slight increase of the S-velocity (from 900 m/s to 1000 m/s) is observed at a depth of about 100 m.

To verify how well this two discontinuities are constrained and to check the stability of the obtained results I perturbed the starting 3-layer model by changing both velocities and layer thicknesses and repeating the inversion procedure. In all the cases the inversion converged to the final model previously described.

The simultaneous inversion provides the best constrained velocity structure because it yields the maximum resolution at the different depths, and therefore I used this model (hereinafter referred to as model A) for the error analysis. The uncertainties that affect this model were estimated by determining the range of shear-wave velocities obtained by the inversion procedure, when one considers the errors associated to the group velocity measurements. In fact, the stacked group velocity values calculated by the Multiple Filter analysis are affected by uncertainties which are quantified in terms of the standard deviation σ. By subtracting and adding 2σ to the group velocity values, I generated the two extreme dispersion curves corresponding to the 95% error limits. These curves were then inverted to infer two extreme velocity models which actually represent the upper and lower bound for the model A. As one can note from fig. 3.12, all the velocity models relative to both single-mode and simultaneous inversion are bounded by the 2σ error bars.

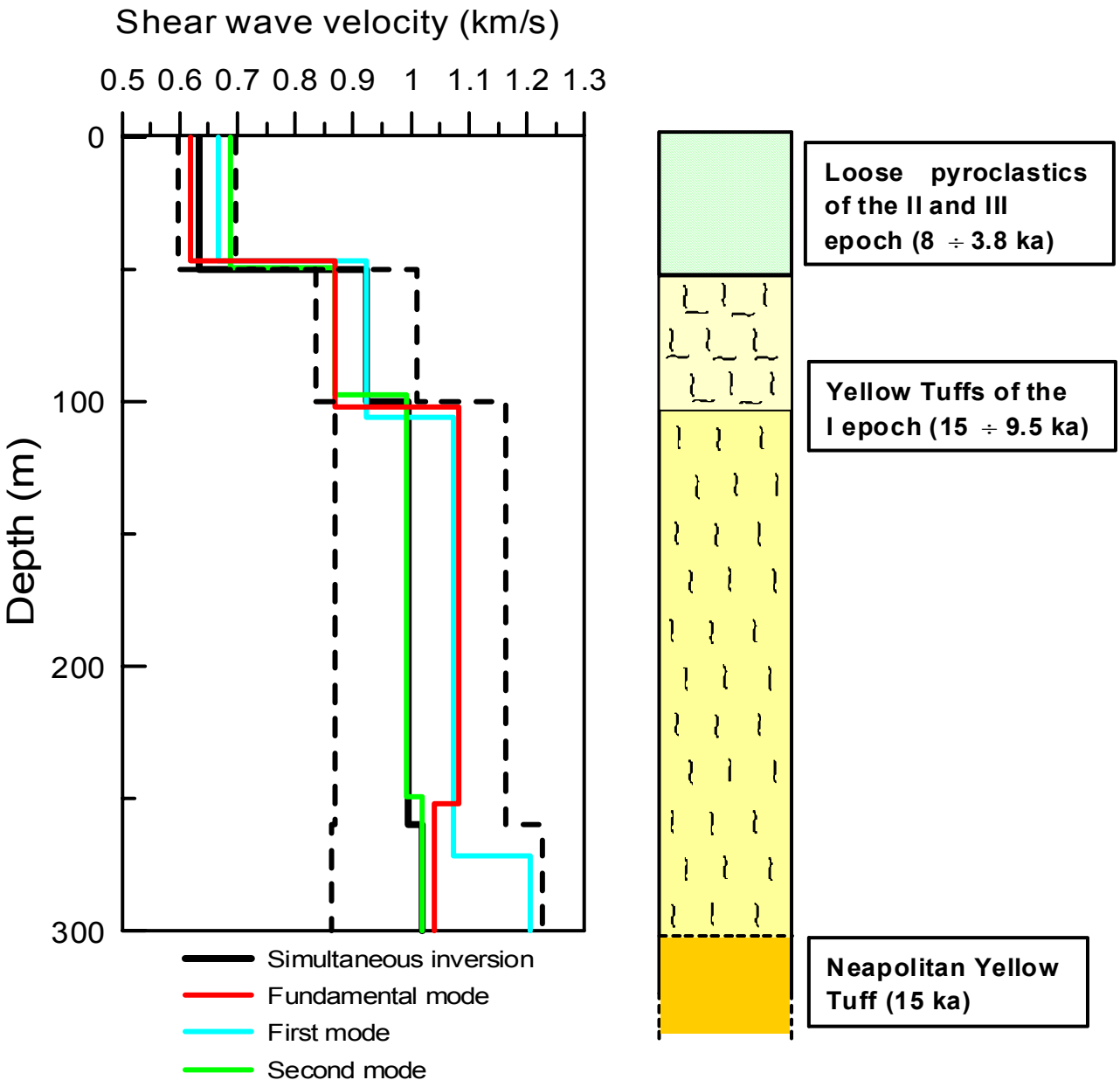

Fig. 3.12 - On the left, shear-wave velocity models obtained from single-mode and simultaneous inversions. The dotted lines bounds the 2σ-width uncertainty region associated to the velocity estimates. On the right, the possible geological interpretation of the velocity structure.

The dispersion curves obtained from MF and SAC (or ESAC) techniques are not directly comparable because they are relative to group and phase velocity measurements respectively. However, a way to compare the results given by these different techniques consists in calculating the predicted phase velocity dispersion curve by using the velocity model (model A) inferred from the inversion of the group velocity dispersion

that was obtained from the MF analysis. This theoretical phase velocity dispersion can be directly compared with the experimental ones obtained from SAC-ESAC measurements. As shown in fig. 3.13, there is a good agreement between the theoretical and the experimental dispersions, for the 2-7 frequency band, which represent the range investigated by both SAC and ESAC methods. This confirms the robustness of the results which have been obtained by using different techniques applied to two completely different data sets (explosions and noise).

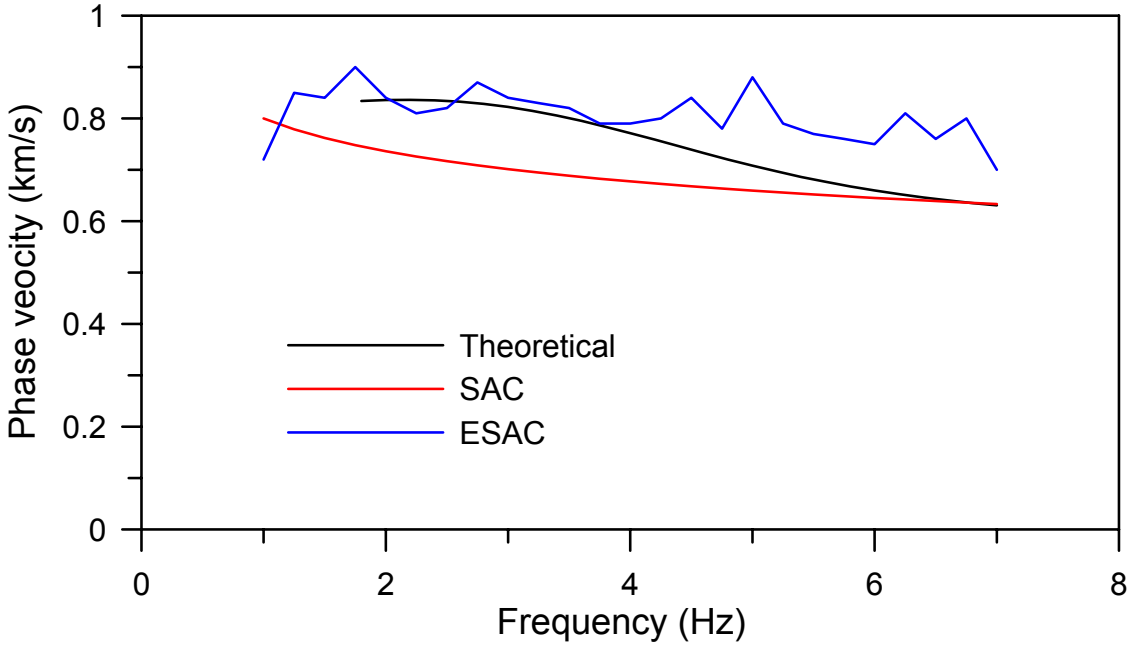

Fig.3.13 - Comparison between experimental phase velocity dispersion obtained from SAC and ESAC, and the theoretical one corresponding to the velocity structure of fig. 3.12.

3.4 Velocity model interpretation

To get more insight into the obtained results, I compared the values I retrieved for the shear-wave velocities with those derived in a previous study from cross- and down-hole measurements (Comune di Napoli, 1994). Although these data come from wells located in the western part of the city of Naples, they are associated with rocks formed after the Neapolitan Yellow Tuff caldera eruption, so they can be considered indicative of the S-wave velocities for the volcanic products which characterize the area of Pozzuoli-Solfatara. The authors observed, for loose and unconsolidated ash deposits, shear-wave velocities strongly depending on the depth and ranging from 180 m/s at

depths of about 5 m to 800 m/s at depth of 85 m, with a value of 550 m/s at a depth of about 50 m. For the compact tuff rocks (lithoid facies of NYT) typical Vs values are about 800-1000 m/s, with a weak dependence on depth.

From field and laboratory measurements Nunziata et al. (1999) evaluated the shear-wave velocities of the Phlegraean soils and tuffs obtaining results in agreement with those reported above. Nunziata et al. found that for pyroclastic products and coastal deposits Vs is influenced by the increasing lithostatic pressure and ranges from 100 to 600 m/s over the 0-20 m depth range, while the compact NYT is characterized by Vs values ranging from 800 to 1100 m/s and weakly depending on the lithostatic load. Slightly lower shear-wave velocities are observed for fractured NYT but those values, unlike for the compact NYT, rapidly increase with pressure due to the closing of the fractures.

Taking into account the volcanological history of the Campi Flegrei area (see section 1.1), the geological constraints and comparison with literature data, I finally give a possible interpretation (fig. 3.12) of the velocity model inferred from surface wave dispersion analysis.

The first 50-m-thick layer could be composed of loose pyroclastic rocks emitted during the III epoch of activity and marine deposits of the La Starza terrace. The Vs value found for this layer is in fact compatible with those reported in Comune di Napoli (1994) and Nunziata et al. (1999) for the same types of rocks. The seismic velocity discontinuity at 50 m can likely mark the transition to the yellow tuffs (which have analogous mechanical characteristics of NYT and hence similar shear-wave velocities) produced during the tuff-cone activity of the I epoch. The second discontinuity at 100-m-depth, which is less marked with respect to the shallower one, has two possible interpretations. It could be due to an effect of the lithostatic pressure which closes cracks and fractures in the tuff rock, with a consequent increase of seismic velocity. An other possible explanation is that this discontinuity marks the contact between the products emitted by two distinct tuff cones which erupted during the I epoch. These units probably overlay the NYT bedrock. The interface with NYT is not resolved by the presented velocity model, whose maximum resolvable depth is of about 250 m. However geological observations suggest a depth of about 300 m for the top of this unit (M. Di Vito, personal communication).

The velocity structure presented in this thesis is in agreement with that recently obtained at larger scale from a 3D seismic tomography by Vanorio et al. (2005), who observe low Vs values (1000-1200 m/s for the first 2 km) in the central part of the caldera. The present results are also compatible with the shallow velocity structure proposed for the Solfatara crater by Bruno et al. (2004). Although the model of Bruno et al. is limited to a depth of about 30 m, a rapid increase of Vs up to 540 m/s is reported for the lower bound of the structure.

3.5 Attenuation analysis and Q_β structure

For the attenuation analysis I selected 9 artificial explosions (vertical component) recorded by the 6 stations composing the linear sub-array A (fig. 3.1) and I applied the methodology reported in section 2.2 to study the spectral decay with distance of Rayleigh wave amplitude, in different frequency bands. I used a 9-s-long time window starting 1 second after the P-wave onset, in order to exclude the body-wave contribution. The data were band-pass filtered around a series of center frequencies spanning the 2.5-8.5 Hz frequency range, with a bandwidth of 1 Hz. I chose this upper limit because for frequencies greater than 8 Hz the noise contribution begins to be strong and hence could mask the attenuation pattern of the Rayleigh waves composing the wavefield associated to the shots. For each frequency band, the matrix equation (2.17) of section 2.2 was solved in order to determine the γ attenuation factor. The geometrical spreading coefficient in (2.17) was set equal to 0.5 because the analysis concerns Rayleigh waves. By solving the (2.17) in the different frequency bands, I recovered the γ attenuation curve shown in fig. 3.14.

To quantify the uncertainties that affect the estimate of the attenuation factor, I calculated the covariance matrix. In terms of the quantities defined in equation (2.17), the expression of the covariance matrix is (Menke, 1984):

$$[\mathrm{cov}(\mathbf{m})] = \left[\left[\mathbf{G}^{\mathrm{T}}\mathbf{G}\right]^{-1}\mathbf{G}^{\mathrm{T}}\right]\sigma_d^2\mathbf{I}\left[\left[\mathbf{G}^{\mathrm{T}}\mathbf{G}\right]^{-1}\mathbf{G}^{\mathrm{T}}\right]^{\mathrm{T}} = \sigma_d^2\left[\mathbf{G}^{\mathrm{T}}\mathbf{G}\right]^{-1}$$

I is the identity matrix and σ_d is the uncertainty affecting the data **d**. As the error on the distances R is negligible respect the uncertainty σ_A that affects the spectral amplitudes A, the quantity σ_d can be expressed in terms of σ_A:

$$\sigma_d^2 = \left|\frac{\partial d}{\partial A}\right|^2 \sigma_A^2 = \frac{1}{A_i^2}\sigma_A^2$$

The error on the spectral amplitude can be calculated following Boatwright (1978):

$$\sigma_A(\omega) = \frac{1}{2} n(\omega)$$

where $n(\omega)$ is the noise spectrum at the angular frequency ω.

In appendix D I include the Mathcad worksheet I prepared for the determination of the γ attenuation curve and for the estimate of the associated uncertainties.

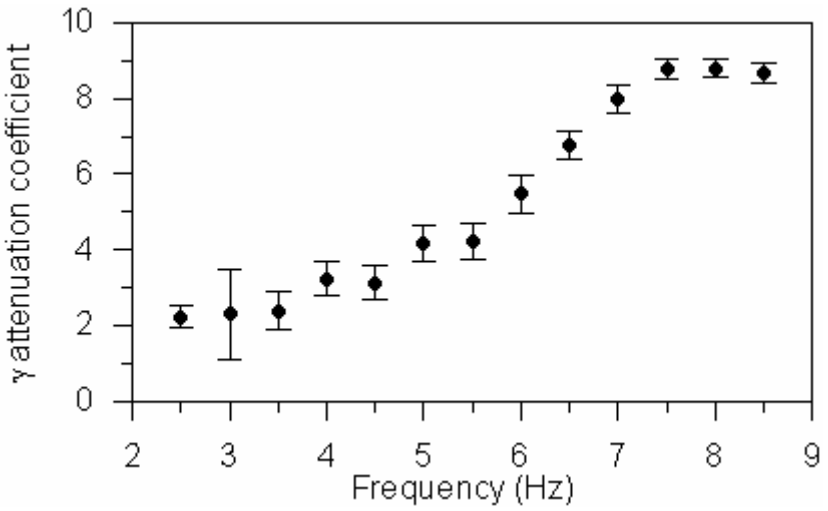

Fig. 3.14 – γ attenuation curve derived from the analysis of the spectral decay with distance.

I used the obtained γ attenuation curve to infer the inverse S-wave quality factor Q_β^{-1} as a function of the depth, that is the 1D attenuation model. To obtain a better constrained model, I performed a simultaneous inversion (Herrmann, 1987) of the γ attenuation curve and the phase velocity dispersion previously obtained from SAC technique. As the γ attenuation curve was retrieved in the 2.5-8.5 Hz frequency range, the corresponding maximum resolvable depth and minimum layers thickness are on the order of 150 m and 30 m, respectively. For the inversion I had to choose a starting model compatible both with the limits imposed by the depth resolution and, at the same time, with the model previously retrieved from the inversion of the group velocity dispersion (that has deeper and slightly finer resolution due to the larger frequency range in which dispersion was retrieved). For this reason, I used as starting model a 2-

layered structure whose thicknesses (50 m for both the layers) and S-wave velocities were constrained by the values of the velocity model derived in section 3.3, and I assigned to the different layers trial values of Q_β, compatible with those usually observed in shallow subsoils of volcanic areas. Several inversions were performed by perturbing the trial values of Q_β, but in any case the inversion procedure always yields stable results, converging to the same final solution despite the differences in the starting Q_β values. The obtained attenuation model presents low Q_β value, being $Q_\beta = 4$ in the first 50-m-thick layer and $Q_\beta = 12$ in the second 50-m-thick layer. The value of the quality factor in the halfspace is not resolved. In the next figures I show the result of the inversion (fig. 3.15), the attenuation model and the resolution kernels (fig. 3.16).

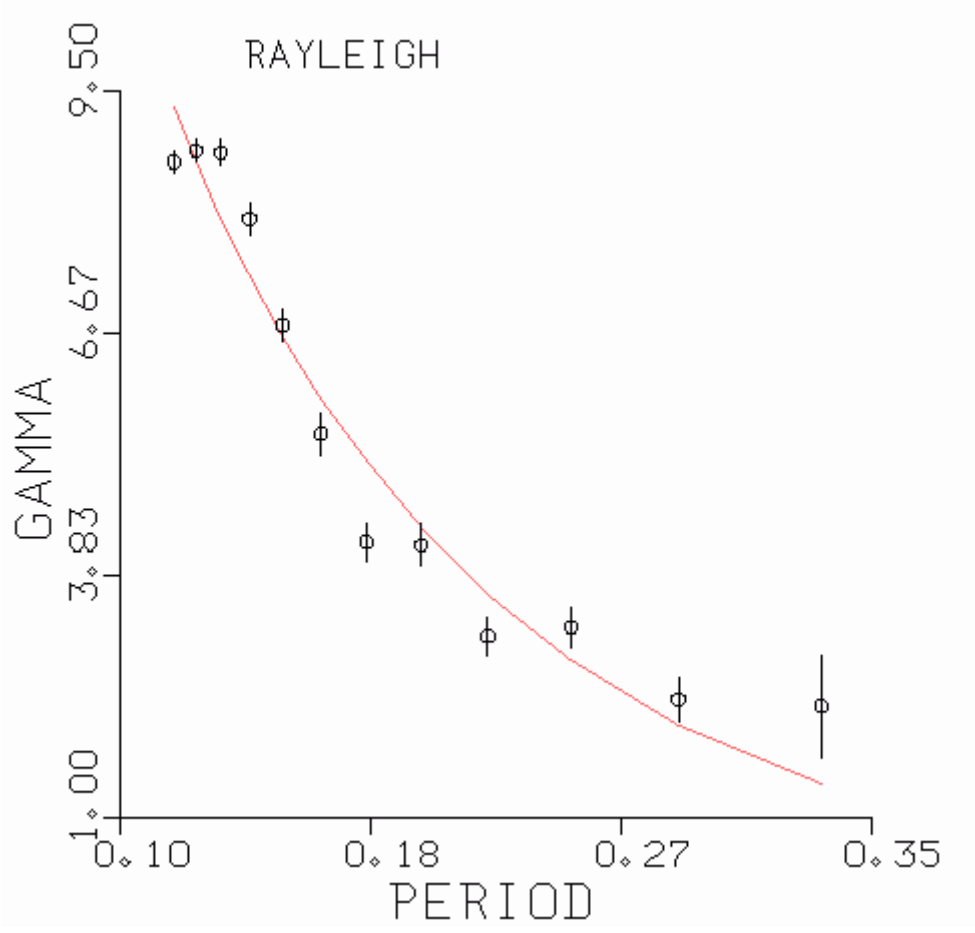

Fig. 3.15 - Result of the inversion of the γ attenuation curve. The solid lines superimposed to the experimental data represent the theoretical dispersions obtained from the inferred attenuation model.

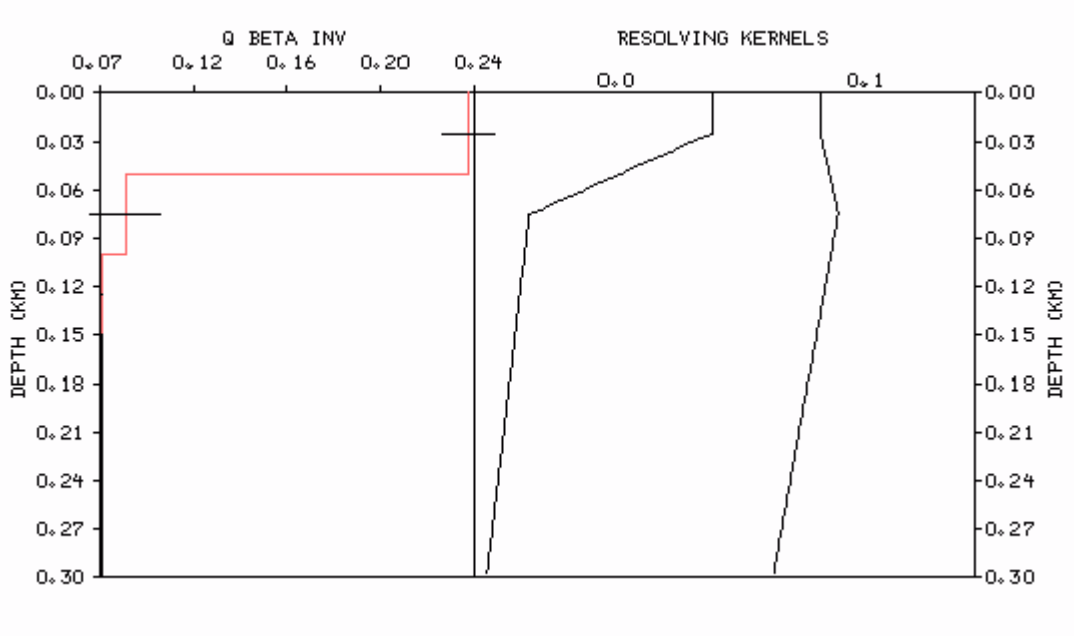

Fig. 3.16 - Attenuation model obtained from the γ curve inversion (on the left) and resolution kernels for the first two layers (on the right).

3.6 Estimate of the theoretical transfer function

In order to estimate the theoretical ground response in the area of Pozzuoli-Solfatara, I considered a vertically-propagating shear-wave in the velocity and attenuation structure derived in section 3.3 and 3.5. For a layered damped soil on an elastic bedrock the transfer function that relates the displacement amplitude at layer *i* to that of layer *j* can be calculated using the relation (Kramer, 1996):

$$F_{ij}(\omega) = \left| \frac{u_i}{u_j} \right| = \left| \frac{A_i(\omega) + B_i(\omega)}{A_j(\omega) + B_j(\omega)} \right|$$

with:

$$A_{m+1} = \frac{1}{2} A_m (1+\alpha_m^*) exp(ik_m^* h_m) + \frac{1}{2} B_m (1-\alpha_m^*) exp(-ik_m^* h_m)$$

$$B_{m+1} = \frac{1}{2} A_m (1-\alpha_m^*) exp(ik_m^* h_m) + \frac{1}{2} B_m (1+\alpha_m^*) exp(-ik_m^* h_m)$$

where h_m is the layer thickness, k_m^* is the complex wave number and α_m^* is the complex impedance of the *m*-th layer. This last two parameters are defined through the complex shear wave velocity, v^* :

$$k_m^* = \frac{2\pi f}{v_m^*} \qquad \alpha_m^* = \frac{\rho_m v_m^*}{\rho_{m+1} v_{m+1}^*} \qquad v_m^* = v_m \cdot (1 + i\xi_m)$$

with ρ_m and ξ_m density and damping of the *m*-th layer, respectively. The damping is related to the quality factor *Q* by the relation:

$$\xi = \frac{1}{2Q}$$

The parameters that I used to calculate the theoretical transfer function are listed in the following table:

Layer number	Shear wave velocity (m/s)	Thickness (m)	Density (g/cm^3)	Quality factor
1 Loose pyroclastics	634	50	1.8	4
2 Fractured Yellow Tuff	923	50	1.9	12
Halfspace Compact Yellow Tuff	993	_	2.0	15

In the table I also report for the halfspace the Q value inferred from the inversion of the attenuation curve, although this is not well constrained due to the lack of resolution at that depth. However, this value does not affect the resonance frequencies and the amplification levels of the theoretical transfer function, as I showed in the numerical simulation reported in appendix E.

The obtained transfer function (fig. 3.17) calculated by using the Mathcad worksheet reported in appendix E, shows two peaks at the resonance frequencies of 2.1 and 5.4 Hz. A further discussion will follow in the next section, after the comparison with the results obtained by applying the method of Nakamura.

3.7 Application of the H/V spectral ratio technique and experimental transfer function.

To obtain the experimental site transfer function, I applied Nakamura's technique to microtremor data collected by station SLF. For the estimate of the H/V spectral ratio, I selected 32 20-s-long time windows of seismic noise recorded between two consecutive air-gun shots. A Konno-Omachi smoothing window (Konno and Omachi, 1998) was applied to the Fourier spectra and, after the quadratic merging of the

horizontal components, the H/V spectral ratios were evaluated for each time window. Finally, these values were averaged to estimate the stacked H/V ratio for the site.

I also calculated the Nakamura spectral ratio using 21 artificial shots of the Serapis data set at station SLF. In this case I used a time window length of 10 s, while the other parameters set for the evaluation of the H/V spectral ratio were the same adopted for the noise analysis.

Finally I applied the method to 29 local earthquakes belonging to the seismic swarm that occurred in the area of the Solfatara on 2005 October 5th (section 1.2). In this case I used the seismic traces recorded at SFT station because the SLF station was removed at the end of the Serapis experiment. In handling earthquake data, I selected a 5-s-long time window starting from the S-wave arrival, in order to analyse the contribution of the shear wave packet. For the H/V ratio estimate, I adopted the procedure previously described for the seismic noise.

The theoretical transfer function (TTF) obtained in section 3.6 was compared with the results from Nakamura's technique. The TTF and the H/V ratios for noise, explosions and earthquakes are shown in fig. 3.17.

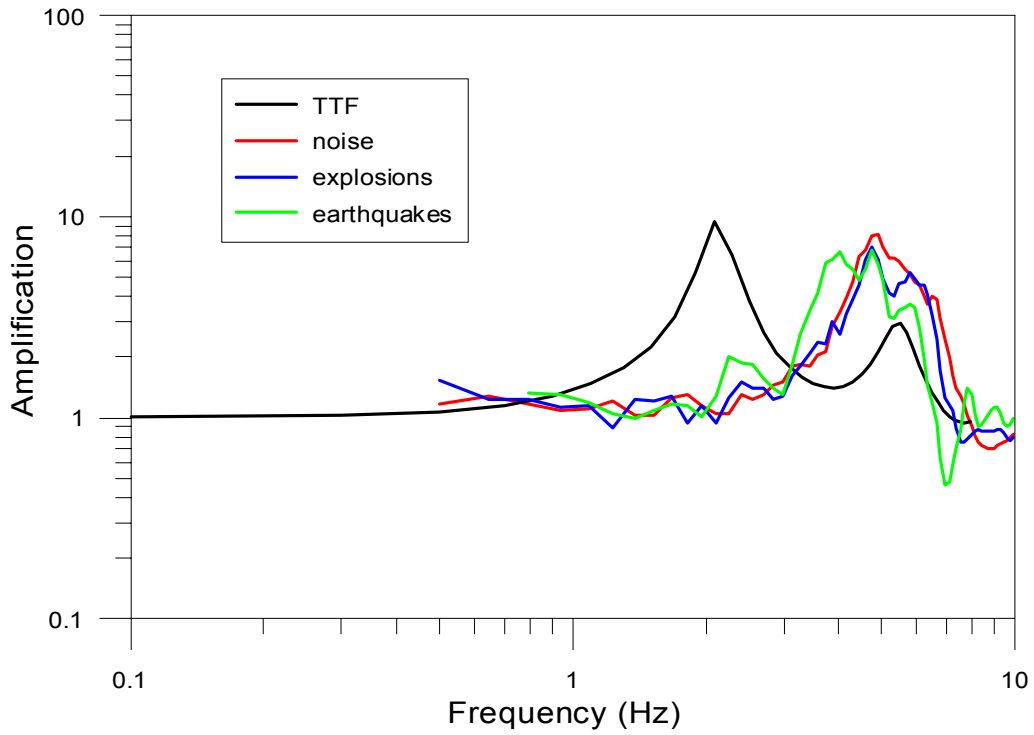

Fig. 3.17 - Theoretical transfer function calculated by using the inferred shear-wave velocity model and H/V spectral ratios obtained from the application of Nakamura's technique to microtremor, explosion and earthquake data.

The first result to note is the good agreement among the three experimental H/V ratios, that evidenced the resonance frequency at:

$f = 4.9 \pm 0.3$ for microtremor

$f = 4.9 \pm 0.4$ for explosions

$f = 4.5 \pm 0.6$ for earthquakes

This resonance frequency, as one can note in fig. 3.17, partially agrees with the second resonance frequency of the theoretical transfer function, although this last is slightly higher (5.4 Hz). On the contrary, there is a quite large discrepancy in the amplification level at this frequency, being the amplification provided by the TTF lower respect to that estimated by the H/V ratio. Above all, the most evident discrepancy is the complete disagreement between the curves for the fundamental resonance frequency of 2.1 Hz which is observed only in the theoretical transfer function. Three possible reasons could explain this discrepancy:

1) The H/V ratio is sensitive to the velocity structure just beneath the station, while the 1D velocity model obtained from the inversion of Rayleigh wave dispersion represents an average model for the medium between the source and the receiver. So I expect that the H/V ratio is compatible with the TTF only if the local structure beneath the station located in the Solfatara crater is exactly the same represented by the average velocity model. However it is possible that in the Solfatara crater a very local thickening or thinning of the shallow layers could produce a shift in the amplification frequencies. In this case the H/V ratio is to be considered indicative of the very local transfer function just for the Solfatara crater, while the transfer function derived from Rayleigh wave dispersion is valid for the area that goes from the shore of Pozzuoli to the external rim of the Solfatara crater.

2) A very local destructive interference occurring in the Solfatara crater, whose basin-like structure is expected to cause significant wave-trapping phenomena, could prevent to observe the 2.1 resonance frequency.

3) Finally, as confirmed by many studies (Luzon et al., 2001; Malischewsky and Scherbaum, 2004) Nakamura's technique gives a good estimate of the fundamental frequency only in the case of large impedance contrast (generally > 2.5), while it often fails once dealing with low impedance contrast. By using the velocity model of 3.6 I estimate for the investigated area an impedance contrast of about 0.6, which is probably

too low for considering reliable the results obtained from the application of Nakamura's technique. In this case, the H/V spectral ratio cannot be considered indicative of the site transfer function.

3.8 PGA estimate from ground motion simulation

I calculated the peak ground acceleration (PGA) due to the expected largest magnitude local earthquake, both for the whole caldera of the Campi Flegrei and locally for the area of Pozzuoli-Solfatara. The first method I used is based on the random vibration theory (RVT). The adopted procedure is summarized in the following steps:

1) the shape of acceleration spectrum $A(f)$ is defined as function of source parameters (f_c, $M_0(M_{max})$), path (Q), radiation pattern ($Y_{\theta\phi}$), geometrical spreading (R), free surface operator (F) and medium characteristics (V_s ρ_0); hereinafter all these parameters are defined as the ensemble $\{K_i\}$;
2) the moments m_k of the squared spectral amplitude of acceleration are evaluated in order to calculate the numbers $N_{z,e}$ of zero crossing and extrema of time series;
3) the ratio (PGA/a_{rms}) of PGA to the root mean square acceleration (a_{rms}) is calculated by using Cartwrigth and Longuet-Higgins equation;
4) Parseval's theorem is used to obtain the estimate of the rms acceleration a_{rms} in terms of the squared amplitude spectrum of ground motion $|A(f,\{K_i\})|^2$;
5) PGA value is calculated by considering the product between the values of (PGA/a_{rms}) evaluated at point 3) and a_{rms}.

The second method that I used for the estimate of PGA estimate can be considered as a slight modification of the first. I describe this method (hereinafter referred to as GMG) in the following steps:

1) the shape of acceleration spectrum $A(f, \{K_i\})$ is defined;
2) Parseval's theorem is used to calculate a_{rms};
3) Ground motion acceleration $A(t)$ is generated using a gaussian distribution with σ equal to a_{rms};
4) PGA is evaluated by considering the maximum amplitude of $A(t)$;

5) the averaged value of PGA is calculated by performing a great number of simulations (N > 50) (the iterative procedure is repeated from point 1) to point 4)).

The definition of spectral ground acceleration $A(f,\{K_i\})$ and the setting of the parameters $\{K_i\}$ are the most important aspects of the three above described methods. The shape of the acceleration spectrum $A(f,\{K_i\})$ is defined as (Boatwright, 1980):

$$A(f,\{K_i\}) = \frac{\Omega_0 \cdot f^2}{\sqrt{1+\left(\frac{f}{f_C}\right)^{2\cdot\gamma}}} \exp\left(-\frac{\pi\, fT}{Q}\right) \tag{3.1}$$

For the area of Pozzuoli-Solfatara I took into account the local site effects considering in equation (3.1) the site contribution too:

$$A^{PS}(f,\{K_i\}) = A(f,\{K_i\}) \cdot G(f)$$

where *G(f)* represents the theoretical amplification function derived in section 3.6.

In the following, I describe how I chose all the parameters of equation (3.1), both for the Campi Flegrei caldera and for the area of Pozzuoli-Solfatara.

I estimated the spectral ground acceleration $A(f, \{K_i\})$ for the maximum expected magnitude M_{max} in the investigated area, for a given recurrence time period. As well known, the number of earthquakes that occurred in a time period τ can be represented by the Gutenberg-Richter relation (Lay and Wallace, 1985):

$$\log N(M) = a - bM \tag{3.2}$$

where N is the number of earthquakes with magnitudes in a fixed range around magnitude M, a and b are parameters respectively related to seismicity level and earth heterogeneity (Scholz, 1968). Equation (3.2) can be used to calculate the expected maximum magnitude M_{max}. If a and b are estimated for data in a time period τ, the ratio a/b gives the value of M_{max} expected in that period. For the Campi Flegrei area, a and b parameters of the Gutenberg-Richter distribution were calculated by De Natale and Zollo (1986). The seismic catalogue used in that work starts form 1975 and ends in 2000, it contains more than 10,000 seismic events ($0 < M_D < 4.2$) mainly related to the bradyseism episode of 1983-84. The completeness threshold of this catalogue is M_D = 0.6. The parameters a and b were obtained using a least square evaluation on the

selected data. Using these values I estimated the value of M_{max} equal to 4.35 ± 0.30 for the Campi Flegrei area, for a recurrence period of 25 years.

After the determination of the expected maximum magnitude, I used the empirical formula derived in Galluzzo et al. (2004) that relates seismic moment to magnitude, in order to calculate the expected maximum moment: $\log M_0 = 9.9 + 0.9 M_D$. By using this relation, it resulted that $M_0(M_{max})$ is equal to $6.5 \cdot 10^{13}$ Nm.

I evaluated the corner frequency f_c associated to the maximum expected magnitude M_{max} by using the Brune formula (Brune, 1970) where the value of the source radius r_c corresponding to $M_0(M_{max})$ is estimated extrapolating the scaling relationships (Galluzzo et al., 2004).

As concerns the attenuation parameters, for the Campi Flegrei caldera I fixed the shear-wave velocity and quality factor Q equal to 3 km/s and 110, respectively, as these values represents an average estimate for the whole area (Del Pezzo et al., 1987). For the local estimate in the area of Pozzuoli-Solfatara, I took into account the velocity and quality factor values derived in this thesis, by considering in equation (3.1) three contributions related to the propagation in the layered structure of section 3.6. Only for the halfspace, I still used the average quality factor Q = 110, as the attenuation structure derived in section 3.5 could not resolve the Q value in the halfspace.

The medium density ρ_0 was considered equal to 2.2 gm/cm^3 in the caldera and 2.1 gm/cm^3 for Pozzuoli-Solfatara. Geometrical spreading factor $1/R$ was obtained by evaluating the average hypocentral distance between the mean of source locations and the nearest station site. I fixed R equal to 2 km being this value the minimum possible hypocentral distance.

Finally, I fixed the radiation pattern term $Y^S_{\theta\varphi}$ equal to 1 in order to take into account the effects due to the maximum radiated energy, while a value of 2 was chosen for the free surface operator F.

Using the above defined parameters, I applied the two techniques (RVT and GMG; see the Mathcad worksheet reported in appendix F) obtaining the following PGA values:

0.04 g	RVT method	Campi Flegrei area
0.04 ± 0.01 g	GMG method	Campi Flegrei area
0.097 g	RVT method	Pozzuoli-Solfatara area
0.096 ± 0.004 g	GMG method	Pozzuoli-Solfatara area

Discussion

In this thesis I contribute to the characterization of the shallow velocity and attenuation structure for the area of Pozzuoli-Solfatara. For this aim, I apply different techniques (combined MFT and PMF, SAC, ESAC) to different kind of data (explosions, seismic noise), providing robust and stable results, which I successfully validated against the available constraints given by the direct and indirect geophysical and geological measurements.

In addition, the techniques adopted for this study represent a cheap manner to obtain fast and reliable measurements of local elastic properties of the earth. These measurements are particularly important for seismic source studies in the investigated area, as the presence of heterogeneous and/or fractured materials can lead to anomalous propagation and site effects that could mask the source contribution in the seismic signals.

I also introduce a new approach based on the autoregressive analysis, for recovering the dispersion curve of surface waves. This method offers some advantages respect to the combined use of MFT and PMF; one is that there is no need to filter the data because this operation is equivalent to the segmentation of the complex frequency series. In addition the computer time required for the elaboration is very small. As I have shown in this thesis, the AR technique applied to real signals generated by the artificial explosions has provided reliable results. The ability of the method in discriminating closely spaced arrival times implies an accurate determination of the dispersion curves. The results presented in this thesis are very promising, although a little effort is now required for the quantification of the uncertainties related to the travel time estimates and their propagation on the group velocity dispersion values. However, in my opinion, this technique could be extensively applied for future studies of surface wave dispersion.

I used the velocity and attenuation structure presented in this thesis to estimate the theoretical transfer function and assess the local site response, that I took into account to better constrain the PGA value for the area of Pozzuoli-Solfatara. Such estimates are very important in an area that is periodically subjected to seismic crises

and where the most part of the seismicity related to the bradysesimic crisis is located. Although this local seismicity is characterised by relatively low energy earthquakes, local amplification occurring at the resonance frequencies can produce great damages to building and infrastructures. All these aspects should be taken into account for the assessment of the seismic hazard in this densely-populated volcanic area.

The comparison between the amplification peak frequencies obtained from the theoretical transfer function and the ones retrieved from the application of Nakamura's technique opens several points for discussion. In section 3.7 I gave 3 possible interpretations that could explain the observed discrepancy. Here I just would like to add that, as remarked in point 1) of section 3.7, local deviations from the average velocity model can produce differences in the transfer function; although the very shallow crustal structure going from Pozzuoli coast to the Solfatara crater rim is not so heterogeneous (as it is inside the flat part of a collapsed caldera), some local variations in the layer thicknesses just beneath the Solfatara crater are possible. I further investigated this aspect by looking at the experimental phase velocity dispersion curve deduced from SAC technique, which is representative of the velocity structure just beneath the array. As shown in fig. 3.13, this curve is quite compatible with the theoretical phase velocity dispersion associated to the velocity model I have retrieved. However, after some numerical simulations, I found that the experimental phase velocity dispersion could also be compatible with a crustal structure formed by a 30-m thick layer of pyroclastic materials on an elastic halfspace composed by fractured yellow tuff. This crustal structure (that would be valid just beneath the array site and that only slightly differs from that of section 3.4) would produce a theoretical transfer function with the fundamental resonance frequency at about 5 Hz. This would agree with Nakamura's spectral ratio.

On these premises, it would be very useful to plan an experiment aimed at the sampling of microtremor in the nodes of a grid densely covering the area which goes from the coast of Pozzuoli to the rim Solfatara crater, as well as the bottom of the whole crater itself. In this way a more punctual evaluation of the H/V Nakamura's spectral ratio would be possible, thus allowing the comparison both with the experimental

transfer functions for different sites and with the theoretical transfer function estimated for the average velocity and attenuation structure presented in this thesis.

Conclusions

- A remarkable result is the robustness of the retrieved surface wave dispersion curves, which have been obtained applying different techniques to both natural and artificial sources.
- The new approach based on AR analysis and proposed for the determination of surface wave dispersion curves has provided encouraging results. In the future this technique could be successfully applied for such kind of studies.
- The obtained seismic velocity and attenuation models contribute to the definition of the surface geology at small-scale in the area of Pozzuoli-Solfatara and constitute a good observational set to be used in all the studies on the seismic source in that area.
- The presented velocity and attenuation structure has been used in this thesis to determine the local site response, in order to contribute to the seismic hazard assessment for the investigated area.
- The present study adds new observations that contribute to the current scientific debate about the applicability of the method of Nakamura.
- The obtained PGA values for the Campi Flegrei and for the area of Pozzuoli-Solfatara were calculated by simulating the ground motion produced by local earthquakes and taking into account the estimated local site response.

Acknowledgments

I am grateful to all the colleagues who helped me in my research activity with their useful suggestions: Edoardo Del Pezzo, Gilberto Saccorotti, Paola Cusano (not only a seismologist but also a good friend), Francesca Bianco, Mario Castellano and Rosalba Maresca. Danilo Galluzzo, Mario La Rocca and Vincenzo Nisii are fully acknowledged both for the interesting scientific discussions and for their contribution to the field work and data management. I wish to thank Mauro Di Vito who provided useful information about the volcanological history of the Campi Flegrei caldera. The technical support of Vincenzo Torello and Giuseppe Borriello was really appreciated. Finally, my special thanks go to Pierpaolo who, sharing my passion for volcanoes, always encouraged me to carry on my studies.

This thesis is dedicated to all the people who firmly persist in reaching their goals.

Appendix A

Derivation of relation (2.2)

In the following I report the demonstration that the expression (2.1) in section 2.1.1 is equivalent to (2.2). The (2.1) is:

$$g(r,t)=\frac{1}{2\pi}\int_{-\omega_c}^{\omega_c}H(\omega)A(\omega+\omega_0,r)\exp\{i[(\omega+\omega_0)t-k(\omega+\omega_0)r]\}d\omega \tag{A.1}$$

Consider the expansion in Taylor series of the spectral amplitude $A(\omega,r)$ around ω_0:

$$A(\omega,r)=\sum_{n=0}^{\infty}\frac{a_n(\omega-\omega_0)}{n!} \tag{A.2}$$

with:

$$a_n=\left(\frac{\partial^n A(\omega,r)}{\partial\omega^n}\right)_{\omega_0}$$

If one defines the function $g_0(t,r)$:

$$g_0(t,r)=\frac{1}{2\pi}\int_{-\omega_c}^{\omega_c}H(\omega)\exp\{i[\omega t-k(\omega+\omega_0)r]\}d\omega \tag{A.3}$$

then the expression (A.1) for $g(t,r)$ becomes:

$$g(t,r)=\left\{\sum_{n=0}^{\infty}\frac{(-i)^n}{n!}a_n\frac{\partial^n g_0(t,r)}{\partial t^n}\right\}\exp(i\omega_0 t) \tag{A.4}$$

Neglecting higher order in the expansion of the complex amplitude $A(\omega,r)$, is equivalent to neglect higher derivatives in (A.4). Now consider the expansion of $k(\omega)$ around $\omega=\omega_0$. As $\frac{dk}{d\omega}=\frac{1}{U}$, with U group velocity, then:

$$k(\omega)=k_0+\frac{1}{U}(\omega-\omega_0)+\frac{1}{2}\frac{d^2k}{d\omega_0^2}(\omega-\omega_0)^2 \tag{A.5}$$

Substituting in equation (A.3):

$$g_0(t,r)=\frac{1}{2\pi}\exp(-ik_0r)\int_{-\omega_c}^{\omega_c}H(\omega)\exp\left(i\left[\omega\left(t-\frac{r}{U_0}\right)-\frac{r}{2}\frac{d^2k}{d\omega_0}\omega^2\right]\right)d\omega \tag{A.6}$$

Moreover, considering the explicit form of the gaussian filter $H(\omega)$:

$$H(\omega)=\begin{cases}\exp\left(-\alpha\,\omega^2/\omega_0\right) & |\omega|\le\omega_c\\ 0 & |\omega|>\omega_c\end{cases}$$

the equation (A.6) becomes:

$$g_0(t,r)=\exp(-ik_0r)\frac{\omega_c}{\pi}\frac{sin\left[\omega_c(t-r/U_0)\right]}{\omega_c(t-r/U_0)}*\frac{1}{2\pi}\sqrt{\frac{\pi}{\gamma}}\exp\left[i\left(\frac{t^2}{4\gamma}-\frac{\pi}{4}\right)\right] \qquad (A.7)$$

where the symbol * denotes the convolution operation and γ is equal to:

$$\gamma=\frac{r}{2}\frac{d^2k}{d\omega_0^2}-\frac{i\alpha}{\omega_0^2}$$

Equation (A.7) can be written as:

$$g_0(t,r)=\frac{1}{2\pi}\sqrt{\frac{\pi}{4\gamma}}\exp\left[i\left(-k_0r+\frac{\beta^2}{4\gamma}-\frac{\pi}{4}\right)\right]erf\left[\frac{1}{\sqrt{\gamma}}\left(\gamma\omega-\frac{\beta}{2}\right)e^{i\pi/4}\right]\Bigg|_{-\omega_c}^{\omega_c} \qquad (A.8)$$

with:

$$erf(z)=\left(\frac{2}{\sqrt{\pi}}\right)\int_0^z\exp\left(-t^2\right)dt \quad \text{and} \qquad \beta=(t-r/U_0)$$

Now assume that $A(\omega,r)$ is constant in the filter band. As one can note from (A.4), in this case the filtered signal is represented by the relation (A.6) multiplied by $\exp(i\omega_0t)$; then the study of (A.4) is equivalent to that of (A.7) or (A.8).

The complex quantity γ can be represented as:

$$\gamma=\frac{r}{2}\frac{d^2k}{d\omega_0^2}-\frac{i\alpha}{\omega_0^2}=\rho e^{i\theta} \qquad (A.9)$$

with:

$$\rho=\sqrt{\left(\frac{r}{2}\frac{d^2k}{d\omega_0^2}+\right)^2+\left(\frac{\alpha}{\omega_0^2}\right)^2} \qquad \pi<\theta<2\pi \qquad (A.10)$$

With this position, the expression of the filtered signal becomes:

$$g(t,r)=\frac{A}{2\pi}\sqrt{\frac{\pi}{4\rho}}\exp\left[i\left(\omega_0 t-k_0 r-\frac{\theta}{2}-\frac{\pi}{4}\right)\right]\exp\left[\frac{\beta^2}{4\rho}\left(sin\theta+i\cos\theta\right)\right]$$

$$\times\left\{erf\left[\sqrt{\rho}\omega_c\exp i(\theta/2+\pi/4)-\frac{\beta}{2\sqrt{\rho}}\exp(-i(\theta/2-\pi/4))\right]\right.$$

$$\left.+erf\left[\sqrt{\rho}\omega_c\exp i(\theta/2+\pi/4)+\frac{\beta}{2\sqrt{\rho}}\exp(-i(\theta/2-\pi/4))\right]\right\} \qquad \text{(A.11)}$$

Under some conditions this expression can be simplified. The error function is an odd function and:

$erf(x+iy)\approx 1$ for $x>|y|$ e $x>2$

$erf(x+iy)\approx -1$ for $x<-|y|$ e $x<-2$

In the following hypothesis:

$\omega_c\rho^{1/2}>1/2\,\beta\rho^{-1/2}$ $\omega_c\rho^{1/2}>2$

the error functions in (A.11) are approximately -1, therefore (A.11) reduces to:

$$g(t,r)=\frac{A}{2\pi}\sqrt{\frac{\pi}{\rho}}\exp\left[i\left(\omega_0 t-k_0 r-\frac{\theta}{2}+\frac{3\pi}{4}\right)\right]\exp\left[\frac{\beta^2}{4\rho}\left(sin\theta+i\cos\theta\right)\right] \qquad \text{(A.12)}$$

If $\frac{r}{2}\frac{dk^2}{d\omega_0^2}=0$, equation (A.12) can be written as:

$$g(t,r)=\frac{A\omega_0}{2\pi}\sqrt{\frac{\pi}{\alpha}}\exp[i(\omega_0 t-k_0 r)]\exp\left[-\frac{\omega_0^2}{4\alpha}\left(t-\frac{r}{U_0}\right)^2\right] \qquad \text{(A.13)}$$

that is the equation (2.2) of section 2.1.1.

Appendix B

A Mathcad worksheet for the AR analysis

I report the Mathcad worksheet I prepared for the AR analysis of a synthetic dispersive signal. Comments are in bold text.

I generate a dispersive synthetic signal composed of 3 wave packet with different frequencies (2, 3 and 5 Hz).

$f1 := 2$
$f2 := 3$ **These are the selected frequencies**
$f3 := 5$

$par := 1.1$
$par2 := 0.9$ **These parameters change the shape of the test signal, acting on the decay rate**
$par3 := 0.8$

$signal(t) := \exp[-(par \cdot f1 \cdot t)] \sin(2 \cdot \pi \cdot f1 \cdot t)$ **The wave packet with frequency f1**
$signal2(t) := \exp[-(par2 \cdot f2 \cdot t)] \cdot \sin(2 \cdot \pi \cdot f2 \cdot t)$ **The wave packet with frequency f2**
$signal3(t) := \exp[-(par3 \cdot f3 \cdot t)] \sin(2 \cdot \pi \cdot f3 \cdot t)$ **The wave packet with frequency f3**

$$quake(t) := \begin{cases} 0 & \text{if } t \le 0 \\ signal(t) & \text{if } t > 0 \end{cases}$$

$$quake2(t) := \begin{cases} 0 & \text{if } t \le 0 \\ signal2(t) & \text{if } t > 0 \end{cases}$$

$$quake3(t) := \begin{cases} 0 & \text{if } t \le 0 \\ signal3(t) & \text{if } t > 0 \end{cases}$$

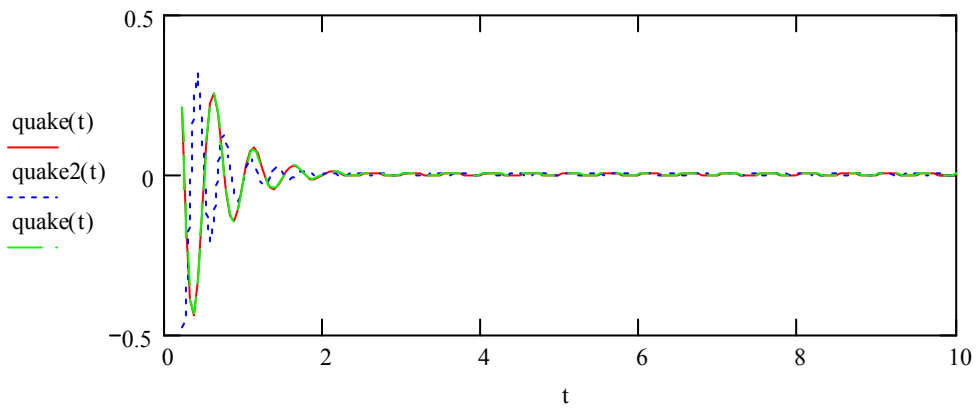

The following routine assigns different time delays to the 3 wave packets.

sampling := 100 **Sampling rate of the time series**

Npti := 999 **Number of points to be generated.**
The time series will have a length of 10 s

$i := 0 .. Npti$

$t_i := \frac{i}{sampling}$

noise_amplitude := 1 **I add to the signals some noise**

I assign the arrival time of the 3 different packets: the 3 arrivals are at 1, 2 and 3 seconds, respectively:

$x_i := t_i - 1$

$k_i := t_i - 2$

$h_i := t_i - 3$

noise := rnorm(Npti + 1, 0, 0.0005) **Generation of the synthetic noise**

$s_i := quake(x_i) + quake2(k_i) + quake3(h_i)$

The synthetic final signal is the sum of the 3 wave packets arriving at different times, plus the noise:

x := s + noise

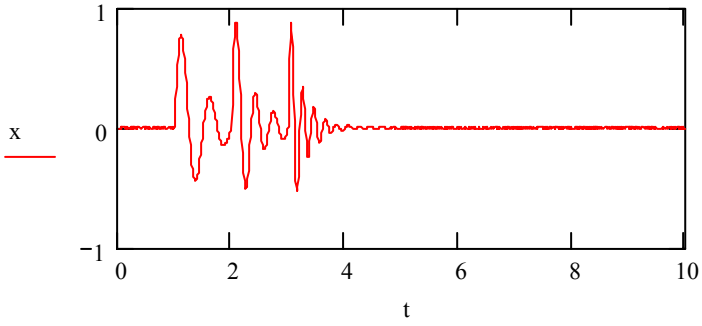

This is the final synthetic dispersive signal. The first packet is at 2 Hz and arrives at 1 s, the second at 3 Hz and arrives at 2 s, the third at 5 Hz and arrives at 3s. Now I transform the oscillating signal in pulses by taking the Hilbert transform.

hil := hilbert(x)

$x := \sqrt{(x)^2 + (hil)^2}$

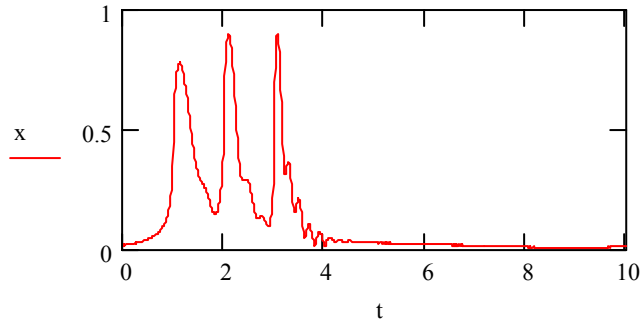

The complex frequency series (amplitude and phase) is obtained by taking the FFT of the pulses.

$i := 1 .. last(x) + 1$

$j := 1 .. \frac{last(x) + 1}{2}$

$t_i := \frac{i}{sampling}$

$fs_j := \frac{sampling}{last(x) + 1} \cdot j$

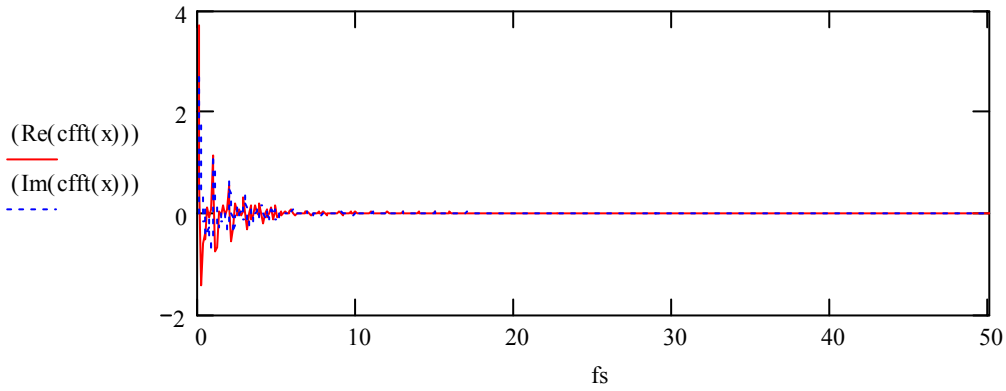

$x := cfft(x)$ **x is the complex frequency series**

$last(cfft(x)) = 999.000$ **The number of points of the complex series**

$\frac{sampling}{last(x) + 1} = 0.100$

$srate := fs_1 - fs_0$ **srate is the unit of frequency discretization**

$srate = 0.100$

$\tau Nyquist := \frac{1}{2srate}$

$\tau Nyquist = 5.000$ **Nyquist travel time for the complex frequency series. It means that I can evaluate the arrival time in the Nyquist time band (-5, 5) seconds, or equivalently in the (0, 10) seconds time range**

I select to analyse the complex frequency series up to 10 Hz:

$x := \text{submatrix}(x, 0, 100, 0, 0)$

$\text{last}(x) = 100.000$ **The selected number of points of the complex series**

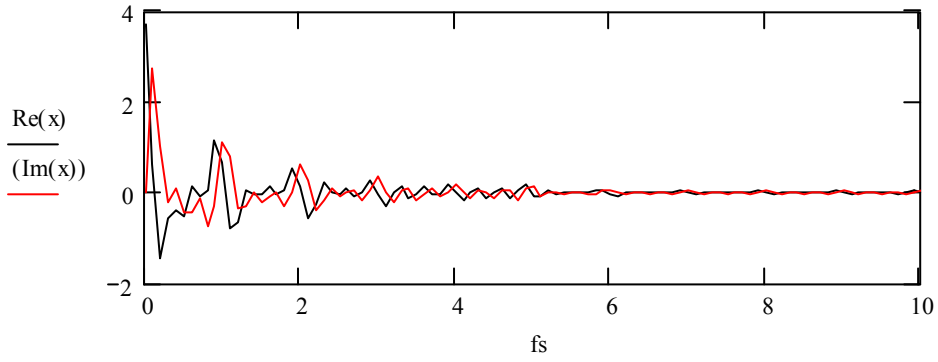

Now I perform the autoregressive analysis. I calculate the eigenvalues and the eigenvectors of the autocovariance matrix of the complex frequency series, for different orders of the filter (from 2 to 14).

$mmax := 14$ **Selection of the maximum filter order**

For each order of the filter, the following routine searches for the minimum eigenvalue.

$m := 0..mmax$

$\lambda 0_m :=$ for $n \in 0..m$

for $k \in 0..n$

for $l \in 0..n$

$$P_{k,l} \leftarrow \frac{1}{(\text{last}(x) + 1) - n} \cdot \left[\sum_{t=n}^{\text{last}(x)} \left[\left(x_{t-k} \right) \cdot \left[\left(\bar{x} \right)_{t-l} \right] \right] \right]$$

$\lambda \leftarrow \text{eigenvals}(P)$

$\lambda \leftarrow \text{sort}(\lambda)$

$\lambda \leftarrow \lambda_0$

The Akaike Information Criterion (AIC) is evaluated to establish the minimum order of the filter required to resolve the number of wave elements in the complex frequency series. In the next plot one can note that AIC decreases until the AR order reaches a value of six. This value is the required minimum filter order.

$AIC_m := (\text{last}(x) + 1) \cdot \ln(\lambda 0_m) + 2 \cdot (m + 1)$ **Evaluation of the Akaike Information Criterion**

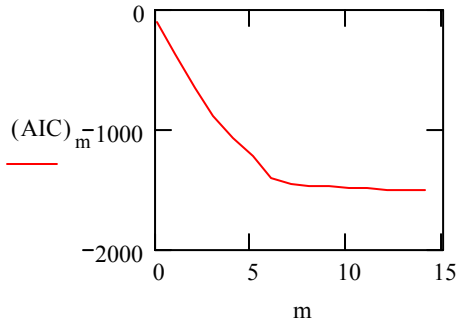

For each order of the filter, the following routine searches for the eigenvectors corresponding to the minimum eigenvalue.

$$\text{eigen}_m := \left| \begin{array}{l} \text{for } n \in 0..m \\ \quad \text{for } k \in 0..n \\ \quad\quad \text{for } l \in 0..n \\ \quad\quad\quad P_{k,l} \leftarrow \dfrac{1}{(\text{last}(x) + 1) - n} \cdot \left[\displaystyle\sum_{t=n}^{\text{last}(x)} \left[\left(x_{t-k} \right) \cdot \left[\left(\bar{x} \right)_{t-l} \right] \right] \right] \\ \lambda \leftarrow \text{eigenvals}(P) \\ \lambda \leftarrow \text{sort}(\lambda) \\ \lambda 0 \leftarrow \lambda_0 \\ a \leftarrow \text{eigenvec}(P, \lambda 0) \end{array} \right.$$

Once the eigenvectors have been found, the characteristic equation (see the section about the description of the method) must be solved in order to obtain the complex travel times.

$N := 0, 2.. (\text{rows}(\text{eigen}) - 1)$ **These instructions write the eigenvector to an ASCII file**

$\text{beta}(N) := \text{concat}("C:\text{Sismologia}\text{phd}\text{eigen}\text{eigen}", \text{num2str}(N))$

$\text{WRITEPRN}(\text{beta}(N)) := \text{eigen}_N$

$c_N := \text{READPRN}(\text{concat}(\text{beta}(N), ".PRN"))$

$$p(y, N) := \sum_{k=0}^{N} \left(c_N \right)_k \cdot y^k$$ **The characteristic equation to be solved**

The following instructions solve the algebraic equation

$N := 2, 4.. (\text{rows}(\text{eigen}) - 1)$

$r_N := \text{polyroots}\left(v_N \right)$

v_N:=p(y,N) coeffs, y

$z_N := \frac{1}{r_N}$ **The roots of the characteristic equation**

$q_N := \frac{i \cdot \ln(z_N)}{2 \cdot 3.14 \cdot srate}$ **The complex travel times**

$\tau_N := Re(q_N)$ **The travel times**

$v_N := Im(q_N)$

$w_N := -2 \cdot v_N$

The results (real and imaginary part of the complex travel times) are written to an ASCII file:

$\tau w_N := augment(\tau_N, w_N)$

beta(N) := ("C:\Sismologia\phd\eigen\tau_w.dat")

APPENDPRN(beta(N)) := τw_N

:=

C:\..\Tau_w.dat

In the following cumulative τ-w plot one can note how the procedure is able to well discriminate the arrival times of the 3 pulses. The arrival times are indicated by the 3 clusters of points at 1, 2 and 3 seconds, while scattered points represent the noise.

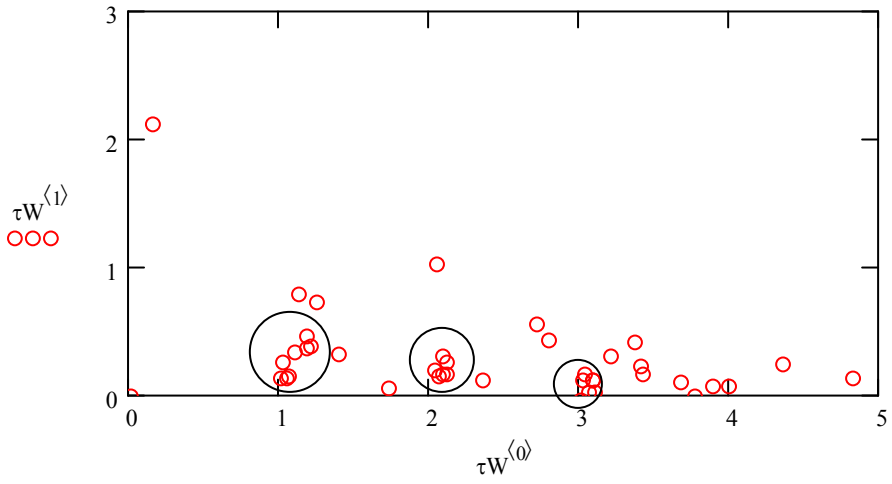

Appendix C

Resolution kernels

In this appendix I report the resolution kernels relative to the inversion of the group velocity dispersion curves in section 3.3.

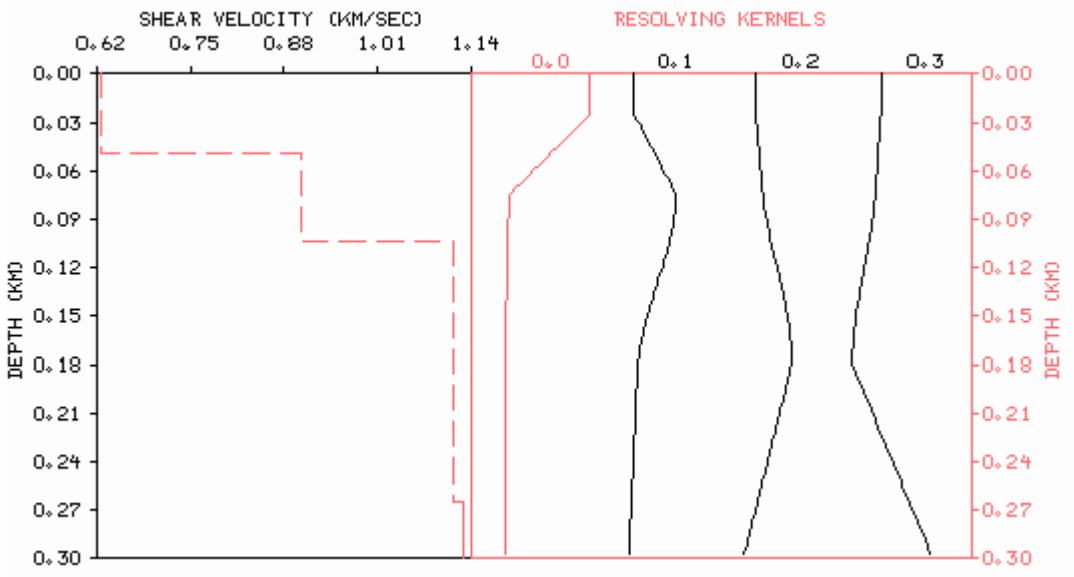

On the left, velocity model inferred from the fundamental mode inversion. On the right, the resolution kernels.

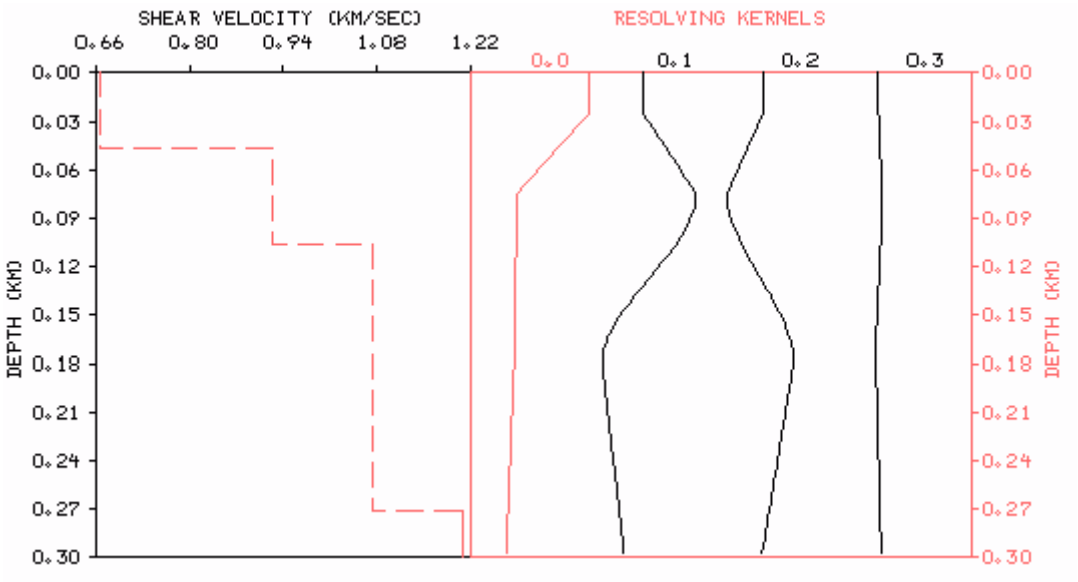

On the left, velocity model inferred from the first mode inversion. On the right, the resolution kernels.

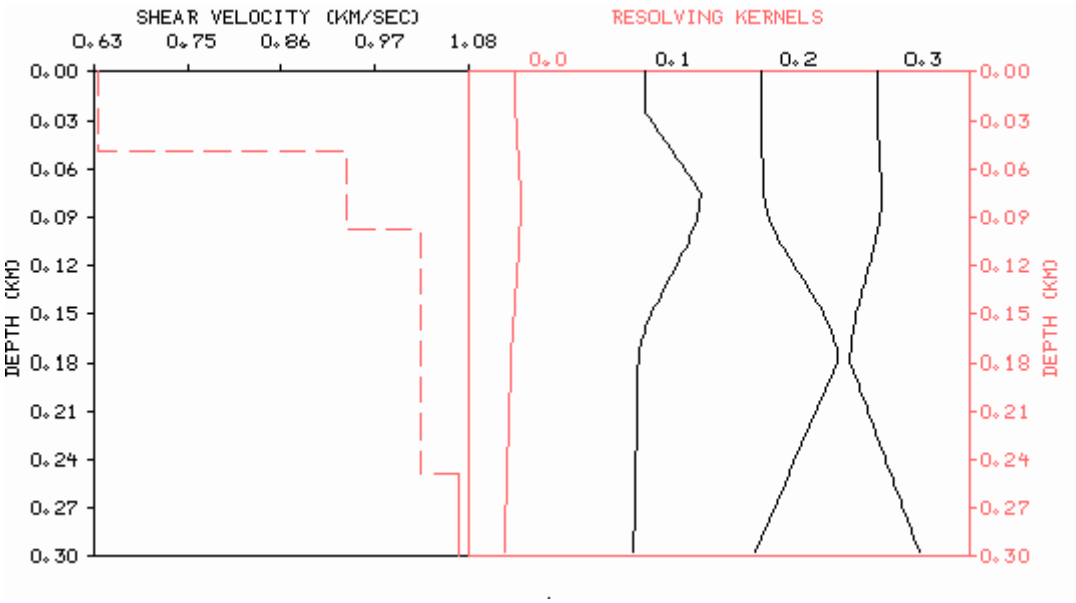

On the left, velocity model inferred from the second mode inversion. On the right, the resolution kernels.

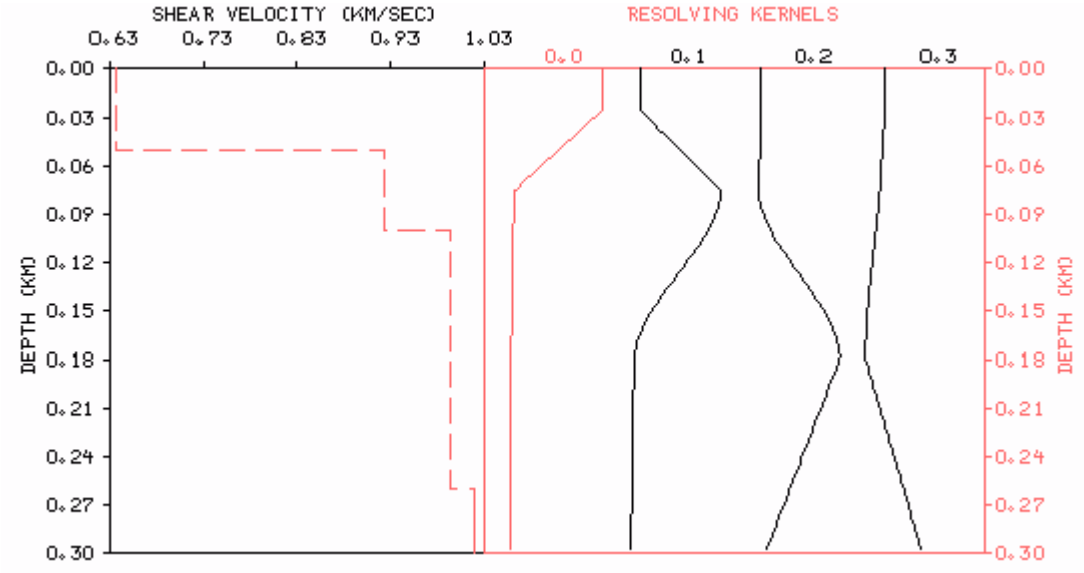

On the left, velocity model inferred from the simultaneous inversion. On the right, the resolution kernels.

Appendix D

A Mathcad worksheet for the attenuation analysis

This appendix contains the Mathcad worksheet I prepared for the attenuation analysis of surface waves. Comments are in bold text.

The seismograms of 9 shots recorded at the 6 stations of the seismic sub-array A are used for the attenuation analysis.

$j := 1 .. \text{cols}(Ev)$

$Ev^{\langle j \rangle} := Ev^{\langle j \rangle} - \text{mean}\left(Ev^{\langle j \rangle}\right)$ **The matrix Ev contains 6 seismic traces for 9 events**

$i := 1 .. \text{last}\left(Ev^{\langle 1 \rangle}\right)$

The sampling rate is srate = 200 Hz

$t_i := \frac{i}{srate}$

This is an example of a shot recorded at the 6 stations of the array

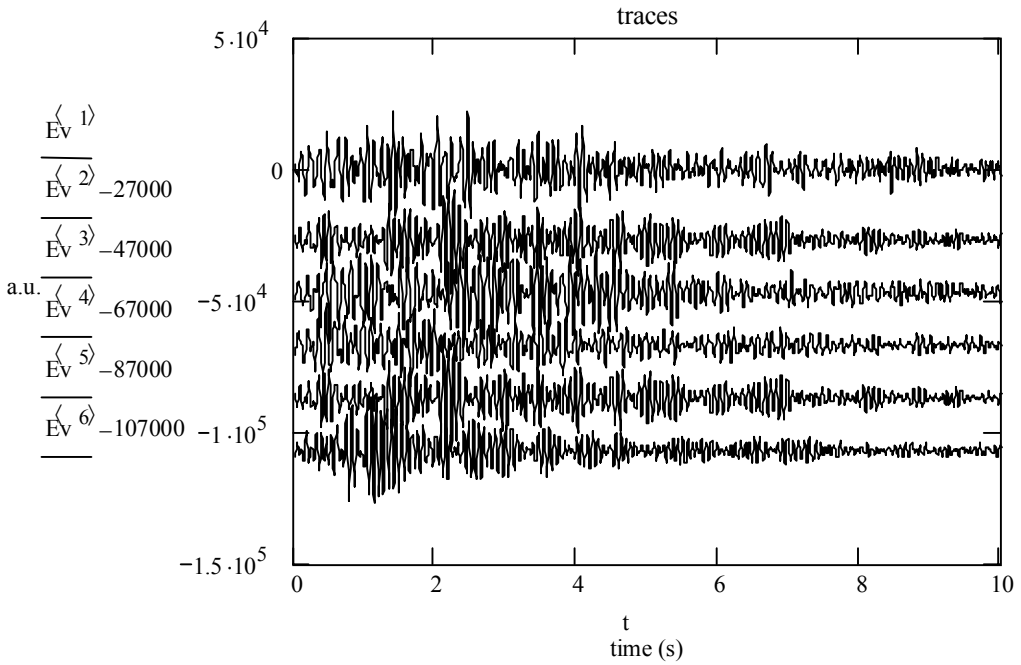

$Ev := \text{submatrix}(Ev, 200, 2000, 1, \text{cols}(Ev))$ **Selection of 9-s-long time window, 1 s after the P-wave arrival**

The signals are filtered in selected frequency bands. In the following example, I apply a band-pass filter between 6 and 7 Hz.

$f1 := 6$

$f2 := 7$

$k := 1 .. \text{cols}(Ev)$

$$Ev^{\langle k \rangle} := FBP\_Bessel\left(Ev^{\langle k \rangle}, srate, f1, f2, 7, 0.7\right)$$

In the next figure I show examples of spectra for some shots. In each plot is reported the spectrum at the 6 stations of the array.

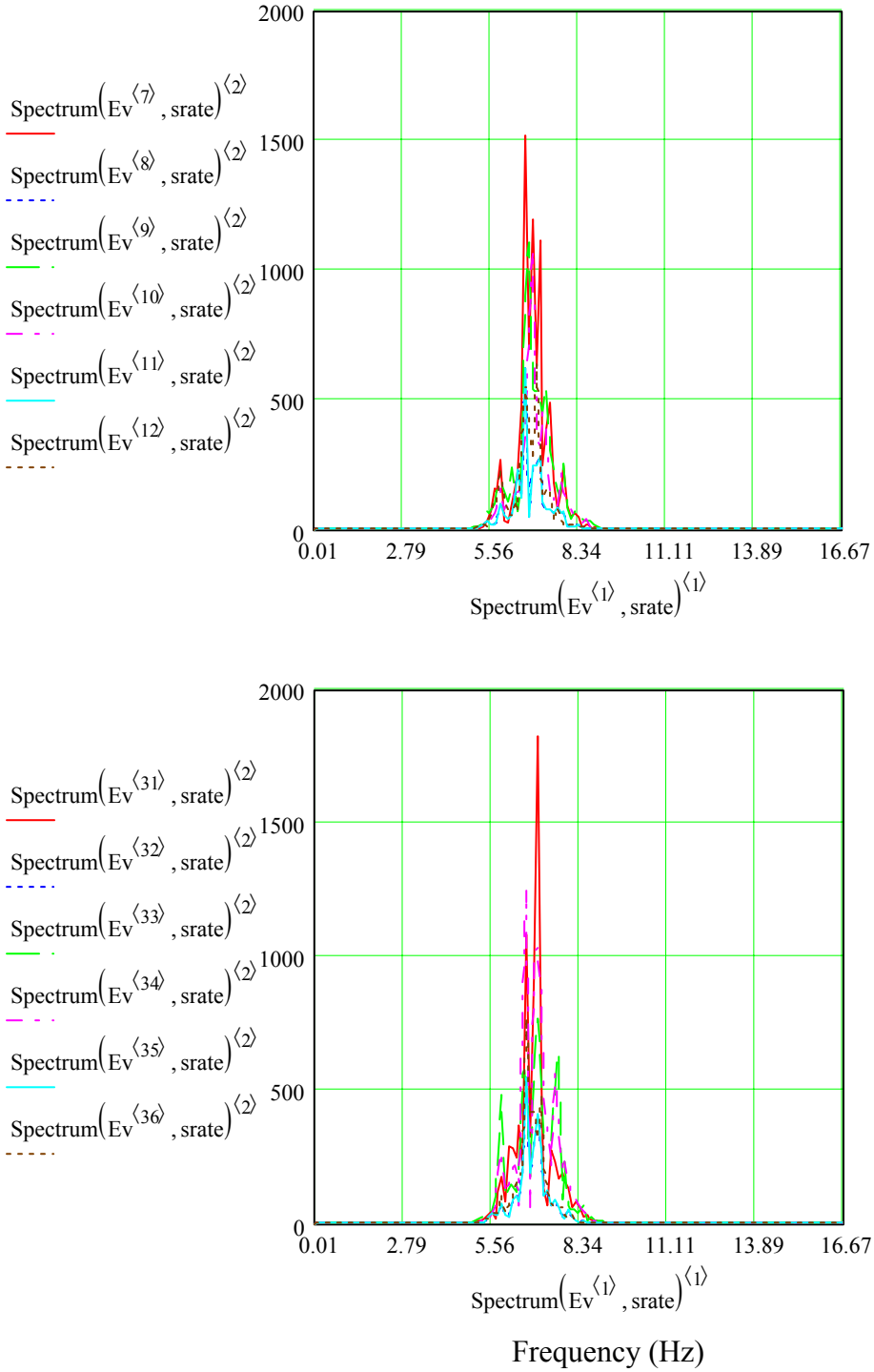

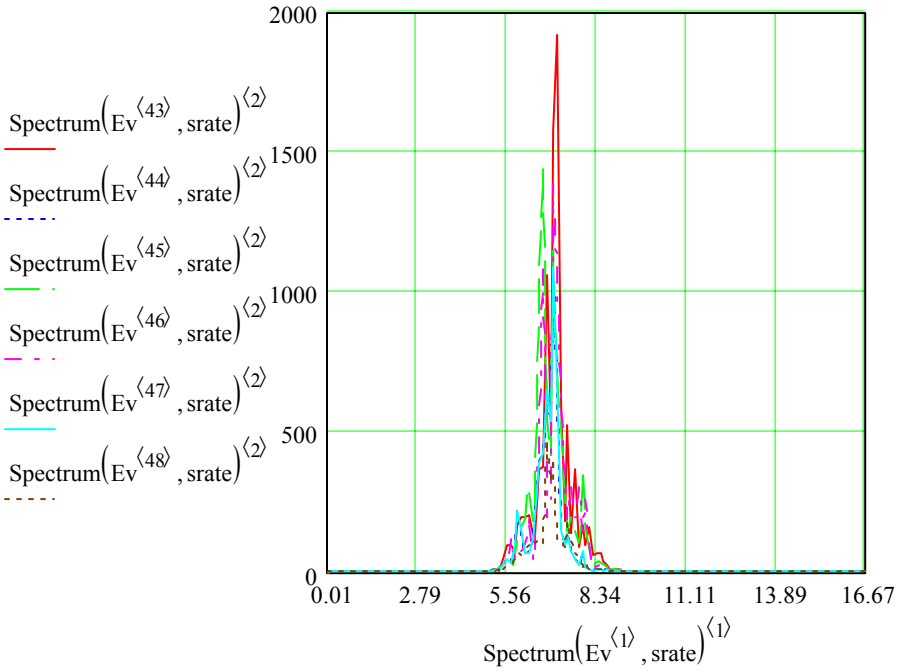

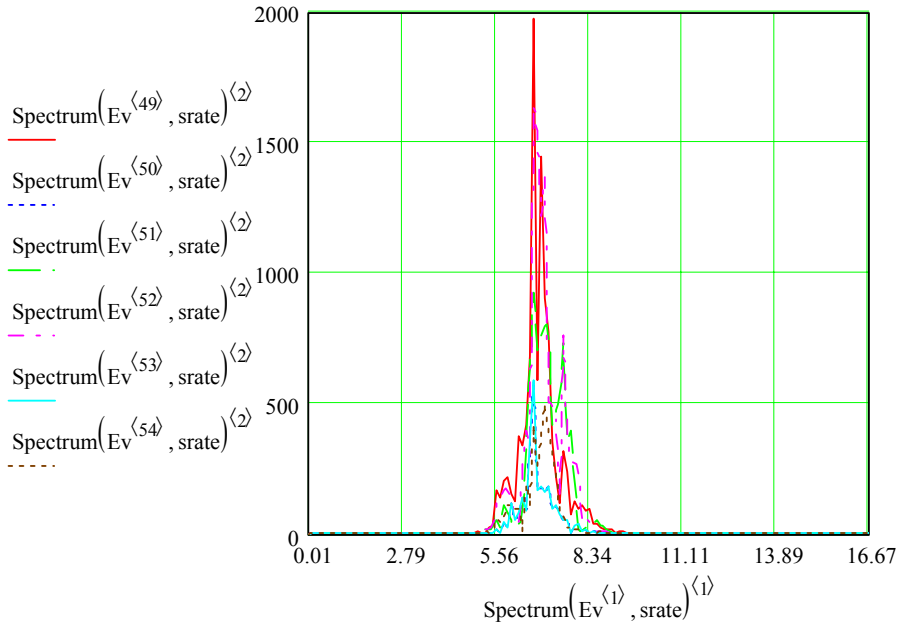

Frequency (Hz)

The following routine calculates the value of the spectral amplitude as a function of the distance for each events. The parameter γ (see definition in the section 2.2) is evaluated by a least-square fitting procedure, by using the whole data-set.

$$f := \text{Spectrum}\left(Ev^{\langle 1\rangle}, srate\right)^{\langle 1\rangle}$$

$$sp^{\langle k\rangle} := \text{Spectrum}\left(Ev^{\langle k\rangle}, srate\right)^{\langle 2\rangle}$$

$$j := 1..\,\text{cols}(Ev)$$

$$Area_j := \left| \begin{array}{l} \text{for } i \in 1..\,\text{last}(f) - 1 \\ \quad \left| A_i \leftarrow \left[\left(sp^{\langle j\rangle}\right)_{i+1} + \left(sp^{\langle j\rangle}\right)_i\right] \cdot \frac{\left[(f)_{i+1} - (f)_i\right]}{2} \right. \\ \quad A \\ AA \leftarrow \sum_{h=1}^{\text{last}(f)-1} \left(A_h\right) \\ AA \end{array} \right.$$

$$areams := \frac{\left(\sum_{j=1}^{\text{cols}(Ev)} Area_j\right)}{\text{cols}(Ev)}$$

$$sg := 0.5$$

$d := sg \cdot \ln(r) + \ln(Area)$ **Definition of the data vector, d, for the inverse problem**

$m := \left(G^T \cdot G\right)^{-1} \cdot G^T \cdot d$ **Solution of the inverse problem**

$m_{10} = -5.836$ **This is the value of the γ parameter obtained from the inversion of all data**

I report an example of the amplitude spectral decay as a function of distance for two events

$j := 1..\,6$

$j := 1..\,6$

$re5 := \text{submatrix}(r, 25, 30, 1, 1)$ **Selection of the 2 events**

$re8 := \text{submatrix}(r, 43, 48, 1, 1)$

$Areae5 := \text{submatrix}(Area, 25, 30, 1, 1)$

$Areae8 := \text{submatrix}(Area, 43, 48, 1, 1)$

$e5_j := sg \cdot \ln\left(re5_j\right) + \ln\left(Areae5_j\right)$ **For each event, fit of the spectral amplitude decay with distance**

$e8_j := sg \cdot \ln\left(re8_j\right) + \ln\left(Areae8_j\right)$

$fite5 := \text{line}(re5, e5)$

$fite8 := \text{line}(re8, e8)$

$fitAe5(re5) := fite5_1 + fite5_2 \cdot re5$

$fitAe8(re8) := fite8_1 + fite8_2 \cdot re8$

$fite5_2 = -8.162$

$fite8_2 = -7.524$

The angular coefficient corresponds to the γ value

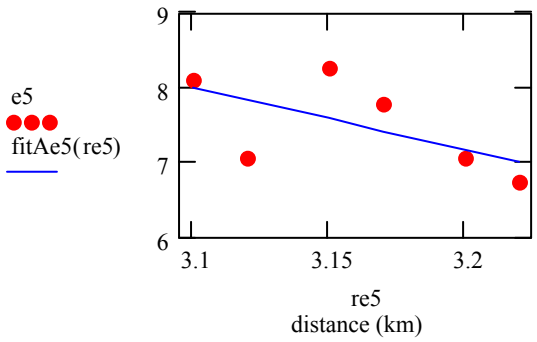

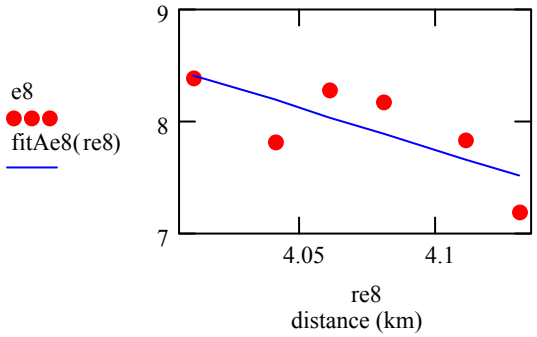

In the following, I evaluate the error on the estimate of the γ parameter, by calculating the variance of the seismic noise.

$Ev := submatrix(Ev, 2200, 4000, 1, cols(Ev))$

Selection of some samples of seismic noise

$Ev^{\langle k \rangle} := FBP\_Bessel\left(Ev^{\langle k \rangle}, srate, f1, f2, 7, 0.7\right)$

$f := Spectrum\left(Ev^{\langle 1 \rangle}, srate\right)^{\langle 1 \rangle}$

$sp^{\langle k \rangle} := Spectrum\left(Ev^{\langle k \rangle}, srate\right)^{\langle 2 \rangle}$

$j := 1..cols(Ev)$

The following routine calculates the noise spectral amplitude:

$$\text{Arean}_j := \left| \begin{array}{l} \text{for } i \in 1..\text{last}(f)-1 \\ \quad \left| A_i \leftarrow \left[\left(sp^{\langle j \rangle}\right)_{i+1} + \left(sp^{\langle j \rangle}\right)_i \right] \cdot \frac{\left[(f)_{i+1} - (f)_i \right]}{2} \right. \\ \quad A \\ AA \leftarrow \sum_{h=1}^{\text{last}(f)-1} \left(A_h\right) \\ AA \end{array} \right.$$

$$\text{areamn} := \frac{\left(\sum_{j=1}^{\text{cols}(Ev)} \text{Arean}_j \right)}{\text{cols}(Ev)}$$

$$\text{areamn} := \frac{\left(\sum_{j=1}^{\text{cols}(Ev)} \text{Arean}_j \right)}{\text{cols}(Ev)}$$

$$\text{sigmadq} := \frac{1}{(\text{areams})^2} \cdot \frac{1}{4} \cdot (\text{areamn})^2$$

$\text{sigmadq} = 0.023$

$\text{areamn} = 407.298$

$Ge := G^T \cdot G$

$\text{sigmamq} := \left(Ge^{-1} \cdot \text{sigmadq}\right)_{10,10}$

$\text{sigmamq} = 0.25$

$\text{sigma} := \sqrt{\text{sigmamq}}$

$m_{10} = -5.836$ **The γ value previously calculated**

$\text{sigma} = 0.5$ **The estimated uncertainty on the γ parameter**

Appendix E

A Mathcad worksheet for the computation of the theoretical transfer function

I prepared the Mathcad worksheet included in this appendix in order to calculate the theoretical transfer function (TTF). I start with some examples of TTF for simple single layer models, considering the effects of the rigid/elastic bedrock and of the undamped/damped soil. Then I consider the velocity and attenuation structure derived for Pozzuoli-Solfatara and calculate the TTF in the hypothesis of damped multiple layers on an elastic halfspace.

Case 1: Uniform undamped soil on rigid rock

I first calculate the transfer function for a single undamped soil on a rigid rock

$vs := 634$ S wave velocity in the layer

$H := 50$ Layer thickness

$f := 0, 0.2 .. 25$

$$F(f) := \frac{1}{\cos\left(\frac{2 \cdot \pi \cdot f \cdot H}{vs}\right)}$$

$$Tf := 4 \cdot \frac{50}{650}$$

$Tf = 0.308$ Fundamental period

$$Ff := \frac{1}{Tf}$$

$Ff = 3.25$ Fundamental frequency

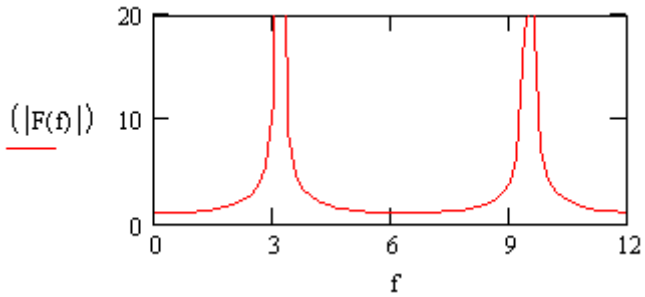

As expected, the fundamental frequency of the transfer function is at about 3 Hz

Case 2: Uniform damped soil on rigid rock

What happen if the single layer soil is damped?

$vs := 634$ Parameters of the layer

$H := 50$

$f := 0, 0.2 .. 25$

To see the effect of the damping on the transfer function, I assign two different quality factors (and hence damping ratios) to the soil.

$Q1 := 15$ Layer quality factor I

$\xi 1 := \frac{1}{2Q1}$

$\xi 1 = 0.033$

$Q2 := 10$ Layer quality factor II

$\xi 2 := \frac{1}{2Q2}$

$\xi 2 = 0.05$

$$Fd1(f) := \frac{1}{\cos\left[\frac{2 \cdot \pi \cdot f \cdot H}{vs \cdot (1 + i \cdot \xi 1)}\right]}$$

$$Fd2(f) := \frac{1}{\cos\left[\frac{2 \cdot \pi \cdot f \cdot H}{vs \cdot (1 + i \cdot \xi 2)}\right]}$$

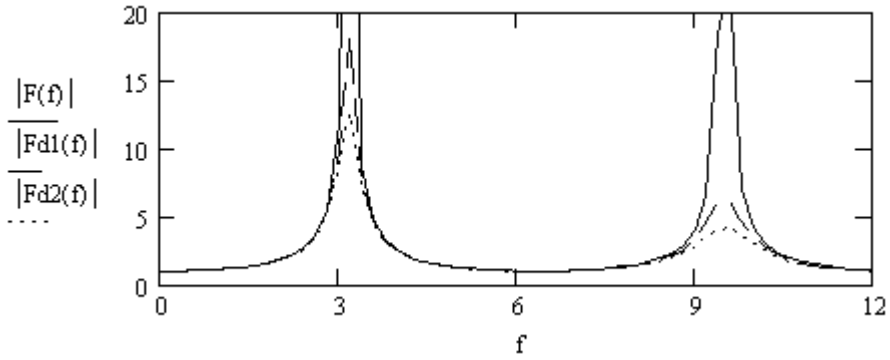

The continuous line is the transfer function for the undamped soil. The dashed line is for a damping corresponding to Q = 15 and the dotted line is for Q = 10. The resonance frequencies remain unchanged (the fundamental is still at 3 Hz), but the amplification levels are lower especially at higher frequencies. However the effect of the damping lowering is observed on the fundamental peak too.

Case 3: Uniform undamped soil on elastic rock

In this example the bedrock is not rigid but it has elastic properties, so it is possible to define its S-wave velocity and the density. If the bedrock is elastic, downward travelling waves at the interface will be partially reflected in the layer and partially transmitted to the bedrock. With this mechanism part of the energy will be removed from the soil layer and we will observe lower amplification level in the transfer function.

$vs := 634$ Layer S-wave velocity

$H := 50$ Layer thickness

$\rho s := 1.8$ Layer density

$f := 0, 0.2 .. 25$

$vr := 923$ S-wave velocity in the bedrock

$\rho r := 1.9$ Bedrock density

$$\alpha := \frac{\rho s \cdot vs}{\rho r \cdot vr}$$ Impedance contrast

$\alpha = 0.651$

$$Fue(f) := \frac{1}{\sqrt{\cos\left(\frac{2 \cdot \pi \cdot f \cdot H}{vs}\right)^2 + \alpha^2 \cdot \sin\left(\frac{2 \cdot \pi \cdot f \cdot H}{vs}\right)^2}}$$

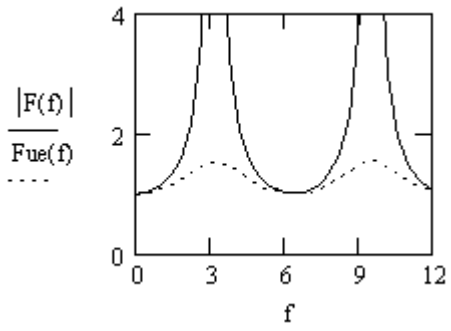

The solid line is the transfer function for the undamped soil on rigid bedrock. The dotted line is the TTF for the undamped soil on elastic bedrock.

Case 4: Uniform damped soil on elastic rock

I consider the effect of the damping for a soil on elastic rock

$vs := 634$ Parameters of the layer $f := 0, 0.2 .. 25$

$H := 50$

$\rho s := 1.8$

$Q1 := 10$

$\xi := \frac{1}{2Q1}$

$\xi = 0.05$

$vr := 923$ Parameters of the bedrock

$\rho r := 1.9$

$vss := vs \cdot (1 + i \cdot \xi)$

$vrr := vr \cdot (1 + i \cdot \xi)$

$\alpha s := \frac{\rho s \cdot vss}{\rho r \cdot vrr}$

$\alpha s = 0.651$

$$Fde(f) := \frac{1}{\cos\left(\frac{2 \cdot \pi \cdot f \cdot H}{vss}\right) + i\alpha s \cdot \sin\left(\frac{2 \cdot \pi \cdot f \cdot H}{vss}\right)}$$

To see the effect of the changes in the impedance contrast I calculate the transfer function for $\alpha s = 0.1$

$\alpha s := 0.1$

$$Fde1(f) := \frac{1}{\cos\left(\frac{2 \cdot \pi \cdot f \cdot H}{vss}\right) + i\alpha s \cdot \sin\left(\frac{2 \cdot \pi \cdot f \cdot H}{vss}\right)}$$

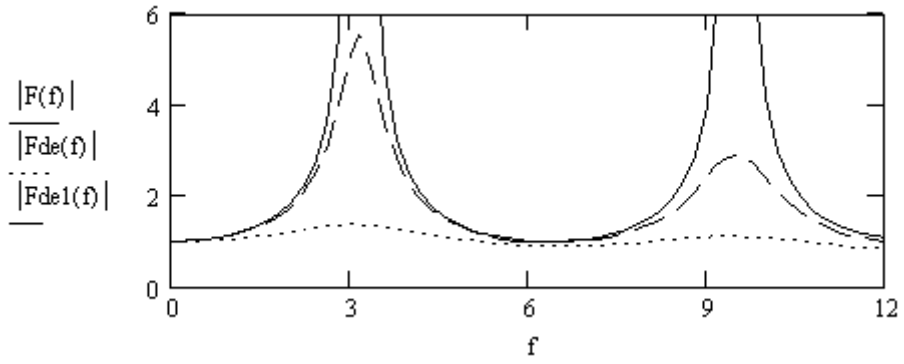

The continuous line is the transfer function for the undamped soil. The dotted line is TTF for an impedance contrast of 0.6 and for a damping corresponding to Q = 10. The dashed line is for an impedance contrast of 0.1 and Q = 10. The resonance frequencies remain unchanged but the amplification levels are lower in the presence of higher impedance contrasts.

Multiple layer models

The case of Pozzuoli-Solfatara: layered damped soil on elastic bedrock

First layer (50 m): poorly unconsolidated pyroclastic and marine deposits:

$f := 0, 0.2 .. 25$

$v1 := 634$

$h1 := 50$

$\rho 1 := 1.8$

$Q1 := 4$

$\xi 1 := \frac{1}{2Q1}$

$\xi 1 = 0.125$

Second layer (50 m): fractured yellow tuff:

$v2 := 923$

$h2 := 50$

$\rho 2 := 1.9$

$Q2 := 12$

$\xi 2 := \frac{1}{2Q2}$

$\xi 2 = 0.042$

Impedance contrast:

$\frac{v1 \cdot \rho 1}{v2 \cdot \rho 2} = 0.651$

The compact yellow tuff unit is considered as bedrock with the following parameters:

$v3 := 993$

$\rho 3 := 2.0$

$Q3 := 15$

$\xi 3 := \frac{1}{2Q3}$

$\xi 3 = 0.033$

$v1s := v1 \cdot (1 + i \cdot \xi 1)$

$v3s := v3 \cdot (1 + i \cdot \xi 3)$

$v2s := v2 \cdot (1 + i \cdot \xi 2)$

$\alpha 1 := \frac{\rho 1 \cdot v1s}{\rho 2 \cdot v2s}$

$\alpha 2 := \frac{\rho 2 \cdot v2s}{\rho 3 \cdot v3s}$

If there were only a single layer on a halfspace, the transfer function would be:

$$A1 := 1$$

$$A2(f) := A1\cdot\left[\frac{1}{2}\cdot(1+\alpha 1)\cdot\exp\left(i\cdot\frac{2\cdot\pi\cdot f}{v1s}\cdot h1\right)+\frac{1}{2}\cdot(1-\alpha 1)\cdot\exp\left(-i\cdot\frac{2\cdot\pi\cdot f}{v1s}\cdot h1\right)\right]$$

$$B2(f) := A1\cdot\left[\frac{1}{2}\cdot(1-\alpha 1)\cdot\exp\left(i\cdot\frac{2\cdot\pi\cdot f}{v1s}\cdot h1\right)+\frac{1}{2}\cdot(1+\alpha 1)\cdot\exp\left(-i\cdot\frac{2\cdot\pi\cdot f}{v1s}\cdot h1\right)\right]$$

$$Fl(f) := \frac{2}{A2(f)+B2(f)}$$

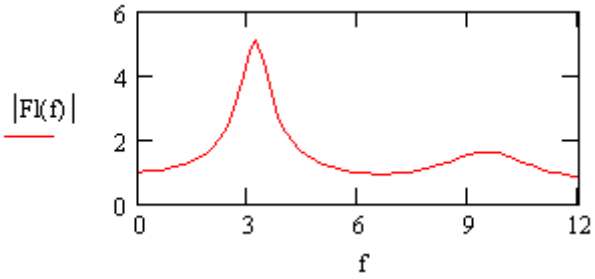

For the area of Solfatara I did not calculate this TTF related to a simple single layer on an elastic bedrock model, but I used the multiple layer model. I calculated the transfer function by considering a vertically SH wave coming from a bedrock composed of compact yellow tuff, and propagating in the first two layers (50 m of fractured yellow tuff and 50 meters of unconsolidated pyroclastic deposits). In this case, the expected fundamental frequency is about:

$$T := 4\cdot\left(\frac{h1}{v1}+\frac{h2}{v2}\right)$$

$$T = 0.532$$

$$Ff := \frac{1}{T}$$

$$Ff = 1.879$$

Expected resonance frequency for the multiple layer model

$$A3(f) := \left[\frac{1}{2}\cdot A2(f)\cdot(1+\alpha 2)\cdot\exp\left(i\cdot\frac{2\cdot\pi\cdot f}{v2s}\cdot h2\right)+\frac{1}{2}\cdot B2(f)\cdot(1-\alpha 2)\cdot\exp\left(-i\cdot\frac{2\cdot\pi\cdot f}{v2s}\cdot h2\right)\right]$$

$$B3(f) := \left[\frac{1}{2}\cdot A2(f)\cdot(1-\alpha 2)\cdot\exp\left(i\cdot\frac{2\cdot\pi\cdot f}{v2s}\cdot h2\right)+\frac{1}{2}\cdot B2(f)\cdot(1+\alpha 2)\cdot\exp\left(-i\cdot\frac{2\cdot\pi\cdot f}{v2s}\cdot h2\right)\right]$$

As one can note, the Q value of the bedrock (halfspace) does not affect the estimate of the TTF because it does not enter in the computation.

$$FL(f) := \frac{2}{A3(f) + B3(f)}$$

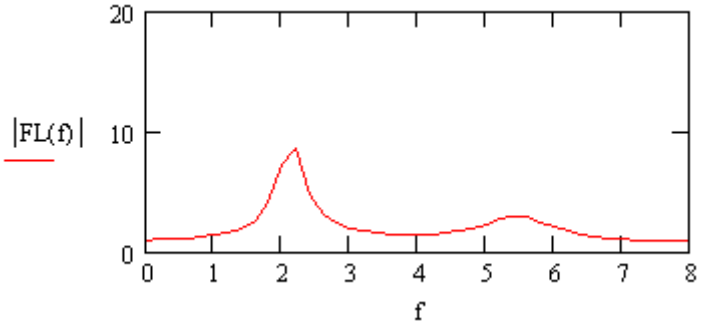

This is the transfer function obtained with the velocity and attenuation model for the area of Pozzuoli-Solfatara.

Appendix F

A Mathcad worksheet for the PGA estimate

For the estimate of the PGA in the area of Pozzuoli-Solfatara, I prepared the following Mathcad worksheet that uses the mathematical formulation derived for both GMG and RVT methods.

Definition of the source and propagation parameters

$a := 4.00$ **a and b values from the Gutenberg-Richter (De Natale and Zollo, 1986)**

$b := 0.92$

$\delta a := 0.10$ **Uncertainties on a and b values**

$\delta b := 0.04$

$Md := 4.35$ **Expected maximum magnitude maxima at Campi Flegrei**

$c := 9.9$ **Parameters of the empirical formula that relates seismic moment and magnitude**

$d := 0.9$

$\delta c := 0.1$ **Uncertainties on c and d values**

$\delta d := 0.01$

$\frac{\delta c}{c} = 0.01$

$\frac{\delta d}{d} = 0.011$

$M := \left[10^{(9.9+0.9Md)}\right] \cdot N \cdot m$ **Relation between seismic moment and magnitude (Galluzzo et al., 2004)**

Now I estimate the seismic moment and the uncertainty:

$M = 6.531 \times 10^{13}\ J$ $\quad Mdyne := 10^{7}\frac{M}{J}$ $\quad Mdyne = 6.531 \times 10^{20}$ **The value of the seismic moment**

$$\delta Md := \sqrt{(\delta a)^2 \cdot \left(\frac{1}{b}\right)^2 + (\delta b)^2 \cdot \left(\frac{a}{b^2}\right)^2}$$

$\delta Md = 0.218$

$\frac{\delta Md}{Md} = 0.05$

$$\delta M := \left[\sqrt{(\delta c)^2 \cdot \left[10^{(c+d\cdot Md)} \log(10) \right]^2 + (\delta d)^2 \cdot \left[10^{(c+d\cdot Md)} \cdot \log(10) \cdot Md \right]^2 + (\delta Md)^2 \cdot \left[10^{(c+d\cdot Md)} \cdot \log(10) \cdot d \right]^2} \right]_{N\cdot m}$$

$\delta M = 1.466 \times 10^{13}\ J$

$\frac{\delta M}{M} = 0.225$ **Relative error on the seismic moment estimate**

$kk := 4$ **Stress drop value in bar (Galluzzo et al., 2004)**

$\Delta\sigma_{kk} := kk \cdot 10^5 \cdot \frac{N}{m^2}$ **Uncertainty on the stress drop**

$r := \left[\frac{(0.44\cdot M)}{1\cdot \Delta\sigma_{kk}} \right]^{\frac{1}{3}}$ **Relation between source radius and seismic moment (Keilis - Borok, 1959)**

$r = 415.717\ m$ **The value of the source radius**

$$\delta r := \sqrt{\left[\left(\frac{0.44}{\Delta\sigma_{kk}} \cdot \frac{1}{3} \right) \cdot \left(M \cdot \frac{0.44}{\Delta\sigma_{kk}} \right)^{\frac{-2}{3}} \right]^2 \cdot (\delta M)^2}$$ **Uncertainty on the source radius**

$\delta r = 31.112\ m$

$\frac{\delta r}{r} = 0.075$ **Relative error on the source radius estimate**

$F := 2$ **Free surface operator (Del Pezzo et al., 1987)**

$R := 2$ **Hypocentral distance in km (insert adimensional values)**

$h1 := 0.05$ **Thickness of the first layer in km (this thesis). Insert adimensional values**

$h2 := 0.05$ **Thickness of the second layer in km (this thesis). Insert adimensional values**

$\rho := \frac{2100 \cdot kg}{m^3}$ **Average density (this thesis)**

$v1 := 634 \cdot \frac{m}{s}$ **Shear wave velocity of the first layer (this thesis)**

$v2 := 923 \cdot \frac{m}{s}$ **Shear wave velocity of the second layer (this thesis)**

$v3 := 1000 \cdot \frac{m}{s}$ **Average shear wave velocity of the halfspace (this thesis)**

$\theta\phi := 1$ **Radiation pattern coefficient (Del Pezzo et al., 1987)**

$Q1 := 4$ **Shear wave quality factor of the first layer (this thesis)**

$Q2 := 12$ **Shear wave quality factor of the second layer (this thesis)**

$Q3 := 110$ **Average quality factor of the halfspace (Del Pezzo et al., 1987)**

$Q(f) := 76 \cdot \left(\frac{f}{Hz}\right)^{0.5}$ **It is also possible to define a frequency dependent quality factor (not used in this simulation)**

$fc := 0.37 \cdot \frac{v3}{r}$ **Corner frequency (Brune,1970)**

$fc = 0.89\,Hz$

$\delta fc := \sqrt{\left(0.37 \cdot \frac{v3}{r^2}\right)^2 \cdot (\delta r)^2}$ **Uncertainty on the corner frequency**

$\Omega := M \cdot F \cdot \frac{\theta\phi}{4 \cdot \pi \cdot \rho \cdot v3^3 \cdot (R1000m + 0.1 \cdot 1000 \cdot m)}$ **Low frequency spectral level**

$\Omega = 2.357 \times 10^{-3}\,ms$

$fN := 50Hz$ **Nyquist frequency**

Now I define the shape of the acceleration spectrum, taking into account that the propagation occurs in the velocity structure derived in this thesis. For this reason, I consider the contribution of 3 terms : 1) propagation in the first layer 2) propagation in the second layer 3) propagation in the halfspace.

$f := 0 \cdot Hz, 0.1 \cdot Hz .. 100 \cdot Hz$

$R3 := R - (h1 + h2)$

$t1 := \frac{h1 \cdot 1000m}{v1}$

$t2 := \frac{h2 \cdot 1000m}{v2}$

$t3 := \frac{R3 \cdot 1000m}{v3}$

$\gamma := 2.5$

$$acc(f) := \Omega \cdot \frac{\exp\left(-\pi \cdot f \cdot t1 \cdot \frac{1}{Q1}\right) \cdot \exp\left(-\pi \cdot f \cdot t2 \cdot \frac{1}{Q2}\right) \cdot \exp\left(-\pi \cdot f \cdot t3 \cdot \frac{1}{Q3}\right) \cdot (2 \cdot \pi \cdot f)^2}{\left[1 + \left(\frac{f}{fc}\right)^{2 \cdot \gamma}\right]^{0.5}}$$

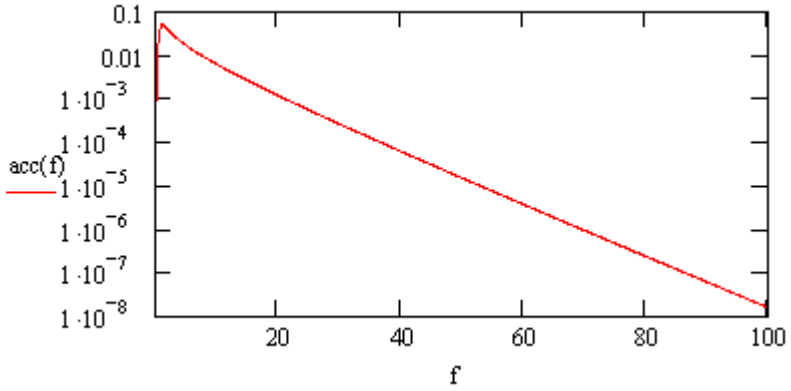

I include the local site effects in the ground motion simulation, by considering the theoretical transfer function (TTF) obtained from the velocity and attenuation structure for the area of Pozzuoli-Solfatara, in the hypothesis of multiple layer model:

$h1 := 50 \cdot m \quad Q1 := 4 \quad \xi 1 := \frac{1}{2Q1} \quad \xi 1 = 0.125 \quad v1 := 634 \cdot \frac{m}{s} \quad \rho 1 := 1.8 \cdot \frac{g}{cm^3}$

$h2 := 50 \cdot m \quad Q2 := 12 \quad \xi 2 := \frac{1}{2Q2} \quad \xi 2 = 0.042 \quad v2 := 923 \cdot \frac{m}{s} \quad \rho 2 := 1.9 \cdot \frac{g}{cm^3}$

$h3 := 160 \cdot m \quad Q3 := 15 \quad \xi 3 := \frac{1}{2Q3} \quad \xi 3 = 0.033 \quad v3 := 993 \cdot \frac{m}{s} \quad \rho 3 := 2.0 \cdot \frac{g}{cm^3}$

$v4 := 1019 \cdot \frac{m}{s} \quad \rho 4 := 2.1 \cdot \frac{g}{cm^3}$

$v1s := v1 \cdot (1 + i \cdot \xi 1) \quad v3s := v3 \cdot (1 + i \cdot \xi 3) \quad v2s := v2 \cdot (1 + i \cdot \xi 2)$

$\alpha 1 := \frac{\rho 1 \cdot v1s}{\rho 2 \cdot v2s} \quad \alpha 2 := \frac{\rho 2 \cdot v2s}{\rho 3 \cdot v3s}$

$A1 := 1$

$A2(f) := A1 \cdot \left[\frac{1}{2} \cdot (1 + \alpha 1) \cdot \exp\left(i \cdot \frac{2 \cdot \pi \cdot f}{v1s} \cdot h1 \right) + \frac{1}{2} \cdot (1 - \alpha 1) \cdot \exp\left(-i \cdot \frac{2 \cdot \pi \cdot f}{v1s} \cdot h1 \right) \right]$

$B2(f) := A1 \cdot \left[\frac{1}{2} \cdot (1 - \alpha 1) \cdot \exp\left(i \cdot \frac{2 \cdot \pi \cdot f}{v1s} \cdot h1 \right) + \frac{1}{2} \cdot (1 + \alpha 1) \cdot \exp\left(-i \cdot \frac{2 \cdot \pi \cdot f}{v1s} \cdot h1 \right) \right]$

$A3(f) := \left[\frac{1}{2} \cdot A2(f) \cdot (1 + \alpha 2) \cdot \exp\left(i \cdot \frac{2 \cdot \pi \cdot f}{v2s} \cdot h2 \right) + \frac{1}{2} \cdot B2(f) \cdot (1 - \alpha 2) \cdot \exp\left(-i \cdot \frac{2 \cdot \pi \cdot f}{v2s} \cdot h2 \right) \right]$

$B3(f) := \left[\frac{1}{2} \cdot A2(f) \cdot (1 - \alpha 2) \cdot \exp\left(i \cdot \frac{2 \cdot \pi \cdot f}{v2s} \cdot h2 \right) + \frac{1}{2} \cdot B2(f) \cdot (1 + \alpha 2) \cdot \exp\left(-i \cdot \frac{2 \cdot \pi \cdot f}{v2s} \cdot h2 \right) \right]$

$TF(f) := \frac{2}{A3(f) + B3(f)}$

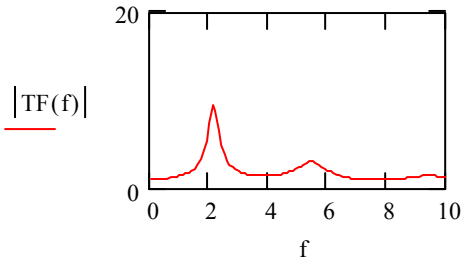

The acceleration spectrum is multiplied by the TTF to take into account local site effects:

$$acc(f) := acc(f)\cdot |TF(f)|$$

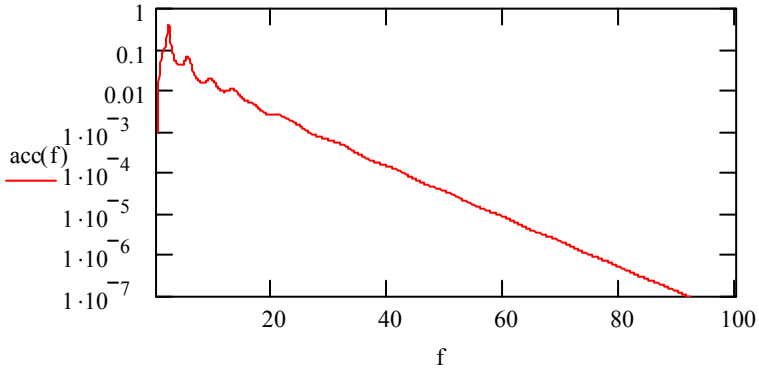

The following routine provides the acceleration spectrum considering the Nyquist frequency

$$hacc(f, fN) := \begin{cases} acc(f) & \text{if } 0 < f \le fN \\ Re(acc(2fN - f)) - i\cdot Im(acc(2fN - f)) & \text{if } fN < f < 2\cdot fN \\ Re\left(acc\left(2fN - f + \frac{1}{2\cdot fN}\right)\right) - i\cdot Im\left(acc\left(2fN - f + \frac{1}{2\cdot fN}\right)\right) & \text{if } f \ge 2\cdot fN \\ acc\left(f + \frac{1}{2\cdot fN}\right) & \text{if } f = 0 \end{cases}$$

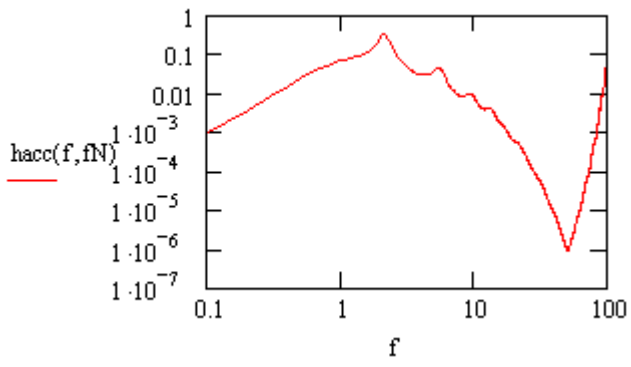

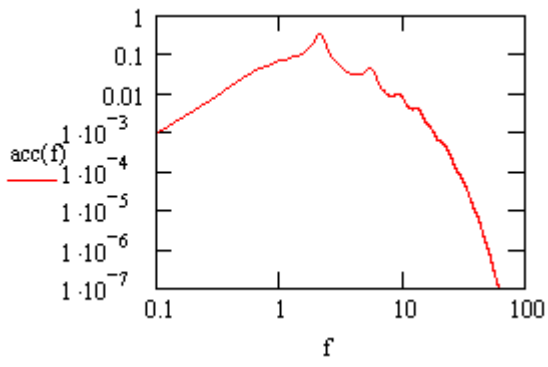

Method 1: GMG

I apply the GMG method to estimate the PGA

$finf := 0 \cdot Hz$

$fsup := 100 \cdot Hz$

$$accrms := \left[2 \cdot fc \cdot \left(\int_{finf}^{fsup} acc(f)^2 \, df \right) \right]^{0.5}$$ **Parseval Theorem**

$mm := 1 .. 2000$

$$tt_{mm} := \frac{1 \cdot mm}{100}$$

$$accrms = 0.324 \frac{m}{s^2}$$

I generate a Gaussian distribution with sigma = accrms

$$d := rnorm\left(2000, 0, accrms \cdot \frac{s^2}{m} \right)$$

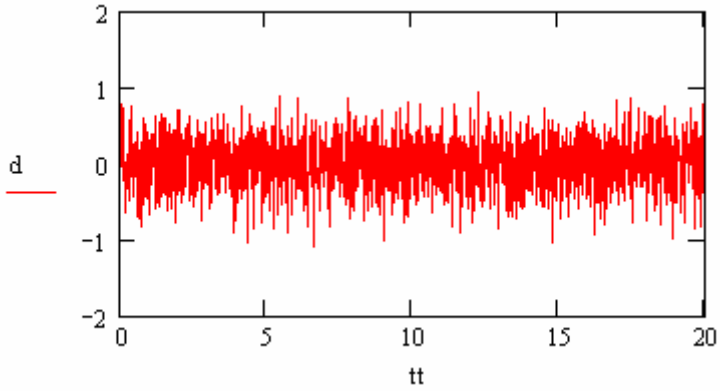

$max(d) = 0.945$

$$pga\_met1 := \frac{max(d)}{9.82}$$

$pga\_met1 = 0.096$ **PGA value**

I calculate the uncertainty on the PGA estimate by propagating the errors that affect the seismic moment and on the corner frequency:

$$daccrmsdM := \frac{\frac{1}{2}\left[2fc\cdot\int_{finf}^{fsup} 2M\cdot\left[\frac{F\cdot\theta\phi\cdot\left(\exp\left(-\pi\cdot f\cdot t1\cdot\frac{1}{Q1}\right)\cdot\exp\left(-\pi\cdot f\cdot t2\cdot\frac{1}{Q2}\right)\cdot\exp\left(-\pi\cdot f\cdot t3\cdot\frac{1}{Q3}\right)\right)\cdot(2\cdot\pi\cdot f)^2}{4\pi\rho\cdot v3^3\cdot(R1000m+0.1\cdot1000\cdot m)\left[1+\left(\frac{f}{fc}\right)^{2\cdot\gamma}\right]^{0.5}}\right]^2 df\right]}{accrms}$$

$$daccrmsdfc := \frac{\frac{1}{2}\left[2\left[\int_{finf}^{fsup}(acc(f))^2\,df\right]+2fc\cdot\int_{finf}^{fsup}\left[\left[\frac{M\cdot F}{4\cdot\pi\cdot\rho\cdot v3^3\cdot(R\cdot1000\cdot m+0.1\cdot1000\cdot m)}\cdot\theta\phi\cdot\left(\exp\left(-\pi\cdot f\cdot t1\cdot\frac{1}{Q1}\right)\cdot\exp\left(-\pi\cdot f\cdot t2\cdot\frac{1}{Q2}\right)\cdot\exp\left(-\pi\cdot f\cdot t3\cdot\frac{1}{Q3}\right)\right)\cdot(2\cdot\pi\cdot f)^2\right]^2\cdot\left[(-1)\cdot\frac{\left[2\cdot\gamma\cdot\left(\frac{f}{fc}\right)^{(2\cdot\gamma-1)}\cdot\left[\frac{-f}{(fc)^2}\right]\right]}{\left[1+\left(\frac{f}{fc}\right)^{2\cdot\gamma}\right]^2}\right]\right]df\right]}{accrms}$$

$$\delta accrms := \sqrt{(daccrmsdfc)^2\cdot(\delta fc)^2+(daccrmsdM)^2\cdot(\delta M)^2}$$

$\delta accrms = 0.023\frac{m}{s^2}$ **Absolute error on the PGA**

$\frac{\delta accrms}{accrms} = 0.06$ **Relative error on the PGA**

Method 2: RVT

I apply the method RVT to estimate the PGA

$fi := 0\cdot Hz$

$fs := 100\cdot Hz$

$fc = 0.89\,Hz$

$T := \frac{1}{fc}$

$T = 1.124\,s$

$$m2 := 2\cdot\int_{fi}^{fs} (2\pi f)^2\left[(acc(f))^2\right] df$$ **Estimate of the moments of the squared spectral amplitude**

$$m4 := 2\cdot\int_{fi}^{fs} (2\pi f)^4\left[(acc(f))^2\right] df$$

$$m1 := 2\cdot\int_{fi}^{fs} (2\pi f)\left[(acc(f))^2\right] df$$

$$m0 := 2\cdot\int_{fi}^{fs} \left[(acc(f))^2\right] df$$

$$fz := \frac{1\cdot\left(\frac{m2}{m0}\right)^{0.5}}{2\pi}$$ **Estimate of the frequencies of zero crossings and extrema**

$$fe := \frac{1\cdot\left(\frac{m4}{m2}\right)^{0.5}}{2\pi}$$

$Tgm := T$ **for small earthquakes (Boore, 2003)**

$Nz := 2fz\cdot Tgm$

$Ne := 2\cdot fe\cdot Tgm$

$\xi := \frac{Nz}{Ne}$

$zmin := 0$

$zmax := \infty$

$$rapp := 2\int_{zmin}^{zmax} \left[1 - \left(1 - \xi\cdot\exp\left(-z^2\right)\right)^{Ne}\right] dz$$

$$drappdne := 2\int_{zmin}^{zmax} \log\left(\left(1 - \xi\cdot\exp\left(-z^2\right)\right)\right)\cdot\left[1 - \left(1 - \xi\cdot\exp\left(-z^2\right)\right)^{Ne}\right] dz$$

$$drappd\,\xi := 2\int_{zmin}^{zmax} Ne\cdot\left(1 - \xi\cdot\exp\left(-z^2\right)\right)^{Ne-1}\left(-1\exp\left(-z^2\right)\right) dz$$

$rapp = 2.951$

$$rms := \left(\frac{m0}{T}\right)^{0.5}$$

$$rms = 0.324\,\frac{m}{s^2}$$

$$\alpha := \left[2\pi\left[1 - \frac{(m1)^2}{(m0 \cdot m2)}\right]\right]^{0.5}$$

$$\alpha = 0.996$$

$$Amax := rms \cdot rapp$$

$$Amax = 0.956\,\frac{m}{s^2}$$

$$pga\_boore\_rvt := \frac{Amax}{9.82 \cdot \frac{m}{s^2}}$$

$pga\_boore\_rvt = 0.097$ **PGA value**

Final results for the two methods:

$pga\_met1 = 0.096$ **GMG**

$pga\_boore\_rvt = 0.097$ **RVT**

References

Aki K., 1957. Space and Time Spectra of Stationary Stochastic Waves, with special reference to microtremors. *Bull. Earthq. Res. Inst. Tokio Univ.*, 25, 415-457.

Aki K., and P.G Richards, 1980. *Quantitative Seismology – Theory and Methods*. W.H. Freeman and company, San Francisco.

Bard P.-Y., and M. Bouchon, 1980. The seismic response of sediment-filled valleys. Part 1: The case of incident SH waves. *Bull. Seism. Soc. Am.*, 70, 1263-1286.

Bard P.-Y., 1999. Microtremor measurements: a tool for site effect estimation?. In *The Effects of Surface Geology on Seismic Motion* (Irikura, Kudo, Okada and Satasani eds.) Balkerna, Rotterdam, 1999), 1251–1279.

Bettig B., Bard P.Y., Scherbaum F., Riepl J., Cotton F., Cornou C., Hatzfeld D, 2001. Analysis of dense array noise measurements using the modified spatial autocorrelation method (SPAC). Application to the Grenoble area. *Boll. Geof. Teor. Appl.*, 42, 15-27.

Bianco F., Del Pezzo E., Saccorotti G., Ventura G., 2004. The role of hydrothermal fluids in triggering the July-August 2000 seismic swarm at Campi Flegrei, Italy: evidence from seismological and mesostructural data. *J. Volcanol. Geotherm. Res.*, 133, 229-246.

Boatwright J., 1978. Detailed spectral analysis of two small New-York state earthquakes. *Bull. Seism. Soc. Am.*, 68, 1117-1131.

Boatwright J., 1980. A spectral theory for circular seismic sources: simple estimates of source dimension, dynamic stress drop and radiated energy. *Bull. Seism. Soc. Am.*, 71, 69–94.

Boore D.M., 2003. Simulation of Ground Motion using the Stochastic Method. *Pure Appl. Geophys.*, 160, 635-676.

Brune J.N., 1970. Tectonic stress and seismic shear waves from earthquakes. *J. Geophys. Res.*, 75, 4997-5009.

Bruno P.P., Bais G., Chiodini G., Godio A., Costi F., 2004. Geophysical study of the shallow hydrothermal system at Solfatara (Campi Flegrei; Italy). *J. Geophys. Res.*, (submitted).

Cartwright D.E., and Longuet-Higgins M.S., 1956. The statistical distribution of the maxima of a random function. *Proc. R. Soc. London*, 237, 212-232.

Castro R., Mucciarelli M., Pacor F., Petrungaro C., 1997. S-wave site response estimates using horizontal to vertical spectral ratios. *Bull. Seism. Soc. Am.*, 87, no. 1, 256–260.

Comune di Napoli, 1994. Indagini geologiche per l'adeguamento del P.R.G. alla legge regionale 07.01.1983 n. 9 in difesa del territorio dal rischio sismico. Indagini per l'applicazione della L.R. n. 9/83.

Del Pezzo E., De Nartale G., Martini M., Zollo A., 1987. Source parameters of microearthquakes at Campi Flegrei (Southern Italy) volcanic area. *Phys.Earth Planet. Inter.*, 47, 25-42.

De Natale G. and Zollo A., 1986. Statistical analysis and clustering features of the Phlegrean Fields earthquake sequence (May 1983-May 1984). *Bull. Seismol. Soc. Am.*, 76 (3), 801-814.

Di Vito M.A., Isaia R., Orsi G., Southon J., de Vita S., D'Antonio M., Pappalardo L., Piochi M., 1999. Volcanism and deformation since 12,000 years at the Campi Flegr ei caldera (Italy). *J. Volcanol. Geotherm. Res.*, 91, 221-246.

Dziewonski A., Bloch S., Landisman M., 1969. A technique for the analysis of transient seismic signals. *Bull. Seism. Soc. Am.*, 59, 427-444.

Fäh D., Kind F., Giardini D., 2001. A theoretical investigation of average H/V ratios. *Geophys. J. Int.*, 145, 535–549.

Field E. H., and K. H. Jacob, 1993. The theoretical response of sedimentary layers to ambient seismic noise. *Geophys. Res. Lett.*, 20, 2925–2928.

Field E. H., and K. H. Jacob, 1995. A comparison and test of various site response estimation techniques including three that are not reference site dependent. *Bull. Seism. Soc. Am.*, 85, 1127–1143.

Galluzzo D., Del Pezzo E., La Rocca M., Petrosino S., 2004. Peak ground acceleration produced by local earthquakes in volcanic areas of Campi Flegrei and Mt. Vesuvius. *Annals of Geophysics*, Vol. 47, N.4: 1377-1389.

Hasada Y, Kumagai H., Kumazawa M., 2001. Autoregressive modeling of transfer functions in frequency domain to determine complex travel times. *Earth Planets Space*, 53, 3–11.

Herrin E., and Goforth, T., 1977. Phase-matched filters: application to the study of Rayleigh waves. *Bull. Seism. Soc Am.*, 67, 1259-1275.

Herrmann R. B., 1973. Some aspects of band-pass filtering of surface waves. *Bull. Seism. Soc. Am.*, 63, 663-671.

Herrmann, R. B., 1987. *Computer Programs in Seismology. User's manual Vol. II-IV*. St. Louis University, Missouri.

Hori S., Fukao Y., Kumazawa M., Furumoto M., Yamamoto A., 1989. A new method of spectral analysis and its application to the Earth's free oscillations: The "Sompi" method. *J. Geophys. Res.*, 94(B6), 7535–7553.

Hough S. E., Borcherdt R. D., Friberg P. A., Busby R., Field E., Jacobs K.H., 1990. The role of sediment-induced amplification in the collapse of the Nimitz freeway during the October 17, 1989 Loma Prieta earthquake. *Nature*, 344, 853-855.

Keilis-Borok V.I., 1959. On estimation of the displacement in an earthquake source dimension. *Ann. Geofis.*, 12, 205-214.

Konno K., and Ohmachi, T., 1998. Ground-Motion Characteristics Estimated from Spectral Ratio between Horizontal and Vertical Components of Microtremor. *Bull. Seism. Soc. Am.*, Vol. 88, No.1, 228-241.

Kramer, S.L. (1996). Geotechnical Earthquake Engineering, Prentice Hall, Inc., Upper Saddle River, New Jersey.

Kumazawa M., Imanishi Y., Fukao Y., Furumoto M., Yamamoto A., 1990. A theory of spectral analysis based on the characteristic property of a linear dynamic system. *Geophys. J. Int.*, 101, 613–630.

Lachet C., and P.-Y. Bard, 1994. Numerical and theoretical investigations on the possibilities and limitations of Nakamura's technique. *J. Phys. Earth.*, 42, 377–397.

Lay T., and Wallace T.C, 1995. *Modern Global Seismology*. (Academic Press, London).

Lermo, J., and Chavez-Garcia F. J., 1993. Site effects evaluation using spectral ratios with only one station. *Bull. Seism. Soc. Am.*, 83, 1574–1594.

Lermo, J., and Chavez-Garcia F. J., 1994. Are microtremors useful in site response evaluation?. *Bull. Seism. Soc. Am.*, 84, 1350–1364.

Lirer L., Pescatore T.S., Corbelli V., Di Vito M., Gattullo V., Romano A., 1987. Geologia delle aree di Monteruscello e del centro storico di Pozzuoli. *Quaderno di documentazione n.1*, ed. Ministero della Protezione Civile, Napoli.

Louie J. N., 2001. Faster, better: Shear–wave velocity to 100 meters depth from refraction microtremor arrays. *Bull. Seism. Soc. Am.*, 91, 347-364.

Luzon F., Al Yuncha Z., Sanchez-Sesma F.J., Ortiz-Aleman C., 2001. A Numerical Experiment on the Horizontal to Vertical Spectral Ratio in Flat Sedimentary Basins. *Pure Appl. Geophys.*, 158, 2451-2461.

Malagnini L., Herrmann R.B., Biella G., de Franco R., 1995. Rayleigh waves in Quaternary alluvium from esplosive sources: determination of shear-wave velocity and Q structure. *Bull. Seism. Soc. Am.*, 85, 900-922.

Malagnini L., 1996. Velocity and attenuation structure of very shallow soils: evidence for a frequency dependent Q. Bull. Seism. Soc. Am., 86, 1471-1486.

Malagnini L., Tricarico P., Rovelli A., Herrmann R.B., Opice S., Biella G., de Franco R., 1996. Explosion, Earthquake, and Ambient Noise Recordings in a Pliocene Sediment-Filled Valley: Inferences on Seismic Response Properties by Reference- and Non-Reference-Site Techniques. *Bull. Seism. Soc. Am.*, 86, 670-682.

Malagnini, L., Hermann R. B., Mercuri A., Opice S., Biella G., de Franco R., 1997. Shear-wave velocity structure of sediments from the inversion of explosion-induced Rayleigh waves: comparison with cross hole measurements. *Bull. Seism. Soc. Am.*, 87, 1413–1421.

Malischewsky P.G., and Scherbaum F., 2004. Love's formula and H/V-ratio (ellipticity) of Rayleigh waves. *Wave Motion*, 40, 57-67.

Matsuura T., Imanishi Y., Imanari M., Kumazawa M., 1990. Application of a new method of high-resolution spectral analysis, "Sompi," for free induction decay of nuclear magnetic resonance. *Appl. Spectrosc.*, 44, 618–626.

Margheriti L., Azzara R. M., Cocco M., Delladio A., Nardi A., 2000. Analysis of Borehole Broadband Recordings: Test Site in the Po Basin, Northern Italy. *Bull. Seism. Soc. Am.*, 90, 1454–1463.

Menke W., 1984. *Geophysical data analysis: discrete inverse theory*. Academic Press, inc., USA.

Midzi V., 2001. 3-D surface wave group velocity distribution in Central-Southern Africa. *J. Seismology*, 5, 559-574.

Nakamura Y., 1989. A Method for Dynamic Characteristics Estimation of Subsurface Using Microtremor on the Ground Surface. *Q. Rept. Railway Tech. Res. Inst.*, 30,1: 25-33.

Nakamura Y., 1996. Real Time Information Systems for Seismic Hazards Mitigation UrEDAS, HERAS and PIC. *Quarterly Report of RTRI*, Vol. 37, No. 3, 112-127.

Nogoshi, M., and Igarashi T., 1971. On the Amplitude Characteristics of Microtremor (Part 2) (in Japanese with English abstract). *Jour. Seism. Soc. Japan*, 24, 26-40.

Nunziata C., Mele R., Natale M., 1999. Shear wave velocities and primary influencing factors of Campi Flegrei-Neapolitan deposits. Engineering Geology, 54, 299-312.

Orsi G., De Vita S., Di Vito M.A., 1996. The restless resurgent Campi Flegrei nested caldera (Italy): constraints on its evolution and configuration. *J. Volcanol. Geotherm. Res.*, 74, 179-214.

Orsi, G., Civetta, L., Del Gaudio, C., De Vita, S., Di Vito, M., Isaia, R., Petrazzuoli, S.M., Ricciardi, G.P., Ricco, C., 1999. Short term ground deformations and seismicity in the resurgent Campi Flegrei caldera (Italy): An example of active block-resurgence in a densely populated area. *J. Volcanol. Geotherm. Res.*, 91, 415-451.

Orsi G., de Vita S., Di Vito M., Isaia R., Nave R., Heiken G., 2003. Facing volcanic and related hazards in the Neapolitan area. In: Heiken G., Fakundiny R, Sutter J. (Eds) "*Earth Sciences in Cities*", American Geophysical Union book, Washington, 56, 121-170.

Petrosino, S., La Rocca M., Del Pezzo E., 1999. Shallow velocity model of the northern flank of Stromboli Volcano, deduced by high frequency surface wave dispersion. *J. Seismology*, 1, 83–94.

Petrosino S., Cusano P., Saccorotti G., Del Pezzo E., 2002. Seismic attenuation and shallow velocity structures at Stromboli Volcano, Italy; *Bull. Seism. Soc. Am.*, Vol 92, 1102-1116.

Saccorotti G., Chouet B., Dawson P., 2003. Shallow-velocity models at the Kilauea Volcano, Hawaii, determined from array analyses of tremor wavefields. *Geophys. J. Int.*, 152, 633-648.

Satoh T., Kawase H., Matsushima S, 2001. Differences Between Site Characteristics Obtained From Microtremors, S-waves, P-waves, and Codas. *Bull. Seism. Soc. Am.*, 91, 313-334.

Sholz C., 1968. The frequency-magnitude relation of microfracturingin rock and its relation to earthquakes. *Bull. Seism. Soc. Am.*, 58, 399-415.

Seekins L.C., Wennerberg L., Margheriti L., Liu H.-P., 1996. Site Amplification at Five Locations in San Francisco, California: A Comparison of S Waves, Codas and Microtremors. *Bull. Seism. Soc. Am.*, 86, 627-635.

Slejko D., Peruzza L., Rebez A., 1998. Seismic hazard maps of Italy. *Ann. Geofis.*, 41(2), 183-214.

Vanorio T., Virieux J., Zollo A., Capuano P., Russo G., 2005. 3-D Seismic Tomography from P- and S- Microearthquake Traveltimes and Rock Physics Characterization in the Campi Flegrei Caldera. *J. Geophys. Res.*, 110, B03201, doi:10.1029/2004JB003102

Vilardo, G., Alessio, G., Luongo, G., 1991. Analysis of the magnitude-frequency distribution for the 1983-1984 earthquake activity of Campi Flegrei, Italy. *J. Volcanol. Geotherm. Res.*, 48, 115-125.

Zollo A., Judenherc S., Auger E., D'Auria L., Virieux J., Capuano P., Chiarabba C., de Franco R., Makris J., Michelini A., Musacchio G., 2003. Evidence for the bouried rim of Campi Flegrei caldera from 3-d active seismic imaging. *Geophys. Res. Lett.*, 30(19), 2002, doi:10.1029/2003GL018173.